

## First Structure-Activity Relationship of 17 $\beta$ -Hydroxysteroid Dehydrogenase Type 14 Nonsteroidal Inhibitors and Crystal Structures in Complex with the Enzyme

Florian Braun, Nicole Bertoletti, Gabriele Möller, Jerzy Adamski, Torsten Steinmetzer, Mohamed Salah, Ahmed Saad Abdelsamie, Chris J van Koppen, Andreas Heine, Gerhard Klebe, and Sandrine Marchais-Oberwinkler

*J. Med. Chem.*, **Just Accepted Manuscript** • DOI: 10.1021/acs.jmedchem.6b01436 • Publication Date (Web): 09 Nov 2016

Downloaded from <http://pubs.acs.org> on November 10, 2016

### Just Accepted

“Just Accepted” manuscripts have been peer-reviewed and accepted for publication. They are posted online prior to technical editing, formatting for publication and author proofing. The American Chemical Society provides “Just Accepted” as a free service to the research community to expedite the dissemination of scientific material as soon as possible after acceptance. “Just Accepted” manuscripts appear in full in PDF format accompanied by an HTML abstract. “Just Accepted” manuscripts have been fully peer reviewed, but should not be considered the official version of record. They are accessible to all readers and citable by the Digital Object Identifier (DOI®). “Just Accepted” is an optional service offered to authors. Therefore, the “Just Accepted” Web site may not include all articles that will be published in the journal. After a manuscript is technically edited and formatted, it will be removed from the “Just Accepted” Web site and published as an ASAP article. Note that technical editing may introduce minor changes to the manuscript text and/or graphics which could affect content, and all legal disclaimers and ethical guidelines that apply to the journal pertain. ACS cannot be held responsible for errors or consequences arising from the use of information contained in these “Just Accepted” manuscripts.

1  
2  
3 **First Structure-Activity Relationship of 17 $\beta$ -Hydroxysteroid Dehydrogenase Type 14**  
4  
5 **Nonsteroidal Inhibitors and Crystal Structures in Complex with the Enzyme**  
6  
7

8 Florian Braun<sup>† $\Delta$</sup> , Nicole Bertoletti<sup>† $\Delta$</sup> , Gabriele Möller<sup>‡</sup>, Jerzy Adamski<sup>‡§§</sup>, Torsten Steinmetzer<sup>†</sup>,  
9  
10 Mohamed Salah<sup>#</sup>, Ahmed S. Abdelsamie<sup># $\Theta$</sup> , Chris J. van Koppen<sup>#</sup>, Andreas Heine<sup>†</sup>, Gerhard Klebe<sup>†</sup>,  
11  
12 Sandrine Marchais-Oberwinkler<sup>†\*</sup>  
13  
14

15 <sup>†</sup> Institute for Pharmaceutical Chemistry, Philipps University Marburg, 35032 Marburg, Germany  
16

17 <sup>‡</sup> German Research Center for Environmental Health, Institute of Experimental Genetics, Genome  
18 Analysis Center, Helmholtz Zentrum München, 85764 Neuherberg, Germany  
19  
20

21 <sup>§</sup> Chair of Experimental Genetics, Technical University Munich, 85350 Freising-Weihenstephan,  
22 Germany  
23  
24

25 <sup>§</sup> German Center for Diabetes Research (DZD), 85764 Neuherberg, Germany  
26  
27

28 <sup>#</sup> ElexoPharm GmbH, Campus A1.2, 66123 Saarbrücken, Germany  
29  
30  
31  
32

33 **Abstract**  
34

35 17 $\beta$ -HSD14 belongs to the SDR family and oxidizes the hydroxyl group at position 17 of estradiol and  
36 5-androstenediol using NAD<sup>+</sup> as cofactor. The goal of this study was to identify and optimize 17 $\beta$ -  
37 HSD14 nonsteroidal inhibitors as well as to disclose their structure-activity relationship. In a first  
38 screen, a library of 17 $\beta$ -HSD1 and 17 $\beta$ -HSD2 inhibitors, selected with respect to scaffold diversity,  
39 was tested for 17 $\beta$ -HSD14 inhibition. The most interesting hit was taken as starting point for chemical  
40 modification applying a ligand-based approach. The designed compounds were synthesized and tested  
41 for 17 $\beta$ -HSD14 inhibitory activity. The two best inhibitors identified in this study have a very high  
42 affinity to the enzyme with a K<sub>i</sub> equal to 7 nM. The strong affinity of these inhibitors to the enzyme  
43 active site could be explained by crystallographic structure analysis, which highlighted the role of an  
44 extended H-bonding network in the stabilization process. The selectivity of the most potent  
45 compounds with respect to 17 $\beta$ -HSD1 and 17 $\beta$ -HSD2 is also addressed.  
46  
47  
48  
49  
50  
51  
52  
53  
54  
55  
56  
57  
58  
59  
60

## Introduction

Human 17 $\beta$ -hydroxysteroid dehydrogenase type 14 (17 $\beta$ -HSD14), also called DHRS10 and retSDR3, is an oxido-reductase belonging to the SDR (Short-chain Dehydrogenase-Reductase) family.<sup>1,2</sup> In vitro, the enzyme oxidizes the hydroxyl group at position 17 of estradiol (E2) and 5-androsten-3 $\beta$ ,17 $\beta$ -diol (5-diol) in presence of the cofactor NAD<sup>+</sup>, however, in vivo, its natural substrate is still unknown.

While Sivik *et al.*<sup>3</sup> described a broad distribution pattern of 17 $\beta$ -HSD14 across various tissues based on immunohistochemistry studies, Northern blotting experiments showed that the enzyme is predominantly expressed in the brain, liver and placenta<sup>2</sup> as well as in the kidney.<sup>4</sup> Furthermore, immunofluorescence studies revealed cytosolic localization.<sup>2</sup>

In order to understand the function of 17 $\beta$ -HSD14, the enzyme needs to be further characterized. Inhibitors are useful chemical tools, which can be used not only to characterize the binding site of an enzyme but also to get insight into the physiological role of the latter upon in vivo administration. With the exception of compound **1**, which we recently presented,<sup>5</sup> no inhibitor has been reported for this enzyme.

The crystal structure of the human 17 $\beta$ -HSD14 has been determined recently as the holo protein (PDB ID: 5JS6 and 5JSF) and as the ternary complex with the nonsteroidal inhibitor **1** (PDB ID: 5ICM). 17 $\beta$ -HSD14 is a tetramer.<sup>5</sup> The binding cavity was shown to be rather lipophilic with a conical shape. The substrate active site is narrow in the vicinity of the catalytic triad and is solvent exposed at the other end. Tyr253' from the C-terminal chain of the adjacent unit in the tetramer reduces the size of the active site.

Up to now 14 different 17 $\beta$ -HSD subtypes have been reported.<sup>6</sup> 17 $\beta$ -HSD1 and 17 $\beta$ -HSD2, the two best characterized subtypes, predominantly catalyze the oxidation and reduction of estrogens and androgens. Inhibitors of these two enzymes have already been reported.<sup>7-20</sup> While 17 $\beta$ -HSD1 is a cytosolic enzyme and shows a reductive activity in vivo (activation of estrogens), 17 $\beta$ -HSD2 is membrane-bound and catalyzes the oxidation of estrogens and androgens to their less potent analogues similarly to 17 $\beta$ -HSD14. However, 17 $\beta$ -HSD2 and 17 $\beta$ -HSD14 differ in their tissue distribution pattern since in contrary to 17 $\beta$ -HSD14, 17 $\beta$ -HSD2 is not present in the human brain temporal lobe.<sup>21</sup>

1  
2  
3 The presence of 17 $\beta$ -HSD14 in the brain might indicate that this enzyme is involved in the regulation  
4  
5 of active estrogens and androgens in this organ.<sup>2</sup>  
6

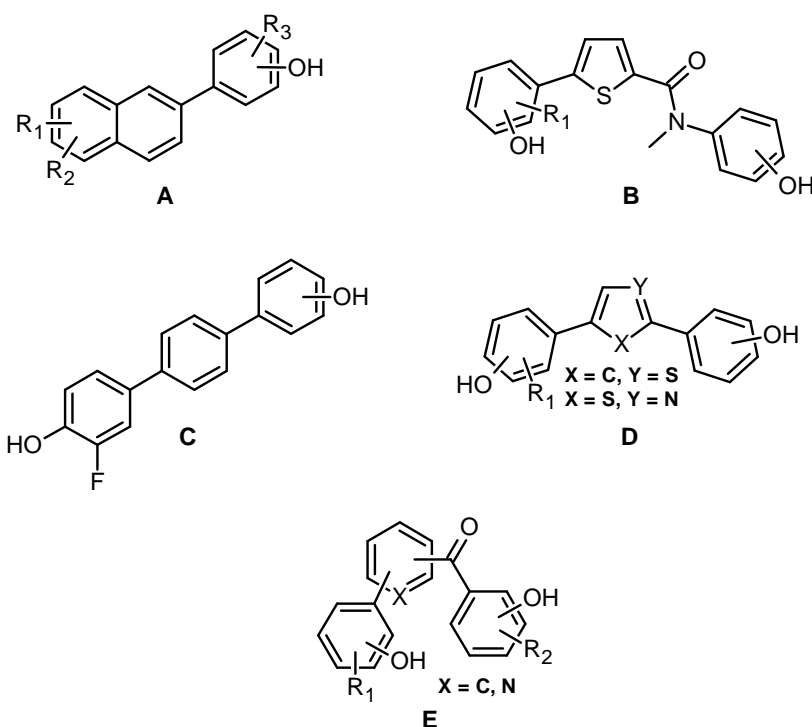
7  
8 The goal of this work was to identify 17 $\beta$ -HSD14 nonsteroidal inhibitors and to optimize their  
9  
10 structures, which led to highly active compounds. The inhibitor optimization was performed following  
11  
12 a ligand-based approach. The synthesis and biological evaluation of highly active compounds with a  
13  
14 nonsteroidal scaffold together with four new crystal structures of the ternary complexes are reported.  
15  
16 Analysis of the crystal structures of the ternary complexes revealed the location of the inhibitor  
17  
18 binding sites as well as the resulting protein-inhibitor interactions and a complex pattern of hydrogen  
19  
20 bonds (H-bonds) contributing to the strong affinity of these compounds to the enzyme. The  
21  
22 physicochemical properties of the new inhibitors as well as selectivity considerations were also  
23  
24 addressed.  
25  
26  
27  
28  
29

## 30 **RESULTS**

### 31 **Design of 17 $\beta$ -HSD14 inhibitor candidates**

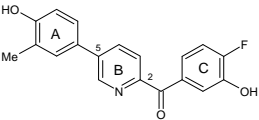
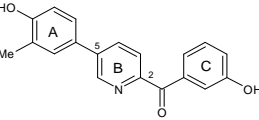
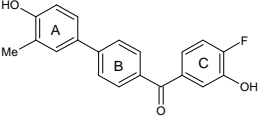
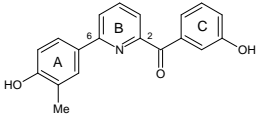
32  
33  
34 Although 17 $\beta$ -HSDs belong to the same superfamily they share a low overall sequence identity.  
35  
36 Nonetheless, considering the fact that 17 $\beta$ -HSD1 and 17 $\beta$ -HSD2 catalyze the same reaction as  
37  
38 17 $\beta$ -HSD14, the substrate binding site of the three enzymes should exhibit a high structural similarity.  
39  
40 Based on this idea, it was assumed that some inhibitors developed for 17 $\beta$ -HSD1 and 17 $\beta$ -HSD2  
41  
42 should also bind to 17 $\beta$ -HSD14 and that a common scaffold could be used as starting point, to  
43  
44 optimize them for 17 $\beta$ -HSD14 binding. In a first screen, a small library of 34 17 $\beta$ -HSD1 and 17 $\beta$ -  
45  
46 HSD2 inhibitors, chosen on the basis of structural diversity (Figure 1), was tested for 17 $\beta$ -HSD14  
47  
48 inhibitory activity using a radioactive displacement assay. This assay was performed with the  
49  
50 recombinantly expressed enzyme in a bacterial suspension since the pure protein was not available at  
51  
52 that time. Thereby sets of active and inactive compounds were identified.  
53  
54  
55  
56  
57  
58  
59  
60

**Figure 1:** Scaffold of inhibitors from a 17 $\beta$ -HSD1 and 17 $\beta$ -HSD2 library tested for 17 $\beta$ -HSD14 inhibitory activity.



While the series of tested naphthalenes **A** and thiophene amides **B** contained mostly inactive compounds, the dihydroxyphenylbenzenes **C**, -thiophenes and -thiazoles **D** showed examples of low to moderate inhibitory activity against 17 $\beta$ -HSD14 (between 10% and 45% inhibition at 1  $\mu$ M). In addition, some of the latter derivatives were also reported to possess very high potency for 17 $\beta$ -HSD1 and/or 17 $\beta$ -HSD2 (IC<sub>50</sub> in the low nM range), which might lead to difficulties achieving high selectivity for 17 $\beta$ -HSD14. These parent scaffolds were therefore not considered for further optimization. Some members of the pyridine ketone class **E** also showed remarkable inhibitory activity for 17 $\beta$ -HSD14, paralleled by rather low or moderate activity against 17 $\beta$ -HSD1 (Table 1, compound **2**), which rendered this class as promising scaffold for further investigations. They were therefore chosen as a starting point for the development of new 17 $\beta$ -HSD14 inhibitors.

**Table 1:** Most interesting compounds identified in a first screen.

Cmpd	Structure	Inhibition of	Inhibition of	Inhibition of
		17 $\beta$ -HSD14	17 $\beta$ -HSD1	17 $\beta$ -HSD2
		% Inh. @ 1 $\mu$ M <sup>a</sup>	IC <sub>50</sub> ( $\mu$ M) <sup>b</sup>	IC <sub>50</sub> ( $\mu$ M) <sup>c</sup>
<b>2</b>		62%	1.27	0.10
<b>3</b>		0%	5.48	0.26
<b>4</b>		19%	0.29	0.04
<b>5</b>		32%	19.65	0.26

<sup>a</sup> Recombinant 17 $\beta$ -HSD14 enzyme, bacterial suspension, substrate [<sup>3</sup>H]-E2 [18.3 nM], NAD<sup>+</sup> [7.5 mM], mean value of 3 determinations; standard deviation < 10 %.

<sup>b</sup> Placental 17 $\beta$ -HSD1 enzyme, cytosolic fraction, substrate [<sup>3</sup>H]-E1 + E1 [500 nM], NADH [0.5 mM], mean value of at least 3 determinations; standard deviation < 20 %.

<sup>c</sup> Placental 17 $\beta$ -HSD2 enzyme, microsomal fraction, substrate [<sup>3</sup>H]-E2 + E2 [500 nM], NAD<sup>+</sup> [1.5 mM], mean value of at least 3 determinations; standard deviation < 20 %.

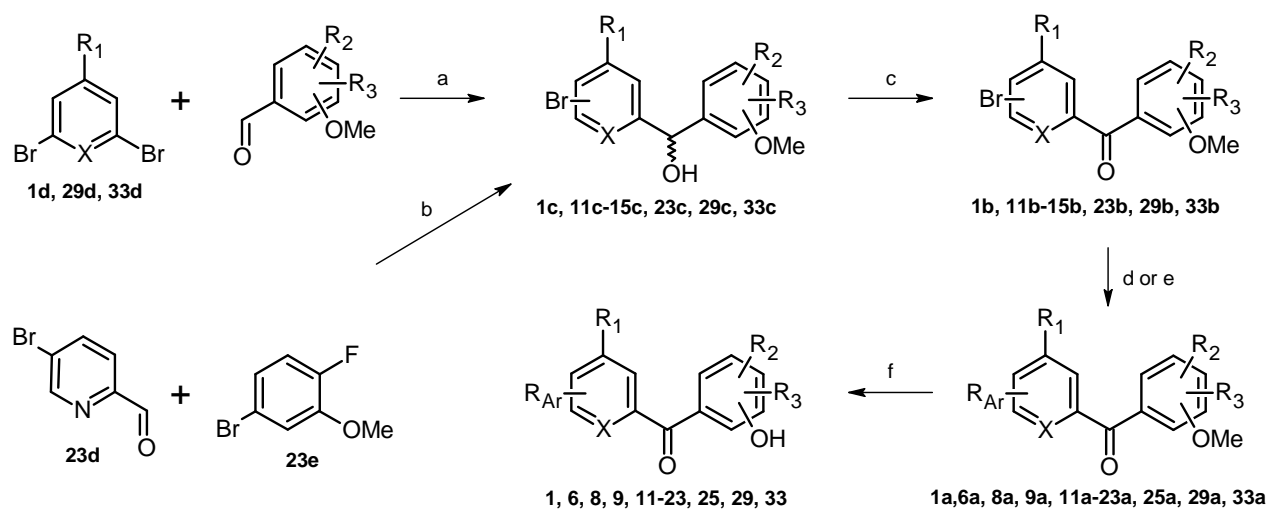
The most interesting hits identified in the preliminary screen are listed in Table 1. The compounds can be categorized into 2,5- (**2**, **3**) and 2,6-substituted (**5**) pyridine ketones and the 1,4-substituted phenyl (**4**). In the 2,5-compound class, **2** and **3** (62% inhibition at 1  $\mu$ M vs 0%) differ by the presence/absence of a fluorine atom in *ortho* position to the OH group of the C-ring, suggesting the importance of this atom for inhibitory activity. Furthermore, comparison of **2** with **4** (62% inhibition at 1  $\mu$ M vs 19%)

1  
2  
3 shows that the pyridine core **B** is more potent than the phenyl analog, pointing toward the importance  
4 of the nitrogen atom in the B-ring for activity. Concerning the 2,6-compound class, comparison of **5**  
5 with 2,5-substituted **3** (32% inhibition at 1  $\mu\text{M}$  vs 0%) shows that moving the A-ring from 5- to 6-  
6 position leads to a gain in activity.  
7  
8  
9

10  
11  
12 Furthermore, considering the selectivity aspect, the poor inhibitory activity of the 2,6-substituted **5**  
13 toward 17 $\beta$ -HSD1 ( $\text{IC}_{50}$ = 19.65  $\mu\text{M}$ ), compared to the 2,5-substituted analog **3** ( $\text{IC}_{50}$ = 5.48  $\mu\text{M}$ )  
14 suggests that the 2,6-substitution pattern might improve selectivity for 17 $\beta$ -HSD14 over 17 $\beta$ -HSD1.  
15 Selectivity against 17 $\beta$ -HSD2 does not become obvious with the set of studied test compounds.  
16  
17 Consequently, the 2,6-pyridine ketone class was selected for optimization and the derivatives, with  
18 modification at the A-ring as well as at the C-ring by substituents with different properties were  
19 synthesized. Special attention was paid to the physicochemical properties of the designed compounds  
20 in order to focus on compounds which should have a promising bioavailability profile according to the  
21 Veber rules<sup>22</sup> and the Lipinski rules of 5.<sup>23</sup>  
22  
23  
24  
25  
26  
27  
28  
29  
30  
31  
32  
33  
34  
35

## 36 Chemistry

37  
38  
39 The synthesis of compounds **1**, **6**, **8**, **9**, **11-23**, **25**, **29** and **33** was achieved in four steps starting from  
40 the dibromopyridine derivatives **1d** and **33d** and analogous benzene **29d**, respectively (Scheme 1).  
41  
42 Lithiation with *n*-butyl lithium<sup>24</sup> and nucleophilic addition to the appropriate aldehyde provided the  
43 alcohol intermediates **1c**, **11c-15c**, **29c** and **33c**. For the synthesis of compound **23** (Scheme 1),  
44 arylbromide **23e** was used to prepare the corresponding Grignard reagent. Nucleophilic addition to the  
45 carbaldehyde **23d** afforded the alcohol intermediate **23c**. Oxidation with 2-iodoxybenzoic acid resulted  
46 in the corresponding ketones **1b**, **11b-15b**, **23b**, **29b** and **33b**. Subsequently, Suzuki couplings<sup>25</sup> with  
47 different arylboronic acids afforded compounds **1a**, **6a**, **8a**, **9a**, **11a-23a**, **25a**, **29a** and **33a** using either  
48 standard conditions ( $\text{Cs}_2\text{CO}_3$ , 80  $^\circ\text{C}$ , overnight) or microwave irradiations ( $\text{Na}_2\text{CO}_3$ , 150  $^\circ\text{C}$ , 60 min,  
49 150 W). Cleavage of the methoxy groups with boron tribromide gave the final compounds **1**, **6**, **8**, **9**,  
50  
51  
52  
53  
54  
55  
56  
57  
58  
59  
60  
**11-23**, **25**, **29** and **33**.

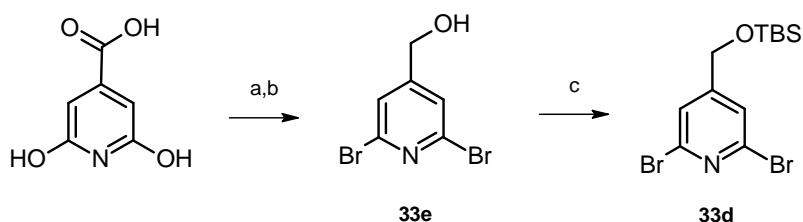
Scheme 1. Synthesis of compounds **1**, **6**, **8**, **9**, **11-23**, **25**, **29** and **33**.

Cmpd	R <sub>Ar</sub>	X	R <sub>1</sub>	R <sub>2</sub>	R <sub>3</sub>	OH-Pos
1	6-(3,4-dihydroxyphenyl)	N	H	4-F	H	3
6	6-(4-hydroxy-3-methylphenyl)	N	H	4-F	H	3
8	6-(3-fluoro-4-hydroxyphenyl)	N	H	4-F	H	3
9	6-(2-fluoro-3-hydroxyphenyl)	N	H	4-F	H	3
11	6-(2-fluoro-3-hydroxyphenyl)	N	H	2-F	4-F	3
12	6-(2-fluoro-3-hydroxyphenyl)	N	H	2-OH	H	3
13	6-(2-fluoro-3-hydroxyphenyl)	N	H	H	H	2
14	6-(2-fluoro-3-hydroxyphenyl)	N	H	3-OH	4-OH	2
15	6-(2-fluoro-3-hydroxyphenyl)	N	H	3-OH	6-OH	2
16	6-phenyl	N	H	4-F	H	3
17	6-(3- <i>N,N</i> -dimethylamino)-phenyl)	N	H	4-F	H	3
18	6-(3-hydroxyphenyl)	N	H	4-F	H	3
19	6-(3-hydroxyphenyl)	N	H	2-OH	H	3
20	6-(3-hydroxy-4-methylphenyl)	N	H	4-F	H	3
21	6-(4-fluorophenyl)	N	H	4-F	H	3
22	6-(3-chloro-4-fluorophenyl)	N	H	4-F	H	3
23	5-(3-fluoro-4-hydroxyphenyl)	N	H	4-F	H	3
25	6-(thiophen-3-yl)	N	H	4-F	H	3
29	3-(2-fluoro-3-hydroxyphenyl)	CH	H	2-OH	H	3
33	6-(2-fluoro-3-hydroxyphenyl)	N	CH <sub>2</sub> OH	4-F	H	3

Reagents and conditions: **a)** *n*-BuLi, anhydrous THF, -80 °C to room temperature, 1 h; **b)** Mg, anhydrous THF, 60 °C, 2 h, 80 °C, 5 h; **c)** 2-iodoxybenzoic acid, anhydrous THF, 60 °C, 2-4 h; **d)** Cs<sub>2</sub>CO<sub>3</sub>, Pd(PPh<sub>3</sub>)<sub>4</sub>, R<sub>Ar</sub>B(OH)<sub>2</sub>, DME/water (2:1), 80 °C, overnight, for compounds **1a**, **6a**, **8a**, **9a**, **12a-15a**, **17a-20a**, **22a**, **23a**, **25a**, **29a** and **33a**; **e)** Na<sub>2</sub>CO<sub>3</sub>, Pd(PPh<sub>3</sub>)<sub>4</sub>, R<sub>Ar</sub>B(OH)<sub>2</sub>, DME/water (2:1), microwave irradiation (60 min, 150 W, 150 °C), for compounds **11a**, **16a** and **21a**; **f)** BBr<sub>3</sub>, CH<sub>2</sub>Cl<sub>2</sub>, -80 °C to room temperature, overnight.

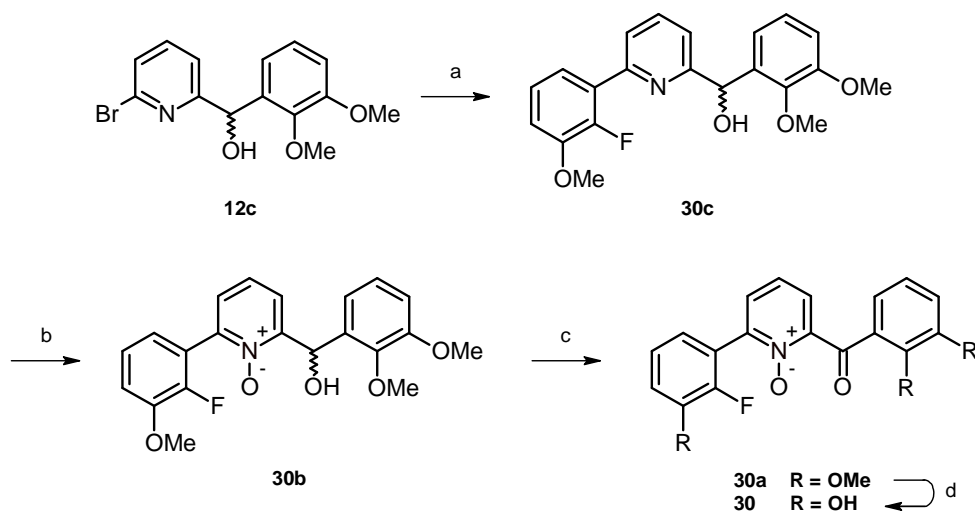
The precursor **33d** was prepared starting from citrazinic acid, which was first brominated with commercial phosphorus oxybromide and then reacted with methanol. Reduction of the formed ester<sup>26</sup> and protection of the primary alcohol **33e** with TBSCl afforded compound **33d** (Scheme 2).

**Scheme 2.** Synthesis of precursor **33d**.



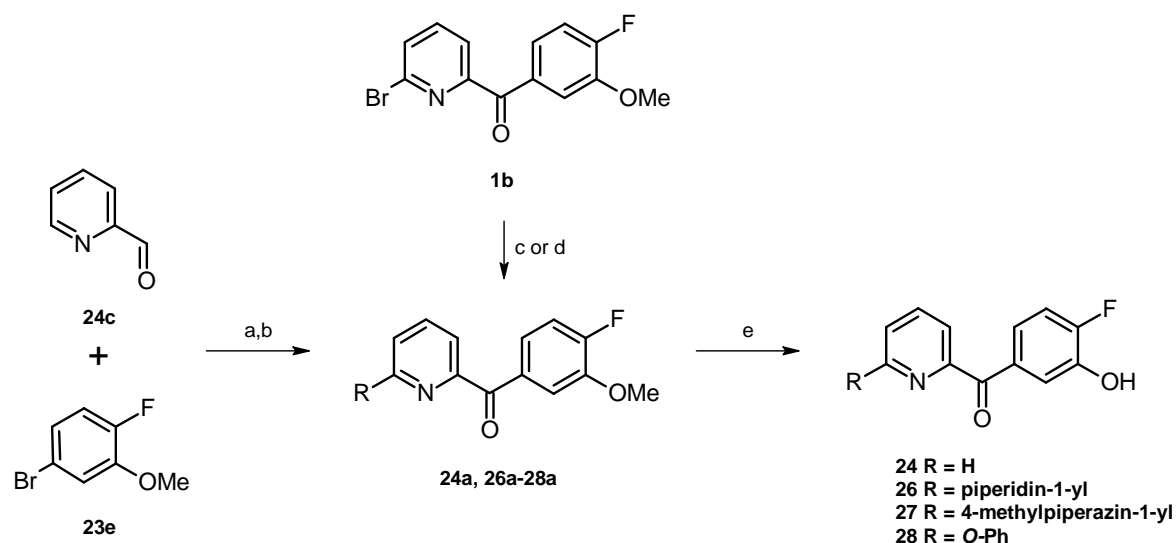
Reagents and conditions: **a)** i) POBr<sub>3</sub>, 130 °C, 0.5 h, 150 °C, 1.5 h, ii) MeOH, room temperature, overnight; **b)** NaBH<sub>4</sub>, EtOH, 85 °C, 3 h; **c)** TBSCl, imidazole, DMF, room temperature, 18 h.

The synthesis of the pyridine *N*-oxide **30** was achieved in four steps starting from the previously described alcohol intermediate **12c**. The Suzuki coupling reaction with 2-fluoro-3-methoxyphenylboronic acid under standard condition afforded compound **30c**. Oxidation into the pyridine *N*-oxide **30b** was performed by means of *meta*-chloroperoxybenzoic acid and further oxidation with 2-iodoxybenzoic acid resulting in ketone **30a**. Cleavage of the methoxy groups with boron trifluoride dimethylsulfide complex afforded the final pyridine *N*-oxide **30** (Scheme 3).

Scheme 3. Synthesis of *N*-oxide **30**.

Reagents and conditions: **a**)  $\text{Cs}_2\text{CO}_3$ ,  $\text{Pd}(\text{PPh}_3)_4$ , 2-fluoro-3-methoxyphenylboronic acid, DME/water (2:1), 80 °C, overnight; **b**) *m*-CPBA (77%),  $\text{CH}_2\text{Cl}_2$ , 0 °C to room temperature, overnight; **c**) 2-iodoxybenzoic acid, anhydrous THF, 60 °C, 2 h; **d**)  $\text{BF}_3 \cdot \text{SMe}_2$ ,  $\text{CH}_2\text{Cl}_2$ , room temperature, overnight.

The synthesis of compound **24**, lacking the A-ring, was performed by coupling of the pyridine carbaldehyde **24c** with the arylbromide **23e** followed by the oxidation to ketone **24a** as previously described (Scheme 4). The synthesis of compounds **26** and **27** was realized by amination of **1b** with different nonaromatic *N*-heterocycles following the procedure described by Bollinger *et al.*<sup>27</sup> to obtain compounds **26a** and **27a**. Compound **28**, with the A-ring linked via an ether bridge to the pyridine moiety, was synthesized by reacting the 6-bromopyridine derivative **1b** in a copper-catalyzed *O*-arylation using picolinic acid as ligand,<sup>28</sup> resulting in compound **28a**. All methoxy groups were cleaved with boron tribromide to provide compounds **24** and **26-28** (Scheme 4).

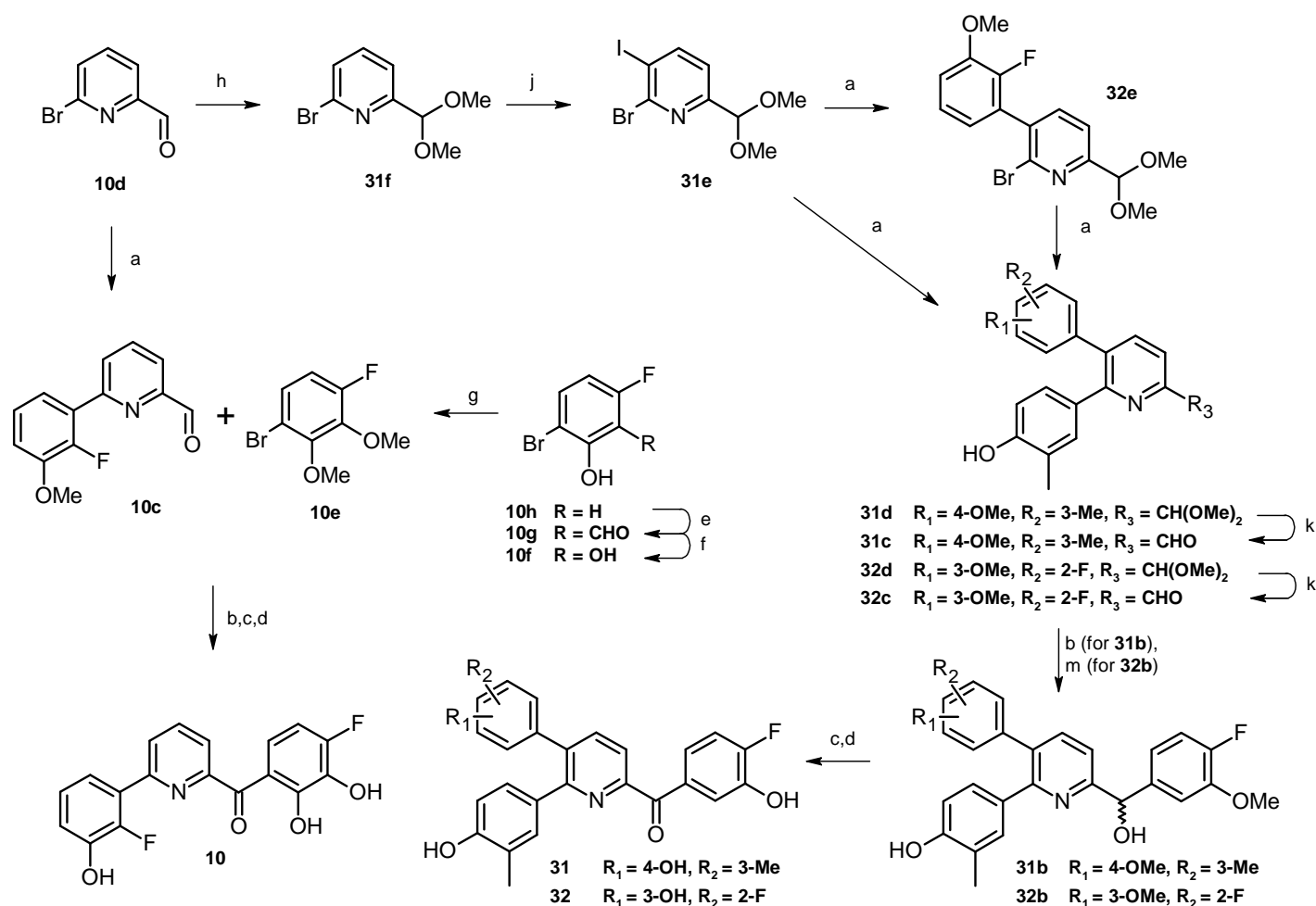
**Scheme 4.** Synthesis of compounds **24** and **26-28**.

Reagents and conditions: **a)** Mg, anhydrous THF, 60 °C, 2 h, 80 °C, 5 h; **b)** 2-iodoxybenzoic acid, anhydrous THF, 60 °C, 3-4 h; **c)** *N*-heterocycles, K<sub>3</sub>PO<sub>4</sub>, 1,4-dioxane, 100 °C, 2-4 d, for compounds **26a** and **27a**; **d)** Cu(I)I, picolinic acid, K<sub>3</sub>PO<sub>4</sub>, DMSO, 80 °C, 3 d, for compound **28a**; **e)** BBr<sub>3</sub>, CH<sub>2</sub>Cl<sub>2</sub>, -80 °C to room temperature, overnight.

The synthesis of the trisubstituted C-ring derivative **10** was achieved in four steps starting from the 6-bromopyridine-2-carbaldehyde **10d** (Scheme 5). Suzuki coupling with 2-fluoro-3-methoxyphenylboronic acid afforded the 6-substituted carbaldehyde **10c**. Nucleophilic addition of the *in situ* formed Grignard reagent of arylbromide **10e**, oxidation of the formed alcohol with 2-iodoxybenzoic acid and cleavage of the methoxy groups with boron tribromide resulted in the desired compound **10**.

The arylbromide **10e** was obtained following a three-step procedure starting from 2-bromo-5-fluorophenol **10h**. First, a modified Casiraghi-formylation reaction using paraformaldehyde in the presence of magnesium chloride and triethylamine gave the intermediate **10g**.<sup>29</sup> Subsequent Dakin reaction with hydrogen peroxide and sodium hydroxide<sup>30</sup> followed by protection of the formed dihydroxy compound **10f** with methyl iodide afforded compound **10e**.

1  
2  
3 The synthesis of trisubstituted pyridines **31** and **32** was achieved in seven and eight steps, respectively,  
4 starting from compound **10d** (Scheme 5). Protection of the aldehyde group with trimethyl  
5 orthoformate gave the 2-dimethoxy derivative **31f**. Iodination with lithium diisopropylamide and  
6 iodine<sup>31</sup> afforded the 5-iodo-6-bromo derivative **31e** in moderate yield. For compound **31**, subsequent  
7 Suzuki coupling with 2.4 equivalents of 4-methoxy-3-methylphenylboronic acid provided the 5,6-  
8 bisubstituted pyridine **31d**. The reaction with 2-fluoro-3-methoxyphenylboronic acid resulted, under  
9 the same conditions, selectively in the mono-coupled derivative **32e**, still brominated in 6-position.  
10 Further, a second Suzuki coupling with 4-methoxy-3-methylphenylboronic acid performed on **32e**  
11 yielded the asymmetric pyridine **32d**. Both, **31d** and **32d** were deprotected with acetic acid to form the  
12 aldehydes **31c** and **32c**. For **31**, a nucleophilic reaction with the *in situ* formed Grignard reagent of  
13 compound **23e** resulted in the alcohol intermediate **31b**. For **32** the corresponding alcohol **32b** was  
14 obtained after lithiation of arylbromide **23e** with butyl lithium and subsequent nucleophilic reaction.  
15 Oxidation with 2-iodoxybenzoic acid and ether cleavage with boron tribromide gave the final  
16 compounds **31** and **32**.  
17  
18  
19  
20  
21  
22  
23  
24  
25  
26  
27  
28  
29  
30  
31  
32  
33  
34  
35  
36  
37  
38  
39  
40  
41  
42  
43  
44  
45  
46  
47  
48  
49  
50  
51  
52  
53  
54  
55  
56  
57  
58  
59  
60

Scheme 5. Synthesis of compounds **10**, **31** and **32**.

Reagents and conditions: **a**) Cs<sub>2</sub>CO<sub>3</sub>, Pd(PPh<sub>3</sub>)<sub>4</sub>, R<sub>Ar</sub>B(OH)<sub>2</sub>, DME/water (2:1), 80 °C, overnight; **b**) Mg, anhydrous THF, 60 °C, 2 h, 80 °C, 5 h; **c**) 2-iodoxybenzoic acid, anhydrous THF, 60 °C, 3-4 h; **d**) BBr<sub>3</sub>, CH<sub>2</sub>Cl<sub>2</sub>, -80 °C to room temperature, overnight; **e**) (CHO)<sub>n</sub>, MgCl<sub>2</sub>, Et<sub>3</sub>N, anhydrous THF, 80 °C, 5 h; **f**) 1 M NaOH, H<sub>2</sub>O<sub>2</sub>, THF, room temperature, 4 h; **g**) MeI, K<sub>2</sub>CO<sub>3</sub>, DMF, room temperature, overnight; **h**) HC(OMe)<sub>3</sub>, *p*-TsOH, anhydrous MeOH, reflux, 4 h; **j**) LDA, anhydrous THF -80 °C, 3 h, I<sub>2</sub>, anhydrous THF, -80 °C to room temperature; **k**) acetic acid/water (2:3), reflux, 2 h; **m**) *n*-BuLi, anhydrous THF, -80 °C to room temperature, 1 h.

### Calculation of physicochemical parameters

For each synthesized compound, the molecular weight (MW) was calculated to be in the range of 300 to 400 g/mol, aside from the trisubstituted compounds **31-33** with a slightly higher MW. The log P was calculated in silico (using Molinspiration<sup>32</sup>) and turned out to be below 5 except for **31-33**. The total polar surface area (TPSA), the number of rotational bonds as well as the number of H-bond donors and acceptors fulfill the Veber rules<sup>22</sup> and the Lipinski rules of 5.<sup>23</sup> In addition, considering the potential role of the enzyme in the brain, the capability of the inhibitors to cross the BBB should also be taken into account. The physicochemical properties to be met by compounds showing a good BBB penetration are described by Pajouhesh and Lenz.<sup>33</sup> These criteria are matched for most of the synthesized compounds especially for **17** and **28** as examples. The solubility range of most of the compounds was also determined by mixing several concentrations of the studied inhibitors in 100 mM phosphate buffer at pH 7.4 and analyzing its precipitation status at different time points (0, 1, 2 and 24 h). A table summarizing the physicochemical parameters can be found in the Supporting Information (Table S3). The pKa values of the OH groups at the A- and at the C-ring were determined in silico for all compounds (using Marvin Sketch), showing that the introduction of a fluorine group in *ortho* position to a OH group decreases the pKa value by about one unit (e.g. pKa OH/C-ring: 7.8 for **8**, 8.8 for **7**).

### Biological evaluation

#### Inhibition of 17 $\beta$ -HSD14 determined with a fluorimetric assay

A fluorimetric assay, quantifying the NADH fluorescence built up during the catalytic reaction, was used to evaluate the inhibitory activity of the synthesized compounds. In the assay, the purified recombinantly expressed human enzyme, E2 as substrate, NAD<sup>+</sup> as cofactor, and the inhibitor were used as already reported.<sup>5</sup> Due to the low sensitivity of the assay, a high enzyme concentration (between 3.0  $\mu$ M and 3.5  $\mu$ M) and a high concentration of substrate E2 (32  $\mu$ M) was necessary. The results are expressed as percent of inhibition measured at an inhibitor concentration of 2  $\mu$ M. The inhibition constant  $K_i$  was experimentally determined using an inhibitor concentration ranging from

1  
2  
3 2.6  $\mu\text{M}$  to 100  $\mu\text{M}$  or 260 nM to 10  $\mu\text{M}$ , depending on the inhibitor potency. As the inhibitor and  
4  
5 protein concentrations were in the same range, no classical kinetic analysis could be applied.<sup>34,35</sup> The  
6  
7 results were analyzed applying the quadratic Morrison equation for tight binding (see Supporting  
8  
9 Information).<sup>36</sup> When the inhibitor was not sufficiently soluble at the required concentration, no  $K_i$   
10  
11 could be determined and the results were expressed as percent inhibition at the highest soluble  
12  
13 concentration of the inhibitor. The results are shown in Tables 2-5. Compounds showing less than 10%  
14  
15 inhibition at a concentration of 100  $\mu\text{M}$  were considered to be inactive.  
16  
17

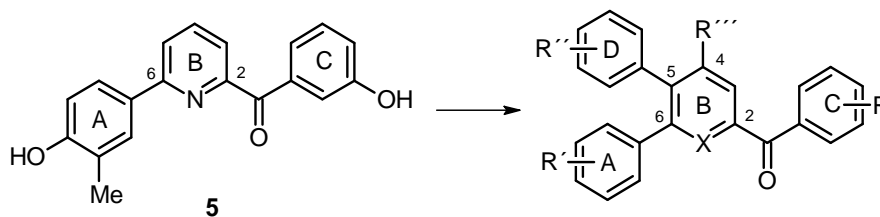
### 18 19 **Aggregation**

20  
21  
22 It was verified that the compounds did not aggregate or induce aggregation of the protein by testing  
23  
24 the compounds with and without detergent (0.5% v/v Tween 20). No significant changes in the  
25  
26 inhibitor activity could be noticed at the different conditions.  
27  
28

### 29 30 **17 $\beta$ -HSD14 inhibitory activity**

31  
32  
33 Starting from the hit pyridine ketone **5**, modifications were undertaken at the C-ring and A-ring by  
34  
35 introduction of different substituents (R, R', Chart 1). These substituents were selected to represent  
36  
37 different electronic properties: electron donating or electron withdrawing, H-bond donor, H-bond  
38  
39 acceptor, lipophilic and hydrophilic. Changes were also performed at the central B-ring by  
40  
41 replacement of the nitrogen by a carbon or a *N*-oxide moiety. An additional phenyl ring (D) with  
42  
43 various substituents (R'') were introduced in 5-position as well as a hydroxymethyl group (R''') in  
44  
45 4-position leading to trisubstituted derivatives.  
46  
47  
48

49 **Chart 1:** Modifications undertaken on the hit compound **5**.



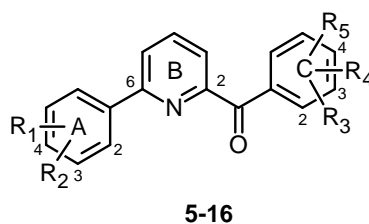
### Substituent variations on the C-ring

In the first inhibitor screen it could be shown, that in the 2,5-pyridine class (Table 1) the addition of a fluorine atom in *ortho* position to the hydroxyl group at the C-ring (**2** compared to **3**) resulted in a notable increase in potency of the inhibitor. The analogous fluorinated compound **6** (2,6-substituted pyridine) was therefore synthesized and proved to bind 10 times more potent than the reference compound **5** ( $K_i = 245$  nM for **6** vs 26 nM for **5**, Table 2). The affinity enhancement caused by the 4-F substituent at the C-ring could also be observed using another substitution pattern at the A-ring: 3-F/4-OH ( $K_i = 467$  nM for **7** vs 36 nM for **8**, Table 2).

The influence of the substituent pattern used for the C-ring was subsequently studied in more detail with compounds containing a 2-F/3-OH phenyl A-ring motif (compounds **9-15**, Table 2). Addition of a 2-OH or a 2-F to the 3-OH/4-F at the C-ring resulted in equipotent compounds ( $K_i = 13$  nM; 11 nM and 9 nM, respectively for **9**, **10** and **11**). Replacing the 3-OH/4-F at the C-ring (**9**) by a 2-OH/3-OH motif (**12**;  $K_i = 64$  nM) led to a slight decrease in affinity. Addition of a 4-OH group (**14**,  $K_i = 405$  nM) or of a 6-OH group at the C-ring (**15**,  $K_i = 796$  nM) resulted in a strong decrease in activity.

The presence of the 3-OMe group at the C-ring (**16a**, inactive at a concentration of 100  $\mu$ M) was detrimental for the inhibitory activity compared to the 3-OH analogue (**16**,  $K_i = 63$  nM).

**Table 2:** 17 $\beta$ -HSD14 inhibitory activity and binding constant ( $K_i$ ) of 2,6-pyridine derivatives with different substituents at the C-ring



Compound	$R_1$	$R_2$	$R_3$	$R_4$	$R_5$	17 $\beta$ -HSD14	
						% inhibition	$K_i$ (nM) <sup>a</sup>
						@ 2 $\mu$ M <sup>a</sup>	
<b>5</b>	3-Me	4-OH	H	3-OH	H	34	245 $\pm$ 21
<b>6</b>	3-Me	4-OH	H	3-OH	4-F	60	26 $\pm$ 3
<b>7</b>	3-F	4-OH	H	3-OH	H	16	467 $\pm$ 91
<b>8</b>	3-F	4-OH	H	3-OH	4-F	67	36 $\pm$ 5
<b>9</b>	2-F	3-OH	H	3-OH	4-F	72	13 $\pm$ 5
<b>10</b>	2-F	3-OH	2-OH	3-OH	4-F	76	11 $\pm$ 3
<b>11</b>	2-F	3-OH	2-F	3-OH	4-F	72	9 $\pm$ 3
<b>12</b>	2-F	3-OH	2-OH	3-OH	H	65	64 $\pm$ 4
<b>13</b>	2-F	3-OH	2-OH	H	H	66	135 $\pm$ 2
<b>14</b>	2-F	3-OH	2-OH	3-OH	4-OH	25	405 $\pm$ 177
<b>15</b>	2-F	3-OH	2-OH	3-OH	6-OH	11	796 $\pm$ 122
<b>16a</b>	H	H	H	3-OMe	4-F	ni	nd
<b>16</b>	H	H	H	3-OH	4-F	57	63 $\pm$ 3

<sup>a</sup> Recombinantly expressed purified 17 $\beta$ -HSD14 enzyme, fluorimetric assay, substrate E2 [32  $\mu$ M], NAD<sup>+</sup> [1.2 mM], 25 $^{\circ}$ C, mean value of at least two independent experiments each with three technical repeats; ni: no inhibition (<10% inhibition at 100  $\mu$ M), nd: not determined.

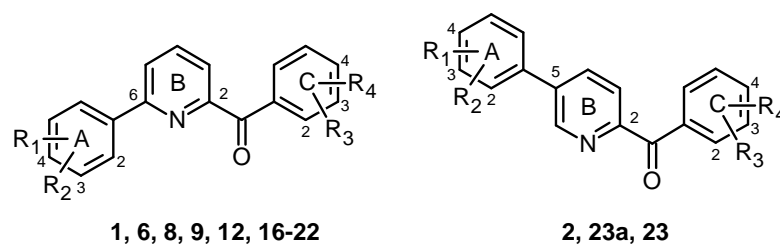
### Substituent variations on the A-ring

2,6-Pyridine derivatives containing the C-ring motif (3-OH/4-F or 2-OH/3-OH) were synthesized with different substituents at varying positions of the A-ring (Table 3).

Compounds with one substituent in the 3- or 4-position (**17**: 3-NMe<sub>2</sub>, K<sub>i</sub>= 7 nM; **18**: 3-OH, K<sub>i</sub>= 7 nM; **19**: 3-OH, K<sub>i</sub>= 44 nM and **21**: 4-F, K<sub>i</sub>= 221 nM) showed that their substitution with a polar moiety at 3-position (**17**, **18**, **19**) led to stronger binding compared to the one with a lipophilic group at 4-position (**21**). This effect is confirmed in case the A-ring is disubstituted (**22**) with the 3-Cl and 4-F substituents, which led to a compound with a similar binding constant as the mono 4-F derivative **21** (K<sub>i</sub>= 190 nM and 221 nM for **22** and **21**, respectively). These lipophilic groups exerted a detrimental effect on the binding affinity, which was lower compared to the unsubstituted phenyl (**16**, K<sub>i</sub>= 63 nM). The compounds with two substituents in 2/3- or in 3/4-positions of the A-ring (**1**: 3-OH/4-OH, K<sub>i</sub>= 7 nM; **6**: 3-Me/4-OH, K<sub>i</sub>= 26 nM; **8**: 3-F/4-OH, K<sub>i</sub>= 36 nM; **9**: 2-F/3-OH, K<sub>i</sub>= 13 nM) had similar binding constants with the exception of **20** (3-OH/4-Me, K<sub>i</sub>= 47 nM) with a slightly decreased affinity. No significant difference in activity could be observed between mono- and disubstituted compounds at the A-ring as long as a 3-OH or a 4-OH moiety was present. In summary, the best affinities were achieved in the presence of a 3-OH or a 3-NMe<sub>2</sub> moiety at the A-ring.

In the 2,5-pyridine class, the affinity of **23** (K<sub>i</sub>= 17 nM) with a 3-F/4-OH substitution pattern at the A-ring was similar to that of compound **2** (K<sub>i</sub>= 24 nM) with a 3-Me/4-OH substitution pattern at the A-ring and fell into the same range of compounds in the 2,6-class. Furthermore the methoxy derivative **23a** was less active compared to the hydroxylated analogue **23** as similarly observed for compound **16a**.

**Table 3:** 17 $\beta$ -HSD14 inhibitory activity and binding constant ( $K_i$ ) of pyridine derivatives with different substituents at the A-ring



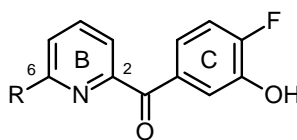
Compound	Position A-ring	R <sub>1</sub>	R <sub>2</sub>	R <sub>3</sub>	R <sub>4</sub>	17 $\beta$ -HSD14	
						% inhibition	$K_i$ (nM) <sup>a</sup>
						@ 2 $\mu$ M <sup>a</sup>	
<b>1</b>	6	3-OH	4-OH	3-OH	4-F	69	7 $\pm$ 1
<b>2</b>	5	3-Me	4-OH	3-OH	4-F	60	24 $\pm$ 9
<b>6</b>	6	3-Me	4-OH	3-OH	4-F	60	26 $\pm$ 3
<b>8</b>	6	3-F	4-OH	3-OH	4-F	67	36 $\pm$ 5
<b>9</b>	6	2-F	3-OH	3-OH	4-F	72	13 $\pm$ 5
<b>12</b>	6	2-F	3-OH	2-OH	3-OH	65	64 $\pm$ 4
<b>16</b>	6	H	H	3-OH	4-F	57	63 $\pm$ 3
<b>17</b>	6	3-NMe <sub>2</sub>	H	3-OH	4-F	57	7 $\pm$ 1
<b>18</b>	6	3-OH	H	3-OH	4-F	65	7 $\pm$ 2
<b>19</b>	6	H	3-OH	2-OH	3-OH	51	44 $\pm$ 3
<b>20</b>	6	3-OH	4-Me	3-OH	4-F	64	47 $\pm$ 7
<b>21</b>	6	H	4-F	3-OH	4-F	37	221 $\pm$ 46
<b>22</b>	6	3-Cl	4-F	3-OH	4-F	44	190 $\pm$ 45
<b>23a</b>	5	3-F	4-OMe	3-OMe	4-F	12	57% $\pm$ 6 <sup>b</sup>
<b>23</b>	5	3-F	4-OH	3-OH	4-F	61	17 $\pm$ 5

<sup>a</sup> Recombinantly expressed purified 17 $\beta$ -HSD14 enzyme, fluorimetric assay, substrate E2 [32  $\mu$ M], NAD<sup>+</sup> [1.2 mM], 25 $^{\circ}$ C mean value of at least two independent experiments each with three technical repeats; <sup>b</sup>% inhibition @ 22,2  $\mu$ M

### Variation of the A-ring

In order to investigate the role of the phenyl A-ring, pyridine derivatives lacking the A-ring (**24**) or derivatives decorated with different heterocycles in 6-position of the B-ring (**25-28**) were designed (Table 4). Comparison of compound **24** ( $K_i = 1541$  nM) with **16** ( $K_i = 63$  nM) showed a decrease in activity. The nonaromatic piperidine **26** ( $K_i = 407$  nM) was also a weaker binder, while the 4-methylpiperazine **27** ( $K_i = 190$  nM) showed a similar inhibitory activity, both compared to **16**.

**Table 4:** 17 $\beta$ -HSD14 inhibitory activity and binding constant ( $K_i$ ) of 2,6-pyridine derivatives with different substituents in 6-position of the pyridine ring (different A-rings)



**16, 24-28**

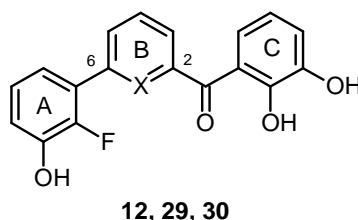
Compound	R	17 $\beta$ -HSD14	
		% inhibition @ 2 $\mu$ M <sup>a</sup>	$K_i$ (nM) <sup>a</sup>
<b>16</b>	phenyl	57	63 $\pm$ 3
<b>24</b>	H	13	1541 $\pm$ 146
<b>25</b>	thiophen-3-yl	50	97 $\pm$ 28
<b>26</b>	piperidin-1-yl	43	407 $\pm$ 16
<b>27</b>	4-methylpiperazin-1-yl	31	190 $\pm$ 21
<b>28</b>	- <i>O</i> -phenyl	55	50 $\pm$ 0

<sup>a</sup> Recombinantly expressed purified 17 $\beta$ -HSD14 enzyme, fluorimetric assay, substrate E2 [32  $\mu$ M], NAD<sup>+</sup> [1.2 mM], 25°C mean value of at least two independent experiments each with three technical repeats

### Variations on the B-ring

In the design section it was reported that in the 2,5-pyridine class the central ring played a crucial role in affinity. This aspect was also investigated in the 2,6-class by the synthesis of the phenyl analogue **29** and the corresponding *N*-oxide **30** (Table 5). Comparison of the biological data of these compounds with the pyridine analogue **12** ( $K_i = 64$  nM) showed that both, the phenyl derivative **29** ( $K_i = 21$  nM) and the *N*-oxide derivative **30** ( $K_i = 132$  nM) had a similar affinity as the pyridine **12**.

**Table 5:** 17 $\beta$ -HSD14 inhibitory activity and binding constant ( $K_i$ ) for compounds with different B-rings



17 $\beta$ -HSD14			
Compound	X	% inhibition @ 2 $\mu$ M <sup>a</sup>	$K_i$ (nM) <sup>a</sup>
<b>12</b>	N	77	64 $\pm$ 4
<b>29</b>	C	60	21 $\pm$ 2
<b>30</b>	N <sup>+</sup> -O <sup>-</sup>	47	132 $\pm$ 13

<sup>a</sup> Recombinantly expressed purified 17 $\beta$ -HSD14 enzyme, fluorimetric assay, substrate E2 [32  $\mu$ M], NAD<sup>+</sup> [1.2 mM], mean value of at least two independent experiments each with three technical repeats

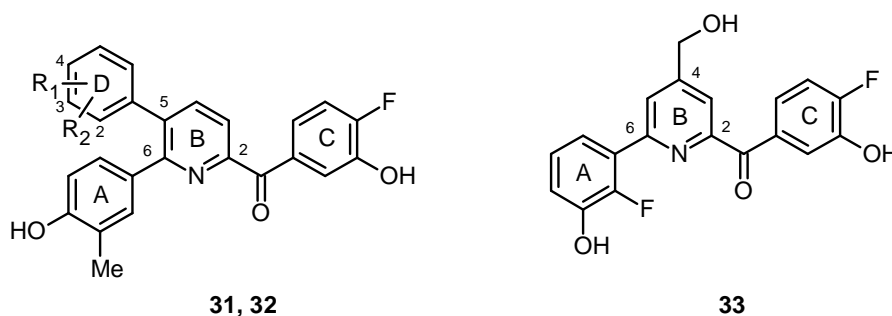
### Trisubstituted pyridines

Based on the hypothesis that the C-ring and the carbonyl group of both the 2,5- and 2,6-pyridines achieve the same interaction as a consequence of binding in the same area, the similarity in affinity of the 2,5-derivative **23** ( $K_i = 17$  nM) and the 2,6-derivative **8** ( $K_i = 36$  nM, Table 3) suggested that the

available space for binding the additional ring must be large, even tolerating an A-ring attached to the 5- or 6-position. Trisubstituted pyridines combining substitutions at the 5- and 6-positions were therefore synthesized (**31** and **32**, Table 6). These trisubstituted compounds turned out to be equipotent (**31**,  $K_i = 9$  nM; **32**,  $K_i = 15$  nM) with a similar affinity compared to the disubstituted derivatives **6** and **23**.

Introducing a hydroxymethyl group at the 4-position of the B-ring led to a slight decrease in activity (**33**  $K_i = 86$  nM compared to **9**  $K_i = 13$  nM, Table 6).

**Table 6:** 17 $\beta$ -HSD14 inhibitory activity and binding constant ( $K_i$ ) of pyridine derivatives with an additional D-ring or a substituent in 4-position



17 $\beta$ -HSD14				
Compound	R <sub>1</sub>	R <sub>2</sub>	% inhibition @ 2 $\mu$ M <sup>a</sup>	$K_i$ (nM) <sup>a</sup>
<b>6</b>			60	26 $\pm$ 3
<b>23</b>			61	17 $\pm$ 5
<b>31</b>	3-Me	4-OH	71	9 $\pm$ 4
<b>32</b>	2-F	3-OH	63	15 $\pm$ 4
<b>33</b>	-	-	47	86 $\pm$ 7

<sup>a</sup> Recombinantly expressed purified 17 $\beta$ -HSD14 enzyme, fluorimetric assay, substrate E2 [32  $\mu$ M], NAD<sup>+</sup> [1.2 mM], mean value of at least two independent experiments each with three technical repeats

### Pan Assay Interference Compounds<sup>37</sup>

All the biologically evaluated compounds were tested *in silico* for nonspecific binding in order to identify false positives using the Pains-remover computer tool.<sup>38</sup> From the compounds analyzed, seven did not pass the filter, including **10**, **12**, **14**, **19**, **20**, **29**, **30** suggested as nonspecific binders. They all share as common characteristic a catechol moiety. It is known that catechols can be toxic,<sup>39</sup> however, the inhibitory data of these compounds are presented as they are useful to establish a better structure-activity relationship comprehension. In case these compounds turn out to be highly interesting, further assays should be performed to characterize their toxicity.

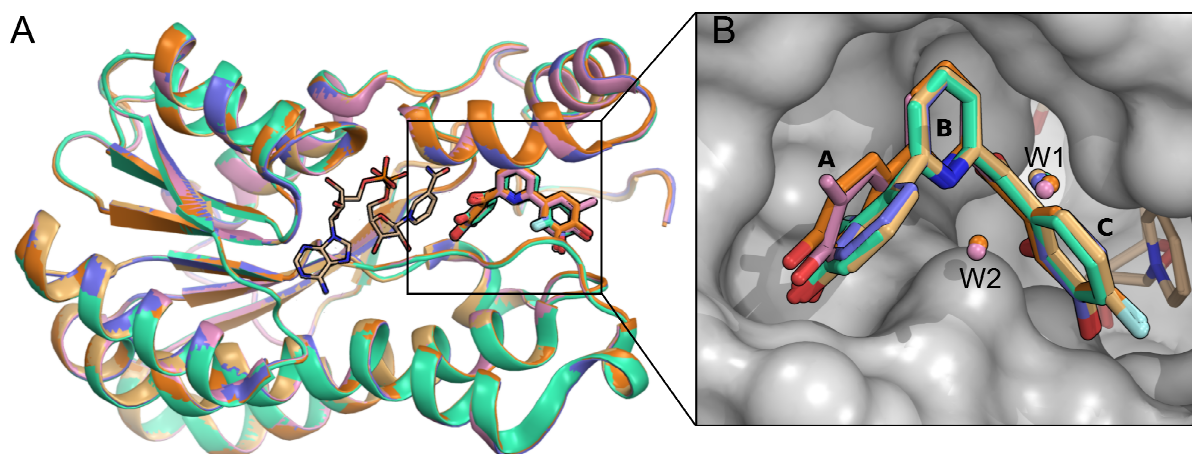
### Crystal structures determination

The inhibitors with the highest binding affinity were selected for crystal structure determination in order to get insight into their binding mode. Crystal structures could be obtained for four different inhibitors by co-crystallization of the protein in complex with cofactor and ligands (**6**, PDB ID: 5L7T; **9**, PDB ID: 5L7Y; **10**, PDB ID: 5L7W; **12**, PDB ID: 5EN4). The data collection, processing, and refinement statistics details are reported in the Supporting Information. The crystals were obtained by two different conditions, however, all crystal structures show the same tetragonal space group (I422) with only one monomer present in the asymmetric unit. The crystal structures disclosed, that the protein is a homotetramer, in accordance with a previous study.<sup>5</sup> The structures obtained have a resolution ranging from 1.52 Å to 2.02 Å. The conformation of the protein in complex with inhibitor **1** (PDB ID: 5ICM) has already been published<sup>5</sup> and will not be the focus here. It will however be included in the structural comparison.

### Description of the inhibitor binding site

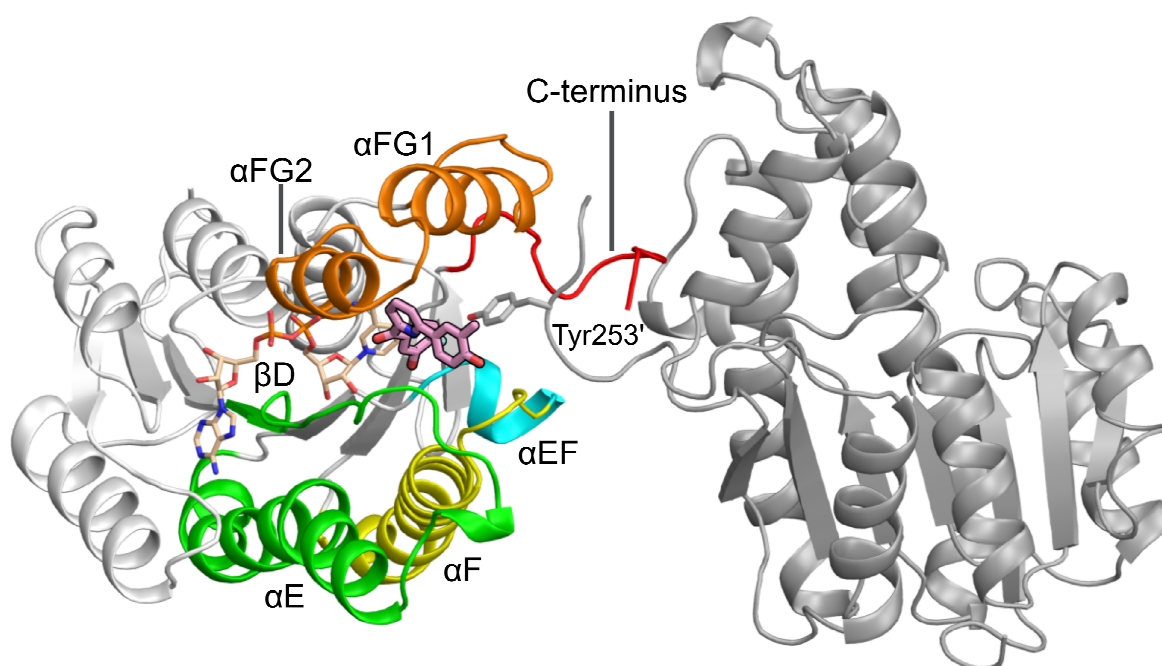
The superimposition of all five ternary complexes reveals that binding of the different ligands does not induce conformational changes of the overall geometry of the protein (Figure 2), showing a mean RMSD of  $0.15 \pm 0.04$  Å between the alignment of the Ca atoms of the structures, as calculated with

1  
2  
3 COOT.<sup>40</sup> The cofactor interacts with the Rossman fold region and experiences similar interactions as  
4  
5 already observed for the 17 $\beta$ -HSD14 holo structure and in complex with inhibitor **1**.<sup>5</sup> The inhibitor  
6  
7 binds into the substrate binding site, which is restricted by two  $\alpha$ -helices from the flexible loop ( $\alpha$ FG1  
8  
9 and  $\alpha$ FG2, residues 189-212, in orange), a portion of the  $\alpha$ F helix (containing the catalytic Tyr154,  
10  
11 Lys158, in yellow), the short  $\alpha$ EF helix (residue 142-146, in cyan), the segment that connects  $\alpha$ E with  
12  
13  $\beta$ D (from Asn89 to Arg98, in green), and the C-terminal tail (in red, Figure 3). Furthermore, Tyr253'  
14  
15 from the adjacent monomer (in gray on the right hand side, Figure 3) is pointing toward the inhibitor  
16  
17 binding site, reducing the volume of the active site cleft. The annotation of the different helices and  $\beta$ -  
18  
19 sheets follows the nomenclature described by Lukacik *et al.*<sup>2</sup> The flexible loop is in a conformation  
20  
21 that closes the binding pocket, reducing the size of the substrate binding site. Furthermore, the  
22  
23 inhibitor binding site is predominantly hydrophobic, with two main hydrophilic regions: The first one  
24  
25 corresponds to the two residues of the catalytic triad Tyr154 and Ser141, and the second one is formed  
26  
27 by His93 and Gln148 (Figure 4). This second region shapes the binding site in a peculiar form and  
28  
29 could be relevant for the achievement of selectivity considering that no other human SDR 17 $\beta$ -HSDs  
30  
31 presents a histidine at this position.  
32  
33  
34  
35



54 **Figure 2.** Superimposition of the crystal structures of 17 $\beta$ -HSD14 obtained in ternary complexes with  
55  
56 five inhibitors: **1**, **6**, **9**, **10**, **12**. (A) The enzyme 17 $\beta$ -HSD14 is shown as ribbon model (5ICM in  
57  
58 orange, 5L7T in pink, 5L7Y in purple blue, 5L7W in ocher and 5EN4 in green); inhibitors are shown  
59  
60 as stick models. The cofactor NAD<sup>+</sup> is shown as thin line. (B) Close-up view on the binding pocket.  
The protein 17 $\beta$ -HSD14 is displayed by use of the solvent accessible surface. The carbon atoms of the

1  
2  
3 inhibitors are shown for **1** in orange **6** in pink, **9** in purple blue, **10** in ocher and **12** in green. Inhibitors  
4  
5 are shown as stick models and cofactor as thin line. The water molecules W1 and W2 are represented  
6  
7 in the same color as the corresponding inhibitor of the individual structures. W1 corresponds to water  
8  
9 molecule 472 in 5ICM, 518 in 5L7T, 508 in 5L7Y, 496 in 5L7W, 450 in 5EN4; W2 corresponds to  
10  
11 water molecule 530 in 5ICM and 502 in 5L7T, in the respective crystal structure. All structural  
12  
13 representations were prepared with PyMOL.<sup>41</sup>  
14  
15  
16  
17  
18  
19  
20  
21  
22  
23  
24  
25  
26  
27  
28  
29  
30  
31  
32  
33  
34  
35  
36  
37  
38  
39  
40



41 **Figure 3.** Ribbon representation of inhibitor **6** in complex with the protein 17 $\beta$ -HSD14 and cofactor  
42 NAD<sup>+</sup>. The inhibitor binding site is delimited by  $\alpha$ FG1 and  $\alpha$ FG2 (orange),  $\alpha$ F (the helix containing  
43 the catalytic Tyr154 and Lys158, yellow),  $\alpha$ EF (cyan),  $\alpha$ E and  $\beta$ D (green) and C-terminal tail (red).  
44 Inhibitor **6** is shown as stick model and its carbon atoms are colored in pink. The symmetry equivalent  
45 molecule containing Tyr253' is shown in gray on the right hand side. The cofactor and Tyr253' are  
46 shown as thin lines.  
47  
48  
49  
50  
51  
52  
53  
54  
55  
56  
57  
58  
59  
60

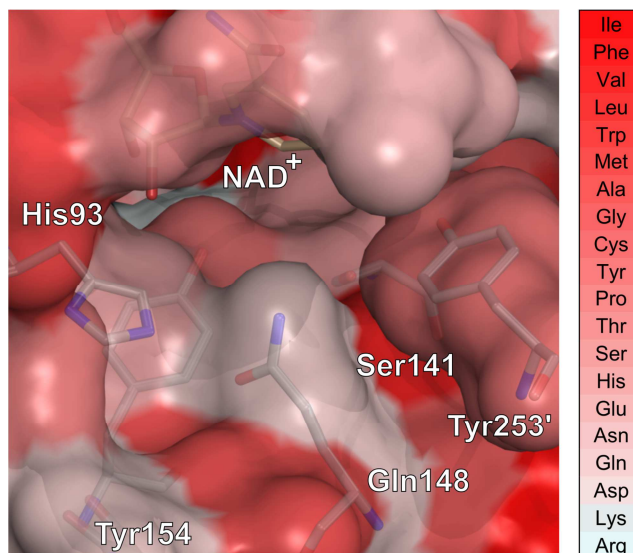


**Figure 4.** Surface representation of 17 $\beta$ -HSD14; color coded according to the Eisenberg hydrophobicity scale (from dark red for highly hydrophobic amino acids to white for highly hydrophilic amino acids).<sup>42</sup> The cofactor NAD<sup>+</sup> and amino acids are shown as stick models. The amino acid of the symmetry equivalent molecule is referred as prime (').

#### Description of the binding mode of inhibitors in complex with 17 $\beta$ -HSD14.

In the surface representation, it is obvious that the V-shape of the inhibitor scaffold matches well with the geometry of the active site (Figure 2B). For all five crystallized inhibitors, additional water molecules are observed in the binding pockets: Water W1 is found for all inhibitors in the same position. W1 is localized between the B- and C-ring, at an approximate 4 Å distance from the B-ring. W1 establishes an H-bond interaction with the side-chain of Asn186 ( $d \approx 2.7$  Å). Water W2 is only observed for **1** and **6** (Figure 2B) and found above the plane of the A-ring. W2 interacts with W1 (H-bond contact  $d \approx 2.6$  Å). In case of the other three inhibitors, the orientation of the A-ring plane is shifted, inducing the displacement of W2.

Due to close similarity, only the interactions of **6** and **12**, as representatives of the series, will be described in detail. The structures and details of the interactions of all inhibitors are shown in Figure 5 (A: **6**, B: **12**; C: **9**; D: **10**). Inhibitors **6** and **12** have the same B-ring scaffold (2,6-pyridine) differing in

1  
2  
3 the nature of their A- and C-ring substituents. At the C-ring, the keto group and the pyridine ring of **6**  
4 and **12** bind exactly at the same position. The angle between the keto group and the phenyl C-ring is  
5 identical in **6** and **12** independent of the presence or absence of the 2-OH group at the C-ring.  
6  
7

8  
9  
10 The 3-OH groups at the C-ring of **6** and **12** interact via remarkably short H-bond interactions with the  
11 side chain of Tyr154 (**6**,  $d= 2.4 \text{ \AA}$ , **12**,  $d= 2.5 \text{ \AA}$ ) and the side chain of Ser141 (**6**,  $d= 2.5 \text{ \AA}$ , **12**,  $d= 2.5$   
12  $\text{\AA}$ ) from the catalytic triad. The 4-F group at the C-ring of **6** is not involved in any specific interaction.  
13  
14

15  
16  
17 The phenyl C-ring of **6** and **12** is stabilized by van der Waals contacts with the nicotinamide moiety of  
18 NAD<sup>+</sup>. The carbonyl group is not involved in any direct interaction. The central pyridine B-ring is  
19 anchored by van der Waals contacts with Trp192 and Leu195, which wrap around the top part of the  
20 pyridine ring. No close contacts are observed with His93.  
21  
22  
23  
24  
25

26  
27 For **6**, an H-bond interaction is formed between the 4-OH at the A-ring with the carbonyl backbone of  
28 Ala149 ( $d= 2.7 \text{ \AA}$ ). The 3-Me group at the A-ring is not involved in any interaction. The aromatic A-  
29 ring is not stabilized by any  $\pi$ -stacking interactions, however, van der Waals interactions with Pro96  
30 are observed. No water mediated H-bond interactions are observed; nonetheless, it is remarkable that  
31 W1 remains present in this lipophilic environment. In total, 91 van der Waals contacts are achieved by  
32 the ligand and its surface is buried to 94.0 % (considering only one monomer of the protein, the  
33 number of van der Waals contacts achieved are summed up to 86 and the buried surface is 87.4 %).  
34  
35  
36  
37  
38  
39  
40  
41

42  
43 In **12**, a rotation of the A-ring plane is observed. Nevertheless, the altered orientation still allows the 3-  
44 OH group at the A-ring to be at H-bond distance to Ala149-CO ( $d= 2.8 \text{ \AA}$ , as observed with **6**). The  
45 aromatic A-ring can also establish a van der Waals interaction with the amino acid Pro96. In summary,  
46 82 van der Waals contacts are observed for **12** with 93.0 % of its surface buried in the protein binding  
47 pocket (considering only one protein monomer, the ligand achieves 80 van der Waals contacts and its  
48 surface is buried to 88.2 %).  
49  
50  
51  
52  
53  
54  
55  
56  
57  
58  
59  
60

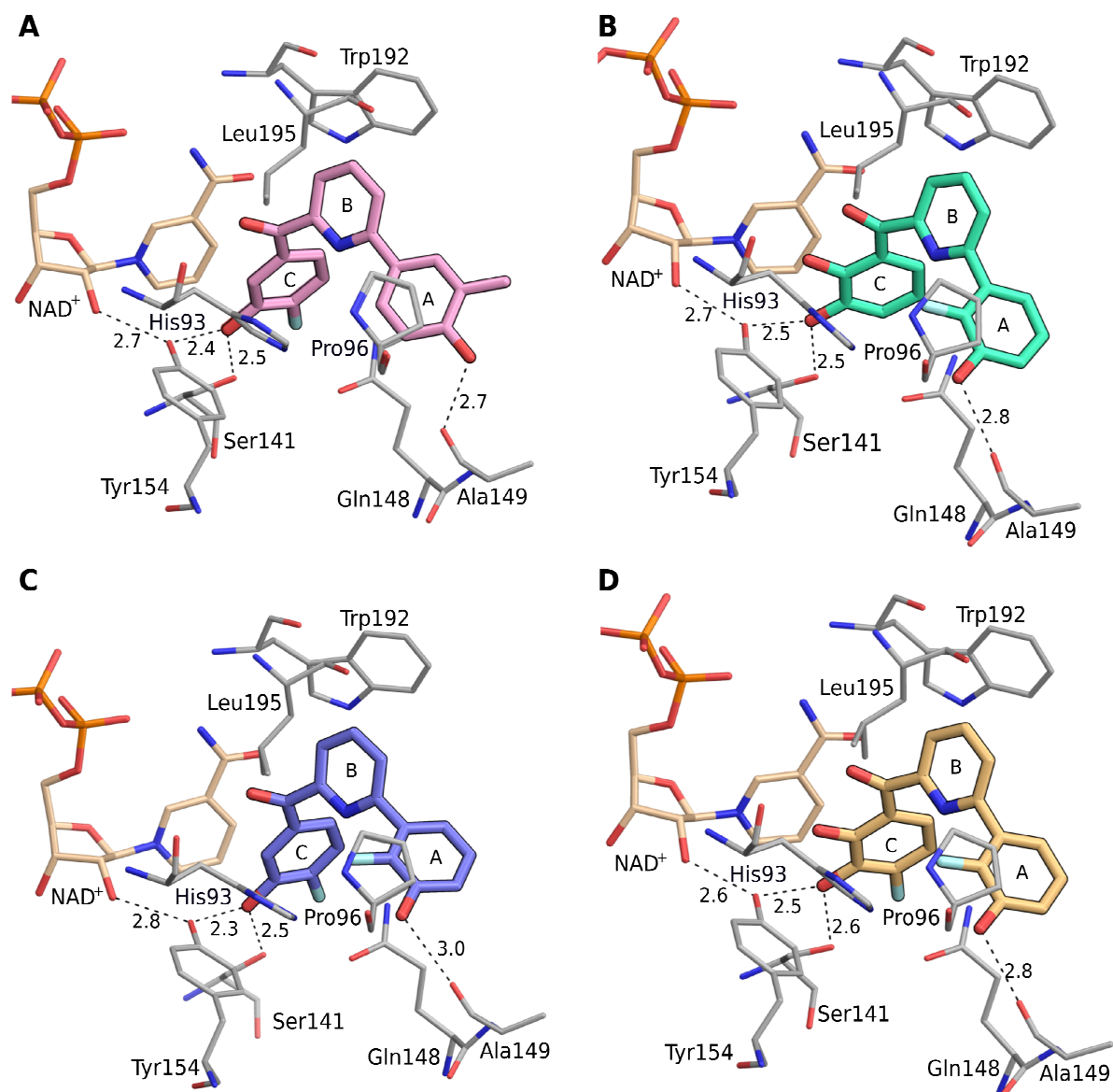
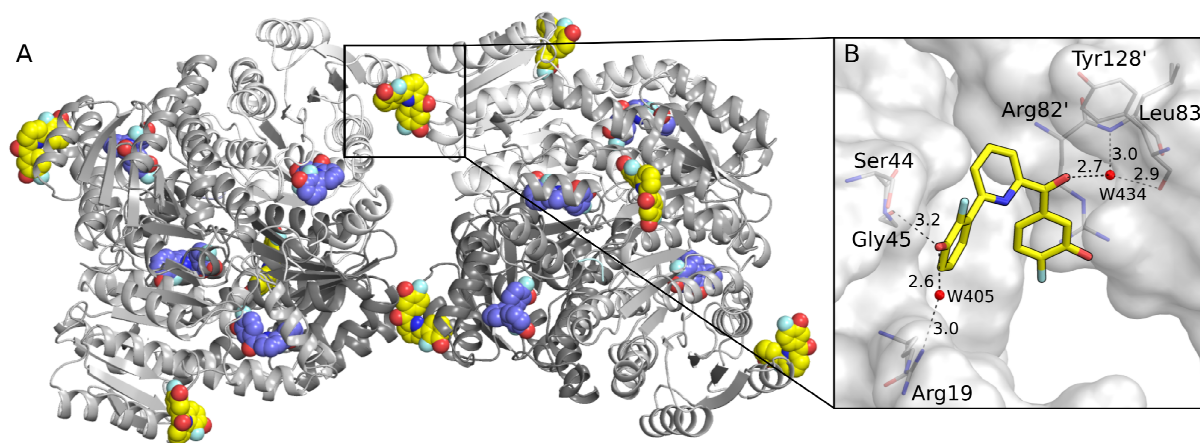


**Figure 5.** Crystal structures of 17β-HSD14 in complex with cofactor NAD<sup>+</sup>, and inhibitors **6** (in pink, A), **12** (in green, B), **9** (in purple blue, C) and **10** (in ocher, D). The inhibitors are shown as stick models. The amino acids, within a distance of 5 Å, and the cofactor are shown as thin lines. H-bonds are depicted as dotted lines. Distances are given in Å.

Interestingly, the crystal structure of **9** in ternary complex with 17β-HSD14 shows the presence of a second inhibitor molecule at the interface between two tetramers (Figure 6A). Close inspection of this interface binding site (Figure 6B) highlights that the inhibitor is stabilized through an H-bond interaction between the 3-OH group at the A-ring to the hydroxyl group of Ser44 side chain ( $d = 3.2$  Å) and with a water molecule W405 ( $d = 2.6$  Å), which is stabilized by Arg19 ( $d = 3.0$  Å). The keto group

1  
2  
3 interacts with the other tetramer through a water molecule W434 ( $d= 2.7 \text{ \AA}$ ), which is also bound to  
4  
5 the NH from the backbone of Leu83' ( $d= 3.0 \text{ \AA}$ ) and the carbonyl group of the backbone of Tyr128'  
6  
7 ( $d= 2.9 \text{ \AA}$ ). The copy of **9** binding to the interface is placed in a rather hydrophilic environment. The  
8  
9 overall geometry of the interface ligand differs from that of the active site ligand: The dihedral angles,  
10  
11 for the ligand in the active site and for the ligand binding at the interface, between the keto group and  
12  
13 C-ring are  $-29^\circ$  and  $4^\circ$  respectively, and between the keto group and the B-ring are  $129^\circ$  and  $-133^\circ$   
14  
15 respectively (considering the plane through the keto group as  $0^\circ$ ). The dihedral angle between  $C_2$  at the  
16  
17 A-ring and the nitrogen at the B-ring is  $131^\circ$  for the ligand in the binding pocket and  $-60^\circ$  for the  
18  
19 ligand present at the interface. A superimposition of the interface and active site compounds can be  
20  
21 seen on Figure 7.  
22  
23  
24  
25



26  
27  
28  
29  
30  
31  
32  
33  
34  
35  
36  
37  
38  
39  
40  
41 **Figure 6.** (A). Overall view of the crystal structure of two 17 $\beta$ -HSD14 tetramers in complex with **9**.  
42  
43 The protein monomers are shown as ribbon models and colored in gray. The inhibitors are shown as  
44  
45 sphere models. The inhibitors located in the substrate binding site are colored in purple blue while the  
46  
47 inhibitors located between the interfaces of the tetramers are shown in yellow. (B). Close-up view of  
48  
49 the second ligand binding site of **9** located at the interface between two tetramers. The enzyme is  
50  
51 displayed by use of the solvent accessible surface. Inhibitor **9** is shown as stick model. The amino  
52  
53 acids are shown as thin lines. The amino acids of the symmetry equivalent molecule are referred to  
54  
55 prime ('). H-bonds are depicted as black dotted lines. Distances are given in  $\text{\AA}$ .  
56  
57  
58  
59  
60

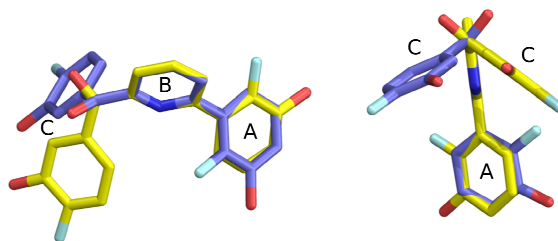


**Figure 7.** Superimposition of compound **9** based on the pyridine B-rings of the ligand at the interface (in yellow) and active site (in purple blue).

### Comparison of the 17 $\beta$ -HSD1, 17 $\beta$ -HSD2 and 17 $\beta$ -HSD14 structures

The existing crystal structure of 17 $\beta$ -HSD1 in ternary complex with the cofactor NADP<sup>+</sup> and E2 (PDB ID: 1FDT) allows the direct comparison with the 17 $\beta$ -HSD14 structure in complex with the cofactor NAD<sup>+</sup> and estrone (E1, PDB ID: 5HS6). The superimposition reveals a structural conservation of the enzymes only in some regions (22% of sequence identity calculated with COOT,<sup>40</sup> Figure 8). Small differences in the NAD<sup>+</sup>/NADP<sup>+</sup> binding site can be observed between type 14 and type 1 (RMSD of 1.6 Å calculated with COOT<sup>40</sup> based on C $\alpha$  alignment). This result was expected since both enzymes bind a different cofactor (NAD<sup>+</sup> for 17 $\beta$ -HSD14 vs NADP<sup>+</sup> for 17 $\beta$ -HSD1). The flexible loop in 17 $\beta$ -HSD1 restricts the end of the binding cavity, while the corresponding loop in 17 $\beta$ -HSD14 is shifted upwards leaving the binding site widely open. This results in a smaller binding pocket for the type 1 enzyme. Furthermore, while the catalytic triad is conserved in both enzymes, the steroids accommodate in the binding sites with different orientations and achieve distinct interactions.

As no crystal structure is available for 17 $\beta$ -HSD2, the comparison between the structures of type 2 and type 14 is not possible.

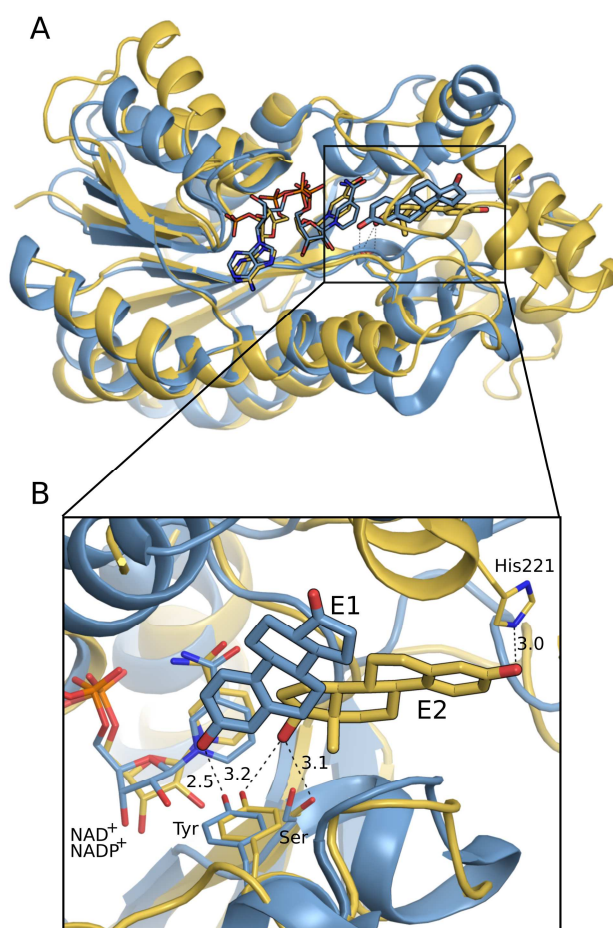


**Figure 8.** (A) Superimposition of 17 $\beta$ -HSD1 (yellow, PDB ID: 1FDT) and 17 $\beta$ -HSD14 (light blue, PDB ID: 5HS6) structures as ternary complexes. (B) Close-up view of the superimposed substrate binding pocket. The proteins are shown as ribbon model. The steroids are shown as stick models. The amino acids, involved in binding of the steroids (Tyr154 for 17 $\beta$ -HSD14; Tyr155, Ser142 and His 221 for 17 $\beta$ -HSD1), and the cofactors are shown as thin lines. The carbon atoms of E1 in complex with 17 $\beta$ -HSD14 are colored in light blue and the carbon atoms of (E2) in complex with 17 $\beta$ -HSD1 are colored in yellow. H-bonds are depicted as black dotted lines. Distances are given in Å.

### Selectivity

Taking into account that the parent scaffold of the new 17 $\beta$ -HSD14 inhibitors was derived from 17 $\beta$ -HSD1 and 17 $\beta$ -HSD2 inhibitors, it was of utmost importance to study their selectivity profile with respect to 17 $\beta$ -HSD1 and 17 $\beta$ -HSD2 binding.

The 17 $\beta$ -HSD1 and 17 $\beta$ -HSD2 inhibition assay was performed using a radioactive assay, quantifying the amount of [<sup>3</sup>H]-labeled E2 (for type 1) and [<sup>3</sup>H]-labeled E1 (for type 2) formed after incubation

1  
2  
3 with protein, cofactor and the inhibitor as previously described.<sup>43</sup> The results are shown in Table 7,  
4  
5 expressed as percent inhibition when tested at an inhibitor concentration of 1  $\mu$ M.  
6

7  
8 As expected the 2,5-pyridine **23** showed the highest affinity for 17 $\beta$ -HSD1 (47% inhibition) compared  
9  
10 to the 2,6-pyridines (**6-20**, 9-23% inhibition), which were all nearly inactive in 17 $\beta$ -HSD1.

11  
12 Inhibition of 17 $\beta$ -HSD2 was slightly higher than that of 17 $\beta$ -HSD1 for the compounds with a 2,6-  
13  
14 substitution pattern (between 30% and 62% inhibition at 1 $\mu$ M concentration for **6-20**) and much  
15  
16 higher for the 2,5-pyridine ketones (64% and 85% when tested at 1  $\mu$ M concentration for **23** and **2**,  
17  
18 respectively).  
19

20  
21 A direct comparison of the 17 $\beta$ -HSD1 and 17 $\beta$ -HSD2 inhibitory activities with those of 17 $\beta$ -HSD14 is  
22  
23 however problematic as different conditions were used in the assays.  
24

25  
26 However, under the applied condition in the 17 $\beta$ -HSD2 inhibition assay, using the Cheng-Prusoff  
27  
28 equation for competitive inhibition, a calculated  $K_i$  ( $cK_i$ ) could be estimated: For a compound with an  
29  
30  $IC_{50}$  of around 1  $\mu$ M (50% inhibition at 1  $\mu$ M) a  $cK_i$  of about 450 nM was expected (with  $K_m$  17 $\beta$ -  
31  
32 HSD2 = 400 nM in this assay<sup>44</sup> and [S]= 500 nM).  
33

34  
35 With 48% and 43% inhibition of 17 $\beta$ -HSD2, compounds **9** and **10** showed a  $cK_i \geq 450$  nM.  
36  
37 Comparison of their  $K_i$  values for 17 $\beta$ -HSD2 and 17 $\beta$ -HSD14 binding allowed to calculate a  
38  
39 selectivity factor (ratio of  $K_i(\text{HSD2})/K_i(\text{HSD14})$ ), which could be estimated to be around 35 for **9** and  
40  
41  $\geq 41$  for **10**. Compounds **9** and **10** are relatively selective 17 $\beta$ -HSD14 inhibitors. The selectivity profile  
42  
43 of **12** toward 17 $\beta$ -HSD2 (with only 30% inhibition at 1  $\mu$ M) should be even better.  
44  
45  
46  
47  
48  
49  
50  
51  
52  
53  
54  
55  
56  
57  
58  
59  
60

**Table 7:** 17 $\beta$ -HSD14 binding constant ( $K_i$ ) and 17 $\beta$ -HSD1/ 17 $\beta$ -HSD2 inhibitory activities (% inhibition) of the most interesting compounds.

Compound	17 $\beta$ -HSD14 $K_i$ (nM) <sup>a</sup>	17 $\beta$ -HSD1 % inhibition @ 1 $\mu$ M <sup>b</sup>	17 $\beta$ -HSD2 % inhibition @ 1 $\mu$ M <sup>c</sup>
<b>2</b>	24 $\pm$ 9	47%	85%
<b>5</b>	245 $\pm$ 21	6%	85%
<b>6</b>	26 $\pm$ 3	9%	62%
<b>9</b>	13 $\pm$ 5	23%	43%
<b>10</b>	11 $\pm$ 3	12%	48%
<b>12</b>	64 $\pm$ 4	13%	30%
<b>18</b>	7 $\pm$ 2	13%	34%
<b>20</b>	47 $\pm$ 7	14%	37%
<b>23</b>	17 $\pm$ 5	47%	64%

<sup>a</sup> Recombinant purified 17 $\beta$ -HSD14 enzyme, fluorimetric assay, substrate E2 [32  $\mu$ M], NAD<sup>+</sup> [1.2 mM], 25°C, mean value of at least two independent experiments each with three technical repeats.

<sup>b</sup> Placental 17 $\beta$ -HSD1 enzyme, cytosolic fraction, substrate [<sup>3</sup>H]-E1 + E1 [500 nM], NADH [0.5 mM], mean value of 2 determinations; standard deviation < 20 %.

<sup>c</sup> Placental 17 $\beta$ -HSD2 enzyme, microsomal fraction, substrate [<sup>3</sup>H]-E2 + E2 [500 nM], NAD<sup>+</sup> [1.5 mM], mean value of 2 determinations; standard deviation < 20 %

As steroidomimetics, the synthesized compounds might show undesired binding affinity to the estrogen receptors (ERs)  $\alpha$  and  $\beta$ . Wetzal *et al.* reported that the most interesting compounds **2-5**, identified in the first screen, showed very low affinities to both ER subtypes (< 0.1 %, taking E2 as

1  
2  
3 100% reference).<sup>45</sup> It is therefore assumed, that the synthesized compounds, which bear the same  
4  
5 scaffold, do not bind tightly to the ERs.  
6  
7  
8  
9

## 10 **DISCUSSION**

11  
12  
13 The combination of the biological results, the crystal structures of the five ligands in ternary complex  
14  
15 with the protein and the physicochemical properties provide the basis for the understanding of the  
16  
17 structure-activity relationship study of the 2,5- and 2,6-substituted pyridine derivatives.  
18  
19

### 20 **Focus on the C-ring part**

21  
22  
23 The 3-OH group at the C-ring achieves important H-bond interactions with Tyr154 and Ser141, which  
24  
25 stabilize the inhibitor in the enzyme binding site. The increase in acidity of this OH moiety, enhanced  
26  
27 by the addition of a fluorine atom in *ortho* position to the OH group, correlates with a gain in binding  
28  
29 affinity. The crystal structures indicate that the H-bond length between the 3-OH group at the C-ring  
30  
31 and Tyr154 is rather short ( $d = 2.3 - 2.5 \text{ \AA}$ ). This result supports the hypothesis of Hwang *et al.*<sup>46</sup> which  
32  
33 describes that in SDR enzymes, the pKa of the OH group from the catalytic tyrosine is decreased  
34  
35 (through electrostatic interaction with the protonated catalytic Lys-NH<sub>3</sub><sup>+</sup> and NAD<sup>+</sup>) and that this Tyr-  
36  
37 OH is present as deprotonated species in the active site. In our structures, the negatively charged (or at  
38  
39 least highly polarized) Tyr154-O<sup>-</sup> can interact via H-bond interactions with 3-OH groups at the C-ring  
40  
41 of the inhibitors, leading to a strong contact between the inhibitor and the protein. This interaction  
42  
43 becomes even more stable in presence of an increasingly acidic OH group at 3-position, once it is  
44  
45 more strongly polarized O( $\delta^-$ )-H( $\delta^+$ ).  
46  
47  
48  
49

50  
51 In addition, it can be seen in the crystal structures that the inhibitors are involved in a more complex  
52  
53 H-bonding network via the interaction with Tyr154, also including the ribose-OH groups of the  
54  
55 cofactor, Lys158, Asn88, Asn89 and two to three water molecules (Figure 9). The highlighted H-  
56  
57 bonding network reinforces the strength of the interaction between Tyr154 and the OH group at the C-  
58  
59 ring of the inhibitor,<sup>47</sup> thereby strongly stabilizing the ligand in the binding pocket.  
60

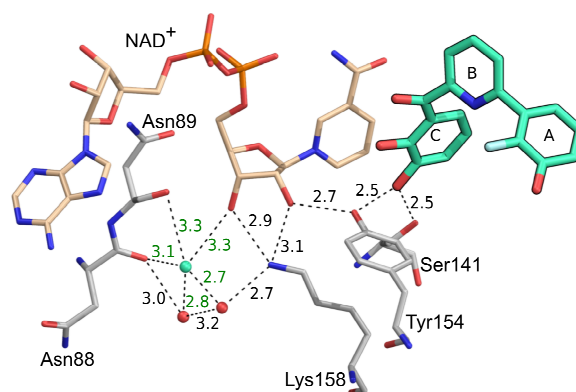


**Figure 9.** H-bonding network stabilizing the inhibitor **12** in the 17 $\beta$ -HSD14 binding site. The carbon atoms of **12** are colored in green and shown as stick model. The amino acids, involved in the H-bonding network, and the cofactor NAD<sup>+</sup> (beige) are shown as thin lines. H-bond interactions are depicted as dotted lines. Distances are given in Å. Water molecules are shown as spheres. The water molecules present in all protein-inhibitor complex structures are colored in red, an additional water molecule is visible in the case of the complexes with **1** and **12** (higher resolution crystal structures) and is colored in green.

The H-bond donor/acceptor profile involved in the interaction between the 3-OH group at the C-ring and Tyr154/Ser141 can be interpreted in more details: a deprotonated Tyr154 implies that the 3-OH group at the C-ring of the inhibitor interacts with Tyr154-O<sup>-</sup> as H-bond donor and with the hydroxyl group of Ser141 as H-bond acceptor. For the inhibitors also bearing a 2-OH group at the C-ring moiety, an intramolecular H-bond with their keto groups can be formed and no interaction with Tyr154 is expected (the OH group of Tyr 154 is already involved in a contact with the ribose-OH and the 3-OH group at the C-ring inhibitor, and is not available for an additional interaction). In addition, it can be remarked that the rigidification induced by the intramolecular H-bond does not correlate with an increase in binding affinity (comparison of compounds **9** and **10**).

Replacing the 3-OH group at the C-ring by a 3-OMe moiety was shown to be detrimental for inhibitory activity (**16a**: no inhibition @100  $\mu$ M compared to **16**: K<sub>i</sub>= 63 nM). When compound **16a** was modeled into the crystal structure of 17 $\beta$ -HSD14 (Figure S1A, Supporting Information), it resulted in a shift of the binding pose (compared to the compounds observed in the crystal structures,

1  
2  
3 see Figure 5), which could allow an H-bond interaction between the oxygen of the 3-OMe group and  
4  
5 the OH group of Tyr154 of the catalytic triad, however, the H-bond contact is only possible when the  
6  
7 3-OMe group acts as an acceptor (Figure S1A, Supporting Information). The inactivity of this  
8  
9 compound confirms the hypothesis that an H-bond donor in 3-position of the C-ring is necessary for  
10  
11 the inhibitory activity of the compound. In addition, no interaction with Ser141 could be observed in  
12  
13 the presence of the 3-OMe group in the model structure.  
14  
15

### 16 17 **Focus on the A-ring part**

18  
19  
20 Based on the biological results, it is evident that the removal of the A-ring leads to a strong decrease in  
21  
22 activity (**16**,  $K_i = 63$  nM compared to **24**  $K_i = 1541$  nM), indicating an important interaction of the  
23  
24 A-ring with the protein. The crystal structures show that no amino acid is able to achieve a  $\pi$ -stacking  
25  
26 interaction in the vicinity of the aromatic A-ring. This result suggests that the aromatic A-ring must be  
27  
28 stabilized by hydrophobic interactions with Pro96.  
29  
30

31  
32 Furthermore, it can be observed that the introduction of a 3-OH or 4-OH group on the A-ring induces  
33  
34 a slight increase in affinity compared to the unsubstituted A-ring. Either these hydroxyl moieties  
35  
36 interact with the carbonyl backbone of Ala149 via a weak H-bond interaction or the benefit of a strong  
37  
38 interaction with Ala149 is decreased by the desolvation cost. It is also striking that neither an electron  
39  
40 donating nor an electron withdrawing group has an influence on the potency.  
41  
42

43  
44 The significant affinity enhancement of the dimethylamino derivative **17** was investigated using the  
45  
46 modeled structure (Figure S1B, Supporting Information). Here, the  $\text{NMe}_2$  moiety comes into close  
47  
48 contact with the carbonyl group of Ala149. A strong interaction would only be possible between the  
49  
50  $\text{NMe}_2$  group and the carbonyl oxygen when the tertiary amine is protonated. However, taking into  
51  
52 account the pKa value of the  $\text{NMe}_2$  group it is unlikely that this group is charged. The gain in affinity  
53  
54 might come from additional hydrophobic interactions between the latter group and Pro96.  
55  
56

57  
58 In the complex structure with **6** the 3-Me group at the A-ring interacts neither with the protein nor with  
59  
60 the solvent. Instead, it is pointing toward an empty cavity, while the 3-OH group of **12** is oriented in  
the opposite direction interacting with Ala149. The swapped orientation of the 3-Me group at the A-

1  
2  
3 ring of **6** might result from electrostatic repulsions between the methyl group and the carbonyl moiety  
4  
5 of Ala149.  
6

7  
8 Regarding the equipotent 2,5- **23** ( $K_i = 17$  nM) and the 2,6-substituted derivative **8** ( $K_i = 36$  nM), it was  
9  
10 previously suggested, that the C-rings of both compounds achieve the same interaction and that the  
11  
12 space available for accommodating the A-ring at either 5- or 6-position must be large to host a ring at  
13  
14 both positions. From the modeled structure of **23** (Figure S1C, Supporting Information), it can be  
15  
16 assumed that the A-ring in 5-position fits well into the binding pocket, interacting through  
17  
18 hydrophobic contacts with Met199. Furthermore, the modeled 2,5,6-trisubstituted derivative **31** ( $K_i = 9$   
19  
20 nM) also suggests that compounds bearing rings at 5- and 6-position can fit in the cavity and may  
21  
22 achieve an intramolecular  $\pi$ -stacking interaction ( $d = 4$  Å, Figure S1D, Supporting Information).  
23  
24  
25

### 26 **Focus on the B-ring part**

27  
28 Investigating the importance of the nitrogen at the B-ring indicates that inhibitor **12** ( $K_i = 64$  nM) and  
29  
30 its phenyl analogue **29** ( $K_i = 21$  nM) show similar affinities. Obviously, the nitrogen does not achieve  
31  
32 any specific interaction with the protein, as confirmed by the crystal structure. However, the pyridine  
33  
34 moiety enhances the solubility for the compounds of this inhibitor class. Concerning the *N*-oxide  
35  
36 derivative **30** ( $K_i = 132$  nM), the previously observed interaction between the 3-OH group at the A-ring  
37  
38 of compound **12** with Ala149 can no longer be accomplished, however, this OH-group can now  
39  
40 address the backbone carbonyl group of Gln150, as observed in the modeled structure (Figure S1E,  
41  
42 Supporting Information). An additional H-bond interaction of  $N^+ - O^-$  with Gln148 could be gained, but  
43  
44 the high desolvation penalty induced by the introduction of the charges might not be compensated,  
45  
46 overall resulting in no increase in affinity.  
47  
48  
49

### 50 **Second binding site for compound 9**

51  
52 For compound **9**, a second binding pose at the tetramer interface was observed. The inhibitor was  
53  
54 refined to an occupancy of 80% at this additional binding site, suggesting that this ligand exhibits a  
55  
56 lower affinity for this region compared to the active site. The binding of the inhibitor in this position  
57  
58 might be irrelevant for the inhibitory process. The presence of compound **9** in this place might be an  
59  
60

1  
2  
3 artefact resulting from crystal packing as the binding at the interface does not induce any  
4  
5 conformational change of the ternary structure and of the ligand binding site. However, it is striking  
6  
7 that Michiels *et al.*<sup>48</sup> reported in their NMR studies that phytoestrogens might also bind at the dimer  
8  
9 interface of 17 $\beta$ -HSD1.  
10

### 11 12 13 **Comparison of the 17 $\beta$ -HSD1, 17 $\beta$ -HSD2 and 17 $\beta$ -HSD14 structures**

14  
15 A positive influence of a fluorine atom in ortho position to a phenolic hydroxyl group was already  
16  
17 reported during the development of 17 $\beta$ -HSD1 dihydroxyphenylthiophenes inhibitors<sup>49</sup> and 17 $\beta$ -HSD2  
18  
19 hydroxyphenyl-*N*-methylsulfonamide thiophenes inhibitors.<sup>50</sup> As no crystal structures of 17 $\beta$ -HSD1  
20  
21 and 17 $\beta$ -HSD2 in complex with these nonsteroidal compounds are available, their binding modes  
22  
23 remain unclear. As 17 $\beta$ -HSD type 1, type 2 and type 14 belong to the SDR superfamily, they share  
24  
25 similarities in the region in the vicinity of the catalytic triad. The presence of the complex H-bonding  
26  
27 network was also identified in the type 1 enzyme after analysis of its crystal structure (PDB ID:  
28  
29 1FDT). It could be expected that the 17 $\beta$ -HSD1 and 17 $\beta$ -HSD2 inhibitors with an acidic OH-phenyl  
30  
31 group have a similar binding mode, interacting with the catalytic triad as observed in the crystal  
32  
33 structure of type 14. Therefore, these new 17 $\beta$ -HSD14 structures in complex with nonsteroidal  
34  
35 inhibitors can represent a useful comparative data for 17 $\beta$ -HSD1 docking studies and 17 $\beta$ -HSD2  
36  
37 homology modelling.  
38  
39  
40

### 41 42 43 **Basis for structure-based drug design**

44  
45 Based on these results, it should be possible to optimize the current ligands using structure-based drug  
46  
47 design. In this compound class the interactions with the catalytic Tyr154 and Ser141, as well as with  
48  
49 Ala149 are very important to anchor the ligand scaffold in the correct position. Specific interactions  
50  
51 involving His93 and Gln148 in inhibitor binding should result in an improved activity and selectivity,  
52  
53 particularly as His93 is not present in other human SDR 17 $\beta$ -HSDs. Addressing the water molecule  
54  
55 W1 should also lead to an additional interaction with the protein. As the active site is open and solvent  
56  
57 exposed, the polar amino acids which are in close neighborhood to the active site next to the surface  
58  
59 could also be targeted by specific interactions.  
60

## CONCLUSION

Nonsteroidal 17 $\beta$ -HSD14 inhibitors have been identified. The initial hits identified in a preliminary screen in the 2,6-substituted pyridine class showed a  $K_i$  around 250 nM/300 nM which was optimized to result in six highly active compounds with  $K_i < 15$  nM and two with a  $K_i$  of 7 nM. The considerations of substituent effects applied during optimization were successful. It appears that at the C-ring, an acidic 3-OH group is essential to achieve high potency, interacting via strong H-bond contacts to Tyr154 and Ser141 thereby stabilizing the interaction through an extensive H-bonding network. The structure-activity relationship found for the A-ring shows, that a 3-OH or a 4-OH group increases the potency of the inhibition by interacting with Ala149. The crystal structures in complex with the inhibitors confirm the rather large active site, reduced by the C-terminal chain from an adjacent monomer. The new 17 $\beta$ -HSD14 inhibitors show good physicochemical properties, which should be associated with a good bioavailability profile. They also present a good selectivity profile toward both closely related subtypes 17 $\beta$ -HSD1 and 17 $\beta$ -HSD2. The determined crystal structures give important insights not only to characterize the novel protein target but also to understand the binding poses of these nonsteroidal inhibitors and provide the basis for their further structure-based optimization.

## EXPERIMENTAL SECTION

### 1. Chemistry

#### 1.1. Chemical methods

Chemical names follow IUPAC nomenclature.

Starting materials were purchased from Acros Organics, Alfa Aesar, Combi-Blocks, Roth and Sigma Aldrich and were used without further purification. Anhydrous THF was freshly distilled from sodium benzophenone ketyl.

Microwave irradiation experiments were carried out in a CEM-Discover apparatus.

1  
2  
3 Column chromatography was performed on silica gel (0.04-0.063 mm, Macherey-Nagel) and reaction  
4 progress was monitored by TLC on aluminium sheets (Silicagel 60 F254, Merck). Visualization was  
5 accomplished with UV light at 254 nm and 366 nm, respectively.  
6  
7

8  
9 Preparative HPLC was performed with a Varian PrepStar 218 gradient system using a ProStar 320  
10 detector. A ProntoSIL C18 column (5.0  $\mu\text{m}$ , 120  $\text{\AA}$ , 250-32 mm) was used as stationary phase with an  
11 acetonitrile/water gradient containing 0.1% TFA at a flow rate of 20 ml/min. All solvents were HPLC  
12 grade. Detection was performed at a wavelength of 254 nm.  
13  
14  
15  
16

17  
18 Mass spectrometry was performed on a Q-Trap 2000 (Applied Biosystems) equipped with an  
19 electrospray interface (ESI).  
20  
21

22  
23  $^1\text{H}$  and  $^{13}\text{C}$  NMR spectra were measured on a JEOL ECX-400 spectrometer (at 400 MHz and  
24 100 MHz, respectively). Chemical shifts are reported in  $\delta$  (parts per million: ppm), using residual  
25 peaks for the deuterated solvents as internal standard:<sup>51</sup> 2.05 ppm ( $^1\text{H}$  NMR), 29.8 ppm and 206.3 ppm  
26 ( $^{13}\text{C}$  NMR), acetone- $d_6$ ; 7.26 ppm ( $^1\text{H}$  NMR), 77.2 ppm ( $^{13}\text{C}$  NMR),  $\text{CDCl}_3$ ; 2.50 ppm ( $^1\text{H}$  NMR), 39.5  
27 ppm ( $^{13}\text{C}$  NMR), DMSO- $d_6$ . Signals are described as s, bs, d, t, q, dd, ddd, dt and m for singlet, broad  
28 signal, doublet, triplet, doublet of doublets, doublet of doublet of doublets, doublet of triplets and  
29 multiplet, respectively. All coupling constants ( $J$ ) are given in Hertz (Hz).  
30  
31  
32  
33  
34  
35  
36  
37

38 Infrared spectroscopy was performed on a Bruker ALPHA FT-IR spectrometer as neat sample.

39  
40 All tested compounds have  $\geq 95\%$  chemical purity as evaluated by HPLC. The Shimadzu<sup>®</sup>-system  
41 consisted of a LC-20AT pump, an SIL-20A autosampler and a SPD-M20A PDA detector. The system  
42 was operated by the standard software LCsolution<sup>®</sup>. A RP C18 NUCLEODUR<sup>®</sup> (125 mm x 4 mm,  
43 5  $\mu\text{m}$ ) column (Macherey-Nagel) was used as stationary phase. All solvents were HPLC grade. In a  
44 gradient run the percentage of acetonitrile was increased from initial concentration of 30% at 0 min to  
45 90% at 15 min and kept at 90% for 5 min. The injection volume was 20  $\mu\text{l}$  at a flow rate of  
46 1.00 ml/min. UV spectra were recorded at a wavelength of 254 nm.  
47  
48  
49  
50  
51  
52

53  
54 Marvin sketch was used for the calculation of the pKa data (Marvin 15.9.14, 2015, Chemaxon  
55 (<http://www.chemaxon.com>)).  
56  
57  
58  
59

60 The following compounds were prepared according to previously described procedures: (**1a**),<sup>5</sup> (**1**),<sup>5</sup>  
(**10g**),<sup>29</sup> (**10f**),<sup>30</sup> (**15d**),<sup>52</sup> (**31f**),<sup>53</sup> (**33f**)<sup>26</sup> (using commercial  $\text{POBr}_3$ , max. temp: 150  $^\circ\text{C}$ ), (**33e**)<sup>26</sup>.

## 1.2. General chemical procedures

### 1.2.1. General procedures for alcohol formation

#### 1.2.1.1. Method A1

A solution of *n*-BuLi (1.0 eq, 2.5 M in hexane) was diluted with anhydrous THF (0.8 M) and arylbromide (1.0 eq) in anhydrous THF was slowly added at -80 °C under argon. The resulting solution was stirred for 15 min at -80 °C, then the appropriate aldehyde (1.0 eq) was added and the reaction solution was stirred for additional 15 min at -80 °C followed by room temperature for 2 h. The mixture was quenched with saturated NH<sub>4</sub>Cl and extracted with ethyl acetate. The combined organic layer was washed with brine, dried over magnesium sulfate, filtered and evaporated to dryness under reduced pressure. The product was purified by column chromatography.

#### 1.2.1.2. Method A2

A mixture of arylbromide (1.0 eq), magnesium turnings (1.1 eq) and a catalytic amount of iodine in anhydrous THF was stirred for 2 h at 60 °C under argon. A solution of the appropriate aldehyde in anhydrous THF was added and the reaction mixture was stirred at 80 °C. The end of the reaction was monitored by TLC. The mixture was quenched with brine and extracted with ethyl acetate. The combined organic layer was dried over magnesium sulfate, filtered and evaporated to dryness under reduced pressure. The product was purified by column chromatography.

### 1.2.2. General procedure for alcohol oxidation - Method B

2-Iodoxybenzoic acid (1.2 eq) was added to a solution of alcohol derivative (1.0 eq) in THF and the reaction mixture was stirred at 60 °C. After the end of the reaction (monitored by TLC) the mixture was cooled to room temperature, quenched with saturated Na<sub>2</sub>S<sub>2</sub>O<sub>3</sub> and extracted with ethyl acetate. The combined organic layer was washed with water and saturated sodium bicarbonate, dried over magnesium sulfate, filtered and evaporated to dryness under reduced pressure. The product was purified by column chromatography.

### 1.2.3. General procedures for Suzuki coupling

### 1.2.3.1. Method C1

A mixture of arylbromide (1.0 eq), boronic acid (1.2 eq), cesium carbonate (4.0 eq) and tetrakis(triphenylphosphine)palladium (0.02 eq) was solved in DME/water (2:1) and degassed with argon. The mixture was stirred overnight at 80 °C. The reaction mixture was cooled down to room temperature, quenched with water and extracted with ethyl acetate. The combined organic layer was washed with brine, dried over magnesium sulfate, filtered and evaporated to dryness under reduced pressure. The product was purified by column chromatography.

### 1.2.3.2 Method C2

A mixture of arylbromide (1.0 eq), boronic acid (1.2 eq), sodium carbonate (2.0 eq) and tetrakis(triphenylphosphine)palladium (0.02 eq) was solved in DME/water (2:1) and degassed with argon. The mixture was exposed to microwave irradiation (60 min, 150 W, 150 °C) and quenched with water after reaching room temperature. The mixture was extracted with ethyl acetate and the combined organic layer was washed with brine, dried over magnesium sulfate, filtered and evaporated to dryness under reduced pressure. The product was purified by column chromatography.

### 1.2.4 General procedure for amination of bromopyridine - Method D

A mixture of bromopyridine (1.0 eq), appropriate *N*-heterocycle (1.1 eq) and potassium phosphate (4.0 eq) in 1,4-dioxane was stirred at 100 °C. At the end of the reaction (monitored by TLC) the mixture was cooled to room temperature, quenched with 1 M sodium hydroxide and extracted with ethyl acetate. The combined organic layer was dried over magnesium sulfate, filtered and evaporated to dryness under reduced pressure. The product was purified by column chromatography.

### 1.2.5. General procedure for ether cleavage - Method E

A solution of methoxy derivative (1.0 eq) in dry dichloromethane was cooled to -80 °C and boron tribromide (1 M in dichloromethane, 5 eq per methoxy function) was slowly added under argon. The reaction mixture was stirred at -80 °C for 1 h and then allowed to warm to room temperature overnight. The mixture was cooled in an ice bath, quenched with water and extracted with ethyl

1  
2  
3 acetate. The combined organic layer was washed with brine, dried over magnesium sulfate, filtered  
4  
5 and evaporated to dryness under reduced pressure. The product was purified by column  
6  
7 chromatography.  
8  
9

### 10 11 12 **1.3. Detailed synthesis procedures and compound characterization**

#### 13 14 **(4-Fluoro-3-hydroxyphenyl)[6-(4-hydroxy-3-methylphenyl)pyridin-2-yl]methanone**

15  
16 **hydrochloride salt (6).** According to method E the title compound was prepared by reaction of (4-  
17  
18 fluoro-3-methoxyphenyl)[6-(4-methoxy-3-methylphenyl)pyridin-2-yl]methanone (**6a**) (110 mg,  
19  
20 0.31 mmol, 1.0 eq) with boron tribromide (3.1 ml, 3.1 mmol, 10 eq) in dichloromethane (6.0 ml). The  
21  
22 crude product was purified by column chromatography (cyclohexane/ethyl acetate 3:1) and the  
23  
24 hydrochloride salt was prepared by means of 2 M hydrogen chloride solution in ether to give 85 mg  
25  
26 (0.24 mmol/ 75%) of the analytically pure compound. C<sub>19</sub>H<sub>14</sub>FNO<sub>3</sub>·HCl; MW: 360; mp: 194-195 °C;  
27  
28 <sup>1</sup>H NMR (DMSO-*d*<sub>6</sub>, 400 MHz): δ 10.29 (bs, 1H), 9.71 (bs, 1H), 8.12-7.96 (m, 2H), 7.85-7.81 (m, 1H),  
29  
30 7.79-7.73 (m, 1H), 7.71 (dd, *J* = 8.8 Hz, 2.2 Hz, 1H), 7.56 (ddd, *J* = 8.4 Hz, 4.5 Hz, 2.1 Hz, 1H),  
31  
32 7.33 (dd, *J* = 11.0 Hz, 8.5 Hz, 1H), 6.89 (d, *J* = 8.4 Hz, 1H), 2.18 (s, 3H); <sup>13</sup>C NMR (DMSO-*d*<sub>6</sub>,  
33  
34 100 MHz): δ 191.9, 157.1, 155.4, 154.2 (d, *J* = 248.2 Hz), 154.1, 144.8 (d, *J* = 12.5 Hz), 138.3, 132.7  
35  
36 (d, *J* = 3.1 Hz), 129.3, 128.5, 125.6, 124.2, 123.2 (d, *J* = 7.8 Hz), 121.7, 121.3, 120.0 (d, *J* = 4.4 Hz),  
37  
38 116.0 (d, *J* = 19.1 Hz), 114.9, 16.2; IR: 3390, 1661, 1611, 1597, 1583, 1526, 1510, 1427, 1235, 1119,  
39  
40 756 cm<sup>-1</sup>; MS (ESI): 324 (M+H)<sup>+</sup>.7 Hz), 115.8 (d, *J* = 6.8 Hz), 56.4; MS (ESI): 310, 312 (M+H)<sup>+</sup>;  
41  
42  
43  
44 HPLC analysis: retention time = 12.29 min; peak area, 97.6%.  
45  
46  
47  
48

#### 49 50 **(4-Fluoro-3-hydroxyphenyl)[6-(3-fluoro-4-hydroxyphenyl)pyridin-2-yl]methanone**

51  
52 **hydrochloride salt (8).** According to method E the title compound was prepared by reaction of (4-  
53  
54 fluoro-3-methoxyphenyl)[6-(3-fluoro-methoxyphenyl)pyridin-2-yl]methanone (**8a**) (148 mg,  
55  
56 0.42 mmol, 1.0 eq) with boron tribromide (4.2 ml, 4.2 mmol, 10 eq) in dichloromethane (8.0 ml). The  
57  
58 crude product was purified by column chromatography (cyclohexane/ethyl acetate 2:1) and the  
59  
60 hydrochloride salt was prepared by means of 2 M hydrogen chloride solution in ether to give 92 mg  
(0.25 mmol/ 61 %) of the analytically pure compound. C<sub>18</sub>H<sub>11</sub>F<sub>2</sub>NO<sub>3</sub>·HCl; MW: 364; mp: 206-207 °C;

<sup>1</sup>H NMR (acetone-*d*<sub>6</sub>, 400 MHz): δ 8.16 (dd, *J* = 8.1 Hz, 1.2 Hz, 1H), 8.11 (dd, *J* = 8.0 Hz, 7.5 Hz, 1H), 7.93 (dd, *J* = 8.5 Hz, 1.7 Hz, 1H), 7.90 (dd, *J* = 3.2 Hz, 1.7 Hz, 1H), 7.88-7.82 (m, 2H), 7.72 (ddd, *J* = 8.5 Hz, 4.5 Hz, 2.1 Hz, 1H), 7.31 (dd, *J* = 10.8 Hz, 8.5 Hz, 1H), 7.13 (t, *J* = 8.7 Hz, 1H); <sup>13</sup>C NMR (acetone-*d*<sub>6</sub>, 100 MHz): δ 192.3, 155.6, 155.4 (d, *J* = 249.3 Hz), 155.2 (d, *J* = 2.35 Hz), 152.6 (d, *J* = 240.0 Hz), 147.2 (d, *J* = 12.9 Hz), 145.5 (d, *J* = 13.3 Hz), 139.3, 134.2 (d, *J* = 3.3 Hz), 131.6 (d, *J* = 5.9 Hz), 124.8 (d, *J* = 7.47 Hz), 124.11 (d, *J* = 3.2 Hz), 123.0, 122.6, 121.3 (d, *J* = 4.2 Hz), 118.9 (d, *J* = 3.0 Hz), 116.6 (d, *J* = 19.2 Hz), 115.3 (d, *J* = 20.0 Hz); IR: 3380, 1660, 1598, 1582, 1524, 1430, 1235, 754 cm<sup>-1</sup>; MS (ESI): 328 (M+H)<sup>+</sup>; HPLC analysis: retention time = 11.63 min; peak area, 98.8%.

**(4-Fluoro-3-hydroxyphenyl)[6-(2-fluoro-3-hydroxyphenyl)pyridin-2-yl]methanone**

**hydrochloride salt (9).** According to method E the title compound was prepared by reaction of (4-fluoro-3-methoxyphenyl)[6-(2-fluoro-3-methoxyphenyl)pyridin-2-yl]methanone (**9a**) (126 mg, 0.35 mmol, 1.0 eq) with boron tribromide (3.5 ml, 3.5 mmol, 10 eq) dichloromethane (6.0 ml). The crude product was purified by column chromatography (cyclohexane/ethyl acetate 2:1) and the hydrochloride salt was prepared by means of 2 M hydrogen chloride solution in ether to give 117 mg (0.32 mmol/ 92%) of the analytically pure compound. C<sub>18</sub>H<sub>11</sub>F<sub>2</sub>NO<sub>3</sub>·HCl; MW: 364; mp: 198-199 °C; <sup>1</sup>H NMR (DMSO-*d*<sub>6</sub>, 400 MHz): δ 8.15 (t, *J* = 7.8 Hz, 1H), 8.00 (ddd, *J* = 7.9 Hz, 2.1 Hz, 0.9 Hz, 1H), 7.92 (dd, *J* = 7.7 Hz, 1.0 Hz, 1H), 7.70-7.64 (m, 1H), 7.55 (ddd, *J* = 8.5 Hz, 4.5 Hz, 2.2 Hz, 1H), 7.31 (dd, *J* = 11.0 Hz, 8.5 Hz, 1H), 7.29-7.22 (m, 1H), 7.12-7.04 (m, 2H); <sup>13</sup>C NMR (DMSO-*d*<sub>6</sub>, 100 MHz): δ 191.7, 154.6, 154.3 (d, *J* = 125.5 Hz), 151.9, 149.2 (d, *J* = 146.2 Hz), 145.6 (d, *J* = 12.6 Hz), 144.9 (d, *J* = 12.4 Hz), 138.4, 132.5, 127.3 (d, *J* = 9.1 Hz), 126.7 (d, *J* = 8.1 Hz), 124.4 (d, *J* = 4.1 Hz), 123.3 (d, *J* = 7.5 Hz), 122.9, 120.2, 119.8 (d, *J* = 4.5 Hz), 118.5 (d, *J* = 3.2 Hz), 116.0 (d, *J* = 19.3 Hz); IR: 3155, 1655, 1593, 1481, 1293, 1225, 750 cm<sup>-1</sup>; MS (ESI): 328 (M+H)<sup>+</sup>; HPLC analysis: retention time = 10.82 min; peak area, 98.4%.

**[6-(3-(*N,N*-Dimethylamino)-phenyl)pyridin-2-yl](4-fluoro-3-hydroxyphenyl)methanone**

**trifluoroacetate salt (17).** According to method E the title compound was prepared by reaction of [6-

(3-(*N,N*-dimethylamino)-phenyl)pyridin-2-yl](4-fluoro-3-methoxyphenyl)methanone (**17a**) (105 mg, 0.30 mmol, 1.0 eq) with boron tribromide (1.5 ml, 1.5 mmol, 5 eq) in dichloromethane (4.0 ml). The crude product was purified by column chromatography (cyclohexane/ethyl acetate 5:1) and preparative HPLC (gradient water/acetonitrile/trifluoroacetic acid 80:20:0.1→35:65:0.1, in 120 min) to give 75 mg (0.22 mmol/ 74%) of the analytically pure compound. C<sub>20</sub>H<sub>17</sub>FN<sub>2</sub>O<sub>2</sub>·TFA; MW: 450; mp: 146-147 °C; <sup>1</sup>H NMR (acetone-*d*<sub>6</sub>, 400 MHz)\*: δ 9.06 (s, 1H), 8.17 (dd, *J* = 8.0 Hz, 1.0 Hz, 1H), 8.09 (t, *J* = 7.8 Hz, 1H), 8.00-7.92 (m, 2H), 7.82 (ddd, *J* = 8.5 Hz, 4.6 Hz, 2.1 Hz, 1H), 7.61 (dd, *J* = 2.5 Hz, 1.7 Hz, 1H), 7.40 (ddd, *J* = 7.7 Hz, 1.5 Hz, 0.9 Hz, 1H), 7.35-7.26 (m, 2H), 6.85 (ddd, *J* = 8.2 Hz, 2.7 Hz, 0.8 Hz, 1H), 2.99 (s, 6H); <sup>13</sup>C NMR (acetone-*d*<sub>6</sub>, 100 MHz)\*: δ 192.1, 157.1, 155.3, 155.3 (d, *J* = 249.3 Hz), 152.1, 145.4, (d, *J* = 13.0 Hz), 139.6, 139.1, 134.3 (d, *J* = 3.4 Hz), 130.2, 124.9 (d, *J* = 7.6 Hz), 123.5, 123.3, 121.6 (d, *J* = 4.3 Hz), 116.5 (d, *J* = 19.2 Hz), 115.7, 114.5, 111.7, 40.6; IR: 3400, 1657, 1594, 1529, 1504, 1580, 1434, 764 cm<sup>-1</sup>; MS (ESI): 337 (M+H)<sup>+</sup>; HPLC analysis: retention time = 14.62 min; peak area, 98.9%. \*measured as base.

## 2. Biological methods

### 2.1. 17β-HSD14 inhibition assay.

In a preliminary study compounds **1-5** were tested using a radioactive displacement assay (Procedure A, % of inhibition at a concentration of 1 μM). The newly synthesized compounds were tested using a fluorimetric assay (Procedure B, as percent inhibition at 2 μM, percent inhibition at the concentration of highest solubility of the compound and K<sub>i</sub>). Procedure A and B use the same enzyme source, obtained from a bacterial culture. In procedure A, the assay is performed with a bacterial suspension, and in procedure B with the purified form of the enzyme. Due to differences in assay conditions only results within the same assay can be compared.

#### 2.1.1. Enzyme expression.

The pET based plasmid containing the coding sequences of the human gene HSD17B14 (using the T205 variant), with a *N*-terminal 6His-tag and a TEV (Tobacco Etch Virus) protease cleavage site was

1  
2  
3 used for the transfection of *E. coli* BL21 (DE3) pLysS competent cells. The transformed bacteria cells  
4  
5 were grown overnight in 100 mL of Terrific Broth medium containing 100 µg/mL of ampicillin at  
6  
7 37°C. Subsequently, 25 mL of the overnight culture were transferred in 1 L of the aforementioned  
8  
9 medium and allowed to grow at 37 °C until an OD<sub>600</sub> of 0.4 was reached. Then the temperature was  
10  
11 lowered to 15° C. When the culture reached the OD<sub>600</sub> of 1.0 the cells were induced with 0.5 mM of  
12  
13 IPTG. The bacteria cells were harvested by centrifugation and conserved at -80° C overnight before  
14  
15 proceeding with the purification.  
16  
17  
18  
19  
20

### 21 **2.1.2. Radioactive assay using Procedure A.**

22  
23  
24 The bacterial pellet obtained was resuspended in 100 mM phosphate buffer pH 7.7. The bacterial  
25  
26 suspension was incubated with [<sup>3</sup>H]-E2 (final concentration: 18.3 nM) in the presence of the potential  
27  
28 inhibitor in DMSO (final concentration in assay: 1µM, final DMSO concentration: 1%) at 37°C. The  
29  
30 enzymatic reaction was started by addition of NAD<sup>+</sup> (7.5 mM) and incubated for 2 h. The reaction was  
31  
32 stopped by addition of 0.21 M ascorbic acid in a methanol/acetic acid mixture (99:1, v/v). Substrate  
33  
34 and product were extracted from the reaction mixture by SPE (Strata C18-E columns from  
35  
36 Phenomenex on a vacuum device). Separation and quantification of the radioactive steroids was  
37  
38 performed with HPLC (Luna 5µm C18(2), 125 x 4.00 mm from Phenomenex, with an  
39  
40 acetonitrile/water mixture (43:57, v.v), flow rate 1mL/min). Substrate conversion in % was calculated  
41  
42 after integration of the product and substrate peaks. Inhibition was calculated based on conversion  
43  
44 without potential inhibitor (DMSO only) which was set to 0% inhibition.  
45  
46  
47  
48  
49  
50  
51

### 52 **2.1.3.. Enzyme purification and Assay using Procedure B.**

#### 53 **2.1.3.1. Enzyme Purification.**

54  
55  
56 The cell pellet, previously obtained after IPTG induction, was resuspended in a buffer containing 50  
57  
58 mM Tris, 500 mM NaCl, 0.5 mM TCEP, 250 mM glucose, 1 mM NAD<sup>+</sup>, 0.5% (v/v) Triton X-100 and  
59  
60 cOmplet Protease Inhibitor Cocktail Tablet (Roche, Germany) adjusted at a pH of 8. The cells were

1  
2  
3 disrupted with a high pressure homogenizer (EmulsiFlex-C5™, AVESTIN, Mannheim, Germany) and  
4  
5 the obtained homogenate was centrifuged at 17700 g for 2h at 4°C. The supernatant was applied to a  
6  
7 Ni-NTA column (5 mL HisTrap FF, GE Healthcare Life Sciences, Freiburg, Germany). Two washing  
8  
9 steps were applied: in the first, to remove the DNA, a buffer composed of 50 mM Tris and 1.5 M NaCl  
10  
11 was run against the Ni-column. The second washing step was then performed with a buffer containing  
12  
13 50 mM Tris, 500 mM NaCl, 0.5 mM TCEP, 250 mM glucose, 0.25 mM NAD<sup>+</sup> and 21 mM imidazole  
14  
15 to remove the unspecific binding proteins. The target protein was eluted by increasing the imidazole  
16  
17 concentration in the buffer to 300 mM. TEV protease was added to the protein mixture to cleave the  
18  
19 *N*-6His-tag and the product solution was dialyzed overnight at 4°C to reduce the imidazole  
20  
21 concentration in the sample (50 mM Tris, 500 mM NaCl, 0.5 mM TCEP, 250 mM glucose and 0.25  
22  
23 mM NAD<sup>+</sup>). A second Ni-NTA column was used for separation of the TEV protease from the 17β-  
24  
25 HSD14. In this step the protein was collected from the flow through of the column, while the TEV  
26  
27 protease remained on the column. With the goal to increase the purity of the protein, an additional  
28  
29 purification step, using a size exclusion chromatography (Superdex 75 26/60, GE Healthcare Life  
30  
31 Sciences, Freiburg, Germany) was performed with a running buffer comprising 50 mM Tris, 500 mM  
32  
33 NaCl, 0.5 mM TCEP and 250 mM glucose. To the isolated target protein, an NAD<sup>+</sup> solution 0.25 mM  
34  
35 (batch for enzymatic assay) or 0.6 mM (batch for crystallization studies) was added. The protein  
36  
37 solution was flash-frozen in liquid nitrogen and stored at -80°C.  
38  
39  
40  
41  
42  
43

#### 44 **2.1.3.2. Fluorimetric assay using Procedure B.**

45  
46  
47 The potential inhibitor (in DMSO, final DMSO concentration in assay: 1%) was added to a mixture of  
48  
49 NAD<sup>+</sup> (1.2 mM) and E2 (32 μM) in 100 mM phosphate buffer pH 8. The enzymatic reaction was  
50  
51 started by addition of the purified enzyme (1 mg/ml) and the production of the fluorescent NADH  
52  
53 formed was measured continuously for 15 min at 25°C. The fluorimetric assays were recorded on a  
54  
55 Tecan Sapphire 2 ( $\lambda_{\text{ex}}$  at 340 nm and  $\lambda_{\text{em}}$  at 496 nm). The slit width for excitation was 7 nm and for  
56  
57 emission 15 nm. Reactions were performed in 200 μL volumes. The assay was run in 96 well-plates in  
58  
59 duplicate, each experiment resulting from three technical repeats. A linear relationship between  
60

1  
2  
3 product formation and reaction time was obtained. The slope of the progress curves was calculated by  
4  
5 linear regression. The inhibitors do not show fluorescence at the concentrations used in the assay.  
6  
7

8 The  $K_i$  values were calculated using the Morrison equation<sup>36</sup> (see Supporting Information). For  
9  
10 calculation, three constants were necessary: the substrate concentration (32  $\mu\text{M}$ ), the  $K_m$  for 17 $\beta$ -  
11  
12 HSD14 with this substrate E2 (6.18  $\mu\text{M}$ <sup>5</sup>) and the concentration in active protein, which was  
13  
14 determined experimentally for each experiment (3.2 or 3.3  $\mu\text{M}$ ), using the procedure detailed by  
15  
16 Copeland.<sup>36</sup> The fitting and data analysis was performed using GraphPad Prism 7.  
17  
18  
19  
20  
21  
22

## 23 **2.2. 17 $\beta$ -HSD1 and 17 $\beta$ -HSD2 inhibition assay.**

24  
25

26 17 $\beta$ -HSD1 and 17 $\beta$ -HSD2 were partially purified from human placenta according to previously  
27  
28 described procedures.<sup>43</sup> The enzyme was incubated with NADH (500  $\mu\text{M}$ ) in the 17 $\beta$ -HSD1 assay and  
29  
30 with NAD<sup>+</sup> (1500  $\mu\text{M}$ ) in the 17 $\beta$ -HSD2 assay, in the presence of the potential inhibitor in DMSO  
31  
32 (final concentration in assay: 1  $\mu\text{M}$ , final DMSO concentration: 1%) at 37°C. The enzymatic reaction  
33  
34 was started by addition of the radioactive substrate (either [<sup>3</sup>H]-E1 (final concentration: 500 nM) in the  
35  
36 17 $\beta$ -HSD1 assay or [<sup>3</sup>H]-E2 (final concentration: 500 nM) in the 17 $\beta$ -HSD2 assay following a  
37  
38 previously described procedure.<sup>54</sup> Separation and quantification of the radioactive steroids were  
39  
40 performed by HPLC coupled to a radiodetector.  
41  
42  
43  
44  
45

## 46 **3. Protein co-crystallization with inhibitors 6, 9, 10, 12.**

47  
48

49 Protein activity was verified before performing the crystallization studies for each inhibitor. The co-  
50  
51 crystallization of 17 $\beta$ -HSD14 in complex with the four inhibitors **6**, **9**, **10** and **12** was performed by  
52  
53 sitting drop vapor diffusion technique.  
54

55 For the crystallization of inhibitors **6** and **9** in complex with the protein an inhibitor stock solution in  
56  
57 pure DMSO was added to the protein solution (9.5 mg/mL) containing 0.6 mM NAD<sup>+</sup> with a final  
58  
59 inhibitor concentration of 0.8 mM and a DMSO concentration of 1%. 2  $\mu\text{L}$  of the mother liquor  
60  
containing 0.1 M CHES, 1 M tri-sodium citrate, pH 9.5, was mixed with 2  $\mu\text{L}$  of the protein solution.

1  
2  
3 After growing for 4 weeks at 18°C, the crystals were exposed to a cryo buffer composed of the mother  
4 liquor with the addition of 20% (w/v) glucose and 0.4 mM of either **6** or **9**, and subsequently flash-  
5 frozen in liquid nitrogen.  
6  
7

8  
9 The inhibitors **10** and **12** were crystallized under different conditions. The same concentration of the  
10 protein containing 0.6 mM of NAD<sup>+</sup>, was mixed with inhibitor and DMSO, to the final concentration  
11 of 4 mM of inhibitor and 5% DMSO. Afterwards, 2 μL of this protein-inhibitor solution were mixed  
12 with 2 μL of mother liquor composed of 0.1 M HEPES, 20% (w/v) PEG6000 and 5% (v/v) DMSO,  
13 adjusted to pH 7.0. Crystals were grown at a temperature of 18°C for four weeks. The crystals  
14 obtained with **10** were exposed to a cryo buffer obtained by the combination of mother liquor with the  
15 addition of 20% glucose and successively flash-frozen with liquid nitrogen. The crystals resulting  
16 from the complex with **12** were kept at room temperature.  
17  
18

19  
20  
21  
22  
23  
24  
25  
26  
27  
28  
29  
30  
31  
32  
33  
34  
35  
36  
37  
38  
39  
40  
41  
42  
43  
44  
45  
46  
47  
48  
49  
50  
51  
52  
53  
54  
55  
56  
57  
58  
59  
60  
Details about the crystallographic data collection, structure determination and refinement can be found  
in the Supporting Information.

## ASSOCIATED CONTENT

Supporting Information.

Chemistry: Chemical methods; General procedures; Detailed synthesis procedures and compound  
characterization; Purity as evaluated by HPLC; Crystallization: Data collection and processing,  
Structure determination and refinement, Crystallographic table; Physicochemical property table of the  
inhibitors; Figures of modeled compounds; Morrison equation.

Accession code:

Atomic coordinates and experimental data for the co-crystal structures of **6** (PDB ID: 5L7T), **9** (PDB  
ID: 5L7Y), **10** (PDB ID: 5L7W), **12** (PDB ID: 5EN4) in complex with 17β-HSD14 will be released  
upon article publication.

## AUTHOR INFORMATION

**Corresponding Author**

\*Phone: +49 6421 28 22880. E-mail: marchais@staff.uni-marburg.de

**Home Address**

<sup>⊙</sup>Ahmed S. Abdelsamie

Chemistry of Natural and Microbial Products Department, National Research Centre,  
Dokki, 12622 Cairo, Egypt

**Author Contributions**

The manuscript was written through contributions of all authors. All authors have given approval to the final version of the manuscript.

<sup>Δ</sup>F.B. and N.B. contributed equally to the work.

**Notes**

The authors declare no competing financial interest.

**ACKNOWLEDGMENT**

We thank Prof. R.W. Hartmann for providing access to the 17 $\beta$ -HSD1 and 17 $\beta$ -HSD2 inhibitors library. HIPS (Helmholtz Institute for Pharmaceutical Sciences, Saarbrücken) is acknowledged for providing the facilities to perform the 17 $\beta$ -HSD1 and 17 $\beta$ -HSD2 assays. The authors are grateful to the Deutsche Forschungsgemeinschaft (MA-5287/1-1 and KL-1204/15-1) for financial support. Part of the research leading to these results has received funding from the European Community's Seventh Framework Programme (FP7/2007-2013) under BioStruct-X (grant agreement N°283570). We are also thankful to the beamline staff at Elettra Sincrotrone (Trieste) and PETRA III (EMBL/DESY, Hamburg) for providing outstanding support during data collection. The authors also thank Laura Sinatra, Lukas Zygalski, Eric Kerste, Laura Toro, Paige Grant and Andreas Schmidt for help during their internships.

1  
2  
3 We are also grateful to ChemAxon Ltd. for providing free access to Marvin Sketch 15.9.14 for the pKa  
4 calculations and to Dr Peter Ertl for providing the free access to the PAINS-remover tool. We are  
5 grateful to the Chemical Computing Group Inc. for granting no cost academic licenses for their  
6 software.<sup>55</sup>  
7  
8  
9  
10

## 11 **ABBREVIATIONS**

12  
13  
14  
15 17 $\beta$ -HSD14: 17 $\beta$ -Hydroxysteroid dehydrogenase type 14; SDR: short-chain dehydrogenase reductase;  
16  
17 E2: estradiol; 5-diol: 5-androstene-3 $\beta$ ,17 $\beta$ -diol; E1: estrone; H-bond: hydrogen bond.  
18  
19  
20  
21  
22  
23  
24  
25  
26  
27  
28  
29  
30  
31  
32  
33  
34  
35  
36  
37  
38  
39  
40  
41  
42  
43  
44  
45  
46  
47  
48  
49  
50  
51  
52  
53  
54  
55  
56  
57  
58  
59  
60

## REFERENCES

- (1) Lukacik, P.; Kavanagh, K. L.; Oppermann, U. Structure and Function of Human 17 $\beta$ -Hydroxysteroid Dehydrogenases. *Mol. Cell. Endocrinol.* **2006**, *248*, 61–71.
- (2) Lukacik, P.; Keller, B.; Bunkoczi, G.; Kavanagh, K. L.; Kavanagh, K.; Lee, W. H.; Hwa Lee, W.; Adamski, J.; Oppermann, U. Structural and Biochemical Characterization of Human Orphan DHRS10 Reveals a Novel Cytosolic Enzyme with Steroid Dehydrogenase Activity. *Biochem. J.* **2007**, *402*, 419–427.
- (3) Sivik, T.; Vikingsson, S.; Gréen, H.; Jansson, A. Expression Patterns of 17 $\beta$ -Hydroxysteroid Dehydrogenase 14 in Human Tissues. *Horm. Metab. Res.* **2012**, *44*, 949–956.
- (4) Haeseleer, F.; Palczewski, K. Short-Chain Dehydrogenases/Reductases in Retina. *Methods Enzymol.* **2000**, *316*, 372–383.
- (5) Bertolotti, N.; Braun, F.; Lepage, M.; Möller, G.; Adamski, J.; Heine, A.; Klebe, G.; Marchais-Oberwinkler, S. New Insights into Human 17 $\beta$ -Hydroxysteroid Dehydrogenase Type 14: First Crystal Structures in Complex with a Steroidal Ligand and with a Potent Non-Steroidal Inhibitor. *J. Med. Chem.* **2016**, *59*, 6961–6967.
- (6) Marchais-Oberwinkler, S.; Henn, C.; Möller, G.; Klein, T.; Negri, M.; Oster, A.; Spadaro, A.; Werth, R.; Wetzel, M.; Xu, K.; Frotscher, M.; Hartmann, R. W.; Adamski, J. 17 $\beta$ -Hydroxysteroid Dehydrogenases (17 $\beta$ -HSDs) as Therapeutic Targets: Protein Structures, Functions, and Recent Progress in Inhibitor Development. *J. Steroid Biochem. Mol. Biol.* **2011**, *125*, 66–82.
- (7) Frotscher, M.; Ziegler, E.; Marchais-Oberwinkler, S.; Kruchten, P.; Neugebauer, A.; Fetzer, L.; Scherer, C.; Müller-Vieira, U.; Messinger, J.; Thole, H.; Hartmann, R. W. Design, Synthesis, and Biological Evaluation of (Hydroxyphenyl)naphthalene and -Quinoline Derivatives: Potent and Selective Nonsteroidal Inhibitors of 17 $\beta$ -

- 1  
2  
3 Hydroxysteroid Dehydrogenase Type 1 (17 $\beta$ -HSD1) for the Treatment of Estrogen-  
4 Dependent Diseases. *J. Med. Chem.* **2008**, *51*, 2158–2169.  
5  
6  
7  
8 (8) Bey, E.; Marchais-Oberwinkler, S.; Negri, M.; Kruchten, P.; Oster, A.; Klein, T.;  
9 Spadaro, A.; Werth, R.; Frotscher, M.; Birk, B.; Hartmann, R. W. New Insights into the  
10 SAR and Binding Modes of Bis(hydroxyphenyl)thiophenes and -Benzenes: Influence  
11 of Additional Substituents on 17 $\beta$ -Hydroxysteroid Dehydrogenase Type 1 (17 $\beta$ -  
12 HSD1) Inhibitory Activity and Selectivity. *J. Med. Chem.* **2009**, *52*, 6724–6743.  
13  
14  
15 (9) Poirier, D. Inhibitors of 17 Beta-Hydroxysteroid Dehydrogenases. *Curr. Med. Chem.*  
16 **2003**, *10*, 453–477.  
17  
18  
19 (10) Poirier, D.; Boivin, R. P.; Tremblay, M. R.; Bérubé, M.; Qiu, W.; Lin, S.-X. Estradiol-  
20 Adenosine Hybrid Compounds Designed to Inhibit Type 1 17 $\beta$ -Hydroxysteroid  
21 Dehydrogenase. *J. Med. Chem.* **2005**, *48*, 8134–8147.  
22  
23  
24 (11) Maltais, R.; Ayan, D.; Trottier, A.; Barbeau, X.; Lagüe, P.; Bouchard, J.-E.; Poirier, D.  
25 Discovery of a Non-Estrogenic Irreversible Inhibitor of 17 $\beta$ -Hydroxysteroid  
26 Dehydrogenase Type 1 from 3-Substituted-16 $\beta$ -(M-Carbamoylbenzyl)-Estradiol  
27 Derivatives. *J. Med. Chem.* **2014**, *57*, 204–222.  
28  
29  
30 (12) Maltais, R.; Trottier, A.; Barbeau, X.; Lagüe, P.; Perreault, M.; Thériault, J.-F.; Lin, S.-  
31 X.; Poirier, D. Impact of Structural Modifications at Positions 13, 16 and 17 of 16 $\beta$ -(M-  
32 Carbamoylbenzyl)-Estradiol on 17 $\beta$ -Hydroxysteroid Dehydrogenase Type 1 Inhibition  
33 and Estrogenic Activity. *J. Steroid Biochem. Mol. Biol.* **2016**, *161*, 24–35.  
34  
35  
36 (13) Lilienkamp, A.; Karkola, S.; Alho-Richmond, S.; Koskimies, P.; Johansson, N.;  
37 Huhtinen, K.; Vihko, K.; Wähälä, K. Synthesis and Biological Evaluation of 17 $\beta$ -  
38 Hydroxysteroid Dehydrogenase Type 1 (17 $\beta$ -HSD1) Inhibitors Based on a  
39 thieno[2,3-D]pyrimidin-4(3H)-One Core. *J. Med. Chem.* **2009**, *52*, 6660–6671.  
40  
41  
42 (14) Allan, G. M.; Lawrence, H. R.; Cornet, J.; Bubert, C.; Fischer, D. S.; Vicker, N.; Smith,  
43 A.; Tutill, H. J.; Purohit, A.; Day, J. M.; Mahon, M. F.; Reed, M. J.; Potter, B. V. L.  
44  
45  
46  
47  
48  
49  
50  
51  
52  
53  
54  
55  
56  
57  
58  
59  
60

- 1  
2  
3 Modification of Estrone at the 6, 16, and 17 Positions: Novel Potent Inhibitors of  
4  
5 17beta-Hydroxysteroid Dehydrogenase Type 1. *J. Med. Chem.* **2006**, *49*, 1325–1345.  
6  
7  
8 (15) Allan, G. M.; Vicker, N.; Lawrence, H. R.; Tutill, H. J.; Day, J. M.; Huchet, M.;  
9  
10 Ferrandis, E.; Reed, M. J.; Purohit, A.; Potter, B. V. L. Novel Inhibitors of 17beta-  
11  
12 Hydroxysteroid Dehydrogenase Type 1: Templates for Design. *Bioorg. Med. Chem.*  
13  
14 **2008**, *16*, 4438–4456.  
15  
16  
17 (16) Schuster, D.; Nashev, L. G.; Kirchmair, J.; Laggner, C.; Wolber, G.; Langer, T.;  
18  
19 Odermatt, A. Discovery of Nonsteroidal 17beta-Hydroxysteroid Dehydrogenase 1  
20  
21 Inhibitors by Pharmacophore-Based Screening of Virtual Compound Libraries. *J. Med.*  
22  
23 *Chem.* **2008**, *51*, 4188–4199.  
24  
25  
26 (17) Brožič, P.; Lanišnik Rižner, T.; Gobec, S. Inhibitors of 17beta-Hydroxysteroid  
27  
28 Dehydrogenase Type 1. *Curr. Med. Chem.* **2008**, *15*, 137–150.  
29  
30  
31 (18) Starčević, Š.; Brožič, P.; Turk, S.; Cesar, J.; Lanišnik Rižner, T.; Gobec, S. Synthesis  
32  
33 and Biological Evaluation of (6- and 7-Phenyl) Coumarin Derivatives as Selective  
34  
35 Nonsteroidal Inhibitors of 17 $\beta$ -Hydroxysteroid Dehydrogenase Type 1. *J. Med. Chem.*  
36  
37 **2011**, *54*, 248–261.  
38  
39  
40 (19) Wetzel, M.; Marchais-Oberwinkler, S.; Hartmann, R. W. 17 $\beta$ -HSD2 Inhibitors for the  
41  
42 Treatment of Osteoporosis: Identification of a Promising Scaffold. *Bioorg. Med. Chem.*  
43  
44 **2011**, *19*, 807–815.  
45  
46  
47 (20) Xu, K.; Al-Soud, Y. A.; Wetzel, M.; Hartmann, R. W.; Marchais-Oberwinkler, S.  
48  
49 Triazole Ring-Opening Leads to the Discovery of Potent Nonsteroidal 17 $\beta$ -  
50  
51 Hydroxysteroid Dehydrogenase Type 2 Inhibitors. *Eur. J. Med. Chem.* **2011**, *46*, 5978–  
52  
53 5990.  
54  
55  
56 (21) Stoffel-Wagner, B.; Watzka, M.; Steckelbroeck, S.; Schramm, J.; Bidlingmaier, J. F.;  
57  
58 Klingmüller, D. Expression of 17beta-Hydroxysteroid Dehydrogenase Types 1, 2, 3  
59  
60 and 4 in the Human Temporal Lobe. *J. Endocrinol.* **1999**, *160*, 119–126.

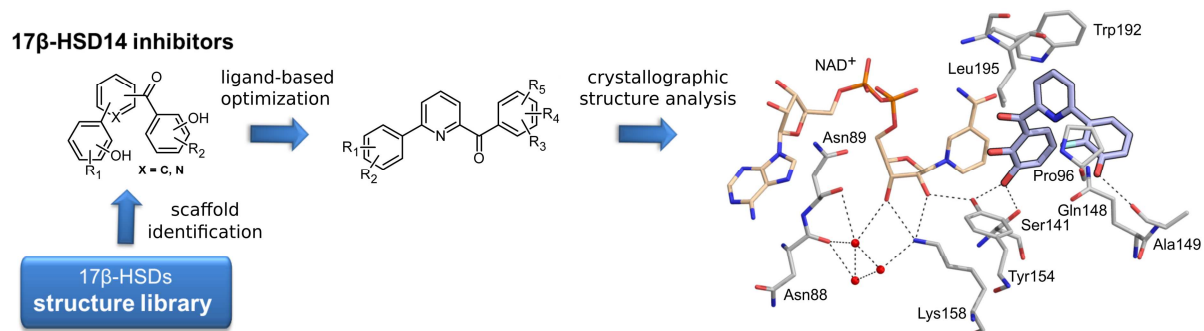
- 1  
2  
3 (22) Veber, D. F.; Johnson, S. R.; Cheng, H.-Y.; Smith, B. R.; Ward, K. W.; Kopple, K. D.  
4  
5 Molecular Properties That Influence the Oral Bioavailability of Drug Candidates. *J.*  
6  
7 *Med. Chem.* **2002**, *45*, 2615–2623.  
8  
9  
10 (23) Lipinski, C. A.; Lombardo, F.; Dominy, B. W.; Feeney, P. J. Experimental and  
11  
12 Computational Approaches to Estimate Solubility and Permeability in Drug Discovery  
13  
14 and Development Settings. *Adv. Drug Deliv. Rev.* **2001**, *46*, 3–26.  
15  
16  
17 (24) Cai, D.; Hughes, D. L.; Verhoeven, T. R. A Study of the Lithiation of 2,6-  
18  
19 Dibromopyridine with Butyllithium, and Its Application to Synthesis of L-739,010.  
20  
21 *Tetrahedron Lett.* **1996**, *37*, 2537–2540.  
22  
23  
24 (25) Miyaura, N.; Suzuki, A. Palladium-Catalyzed Cross-Coupling Reactions of  
25  
26 Organoboron Compounds. *Chem. Rev.* **1995**, *95*, 2457–2483.  
27  
28  
29 (26) Amb, C. M.; Rasmussen, S. C. 6,6'-Dibromo-4,4'-Di(hexoxymethyl)-2,2'- Bipyridine:  
30  
31 A New Solubilizing Building Block for Macromolecular and Supramolecular  
32  
33 Applications. *J. Org. Chem.* **2006**, *71*, 4696–4699.  
34  
35  
36 (27) Bolliger, J. L.; Oberholzer, M.; Frech, C. M. Access to 2-Aminopyridines –  
37  
38 Compounds of Great Biological and Chemical Significance. *Adv. Synth. Catal.* **2011**,  
39  
40 *353*, 945–954.  
41  
42  
43 (28) Maiti, D.; Buchwald, S. L. Cu-Catalyzed Arylation of Phenols: Synthesis of Sterically  
44  
45 Hindered and Heteroaryl Diaryl Ethers. *J. Org. Chem.* **2010**, *75*, 1791–1794.  
46  
47  
48 (29) Castro, A.; Depew, K.; Grogan, M.; Holson, E.; Hopkins, B.; Johannes, C.; Keaney, G.;  
49  
50 Koney, N.; Liu, T.; Mann, D.; Nevalainen, M.; Peluso, S.; Perez, L.; Snyder, D.;  
51  
52 Tibbitts, T. Compounds and Methods for Inhibiting the Interaction of Bcl Proteins with  
53  
54 Binding Partners. WO2008024337 (A2), February 28, 2008.  
55  
56  
57 (30) Eckelbarger, J.; Epp, J.; Fischer, L.; Lowe, C.; Petkus, J.; Roth, J.; Satchivi, N.;  
58  
59 Schmitzer, P.; Siddall, T. 4-Amino-6-(Heterocyclic)picolinates and 6-Amino-2-  
60

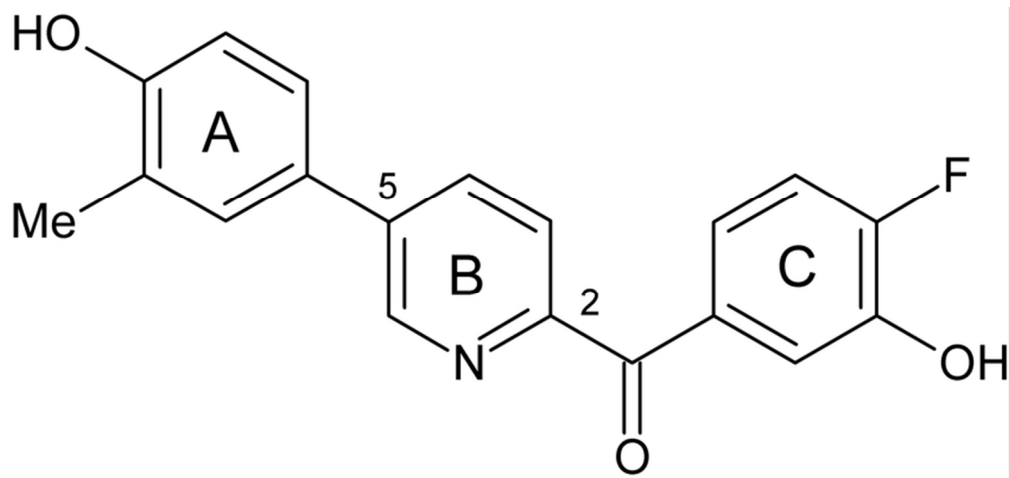
- 1  
2  
3 (Heterocyclic)pyrimidine-4-Carboxylates and Their Use as Herbicides.  
4  
5  
6 WO2014151008 (A1), September 25, 2014.  
7  
8 (31) Duan, X.-F.; Li, X.-H.; Li, F.-Y.; Huang, C.-H. A Concise Synthesis of 2,4-  
9  
10 Disubstituted Pyridines: A Convenient Synthesis of 2-Bromo-4-Iodopyridine via  
11  
12 Halogen Dance and Its Successive One-Pot Disubstitutions. *Synthesis* **2004**, *2004*,  
13  
14 2614–2616.  
15  
16  
17 (32) <http://www.molinspiration.com/>, April 18, 2016.  
18  
19 (33) Pajouhesh, H.; Lenz, G. R. Medicinal Chemical Properties of Successful Central  
20  
21 Nervous System Drugs. *NeuroRx* **2005**, *2*, 541–553.  
22  
23  
24 (34) Morrison, J. F. The Slow-Binding and Slow, Tight-Binding Inhibition of Enzyme-  
25  
26 Catalysed Reactions. *Trends Biochem. Sci.* **1982**, *7*, 102–105.  
27  
28  
29 (35) Morrison, J. F. Kinetics of the Reversible Inhibition of Enzyme-Catalysed Reactions by  
30  
31 Tight-Binding Inhibitors. *Biochim. Biophys. Acta* **1969**, *185*, 269–286.  
32  
33  
34 (36) Copeland, R. A. *Enzymes: A Practical Introduction to Structure, Mechanism, and Data*  
35  
36 *Analysis*, 2nd ed.; Wiley-VCH: New York, 2000.  
37  
38  
39 (37) Baell, J. B.; Holloway, G. A. New Substructure Filters for Removal of Pan Assay  
40  
41 Interference Compounds (PAINS) from Screening Libraries and for Their Exclusion in  
42  
43 Bioassays. *J. Med. Chem.* **2010**, *53*, 2719–2740.  
44  
45  
46 (38) [http://Cbligand.org/PAINS/Search\\_struct.php](http://Cbligand.org/PAINS/Search_struct.php). July 08, 2016.  
47  
48 (39) Schweigert, N.; Zehnder, A. J. B.; Eggen, R. I. L. Chemical Properties of Catechols and  
49  
50 Their Molecular Modes of Toxic Action in Cells, from Microorganisms to Mammals.  
51  
52 *Environ. Microbiol.* **2001**, *3*, 81–91.  
53  
54  
55 (40) Emsley, P.; Lohkamp, B.; Scott, W. G.; Cowtan, K. Features and Development of *Coot*.  
56  
57 *Acta Crystallogr. D Biol. Crystallogr.* **2010**, *66*, 486–501.  
58  
59  
60 (41) *The PyMOL Molecular Graphics System, Version 1.7.x Schrödinger, LLC.*

- 1  
2  
3 (42) Eisenberg, D.; Schwarz, E.; Komaromy, M.; Wall, R. Analysis of Membrane and  
4 Surface Protein Sequences with the Hydrophobic Moment Plot. *J. Mol. Biol.* **1984**, *179*,  
5 125–142.  
6  
7  
8  
9  
10 (43) Kruchten, P.; Werth, R.; Marchais-Oberwinkler, S.; Frotscher, M.; Hartmann, R. W.  
11 Development of a Biological Screening System for the Evaluation of Highly Active  
12 and Selective 17 $\beta$ -HSD1-Inhibitors as Potential Therapeutic Agents. *Mol. Cell.*  
13 *Endocrinol.* **2009**, *301*, 154–157.  
14  
15  
16  
17 (44) Kruchten, P. Entwicklung Eines Screeningsystems Zur Identifizierung Hochaktiver  
18 Und Selektiver Hemmstoffe Der 17 $\beta$ -Hydroxysteroid-Dehydrogenase Typ 1  
19 (17 $\beta$ HSD1). Dissertation, Saarland University, Saarbrücken, 2009.  
20  
21  
22  
23  
24  
25  
26 (45) Wetzel, M.; Gargano, E. M.; Hinsberger, S.; Marchais-Oberwinkler, S.; Hartmann, R.  
27 W. Discovery of a New Class of Bicyclic Substituted Hydroxyphenylmethanones as  
28 17 $\beta$ -Hydroxysteroid Dehydrogenase Type 2 (17 $\beta$ -HSD2) Inhibitors for the Treatment  
29 of Osteoporosis. *Eur. J. Med. Chem.* **2012**, *47*, 1–17.  
30  
31  
32  
33  
34  
35 (46) Hwang, C.-C.; Chang, Y.-H.; Hsu, C.-N.; Hsu, H.-H.; Li, C.-W.; Pon, H.-I.  
36 Mechanistic Roles of Ser-114, Tyr-155, and Lys-159 in 3 $\alpha$ -Hydroxysteroid  
37 Dehydrogenase/Carbonyl Reductase from *Comamonas Testosteroni*. *J. Biol. Chem.*  
38 **2005**, *280*, 3522–3528.  
39  
40  
41  
42  
43  
44  
45 (47) Bissantz, C.; Kuhn, B.; Stahl, M. A Medicinal Chemist's Guide to Molecular  
46 Interactions. *J. Med. Chem.* **2010**, *53*, 5061–5084.  
47  
48  
49  
50 (48) Michiels, P. J. A.; Ludwig, C.; Stephan, M.; Fischer, C.; Möller, G.; Messinger, J.; van  
51 Dongen, M.; Thole, H.; Adamski, J.; Günther, U. L. Ligand-Based NMR Spectra  
52 Demonstrate an Additional Phytoestrogen Binding Site for 17 $\beta$ -Hydroxysteroid  
53 Dehydrogenase Type 1. *J. Steroid Biochem. Mol. Biol.* **2009**, *117*, 93–98.  
54  
55  
56  
57 (49) Bey, E.; Marchais-Oberwinkler, S.; Negri, M.; Kruchten, P.; Oster, A.; Klein, T.;  
58 Spadaro, A.; Werth, R.; Frotscher, M.; Birk, B.; Hartmann, R. W. New Insights into the  
59  
60

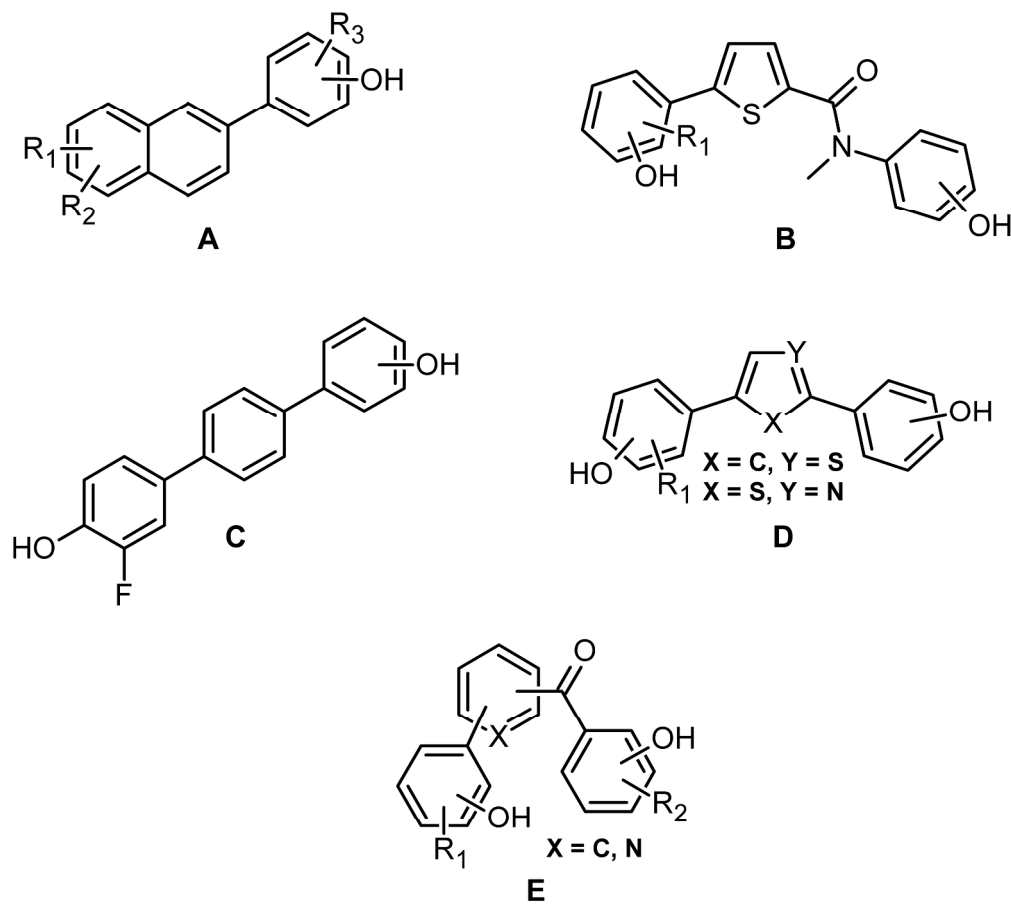
- 1  
2  
3 SAR and Binding Modes of Bis(hydroxyphenyl)thiophenes and -Benzenes: Influence  
4 of Additional Substituents on 17 $\beta$ -Hydroxysteroid Dehydrogenase Type 1 (17 $\beta$ -  
5 HSD1) Inhibitory Activity and Selectivity. *J. Med. Chem.* **2009**, *52*, 6724–6743.  
6  
7  
8  
9  
10 (50) Perspicace, E.; Giorgio, A.; Carotti, A.; Marchais-Oberwinkler, S.; Hartmann, R. W.  
11 Novel N-Methylsulfonamide and Retro-N-Methylsulfonamide Derivatives as 17 $\beta$ -  
12 Hydroxysteroid Dehydrogenase Type 2 (17 $\beta$ -HSD2) Inhibitors with Good ADME-  
13 Related Physicochemical Parameters. *Eur. J. Med. Chem.* **2013**, *69*, 201–215.  
14  
15  
16  
17 (51) Gottlieb, H. E.; Kotlyar, V.; Nudelman, A. NMR Chemical Shifts of Common  
18 Laboratory Solvents as Trace Impurities. *J. Org. Chem.* **1997**, *62* (21), 7512–7515.  
19  
20  
21  
22 (52) Andrus, M. B.; Meredith, E. L.; Sekhar, B. B. V. S. Synthesis of the Left-Hand Portion  
23 of Geldanamycin Using an Anti Glycolate Aldol Reaction. *Org. Lett.* **2001**, *3*, 259–262.  
24  
25  
26  
27 (53) Hicks, R. G.; Koivisto, B. D.; Lemaire, M. T. Synthesis of Multitopic Verdazyl Radical  
28 Ligands. Paramagnetic Supramolecular Synthons. *Org. Lett.* **2004**, *6*, 1887–1890.  
29  
30  
31  
32 (54) Kruchten, P.; Werth, R.; Marchais-Oberwinkler, S.; Bey, E.; Ziegler, E.; Oster, A.;  
33 Frotscher, M.; Hartmann, R. W. Development of Biological Assays for the  
34 Identification of Selective Inhibitors of Estradiol Formation from Estrone in Rat Liver  
35 Preparations. *Comptes Rendus Chim.* **2009**, *12*, 1110–1116.  
36  
37  
38  
39 (55) Molecular Operating Environment (MOE), 2013.08; Chemical Computing Group Inc.,  
40 1010 Sherbooke St. West, Suite #910, Montreal, QC, Canada, H3A 2R7, 2016.  
41  
42  
43  
44  
45  
46  
47  
48  
49  
50  
51  
52  
53  
54  
55  
56  
57  
58  
59  
60

## Table of Content graphic





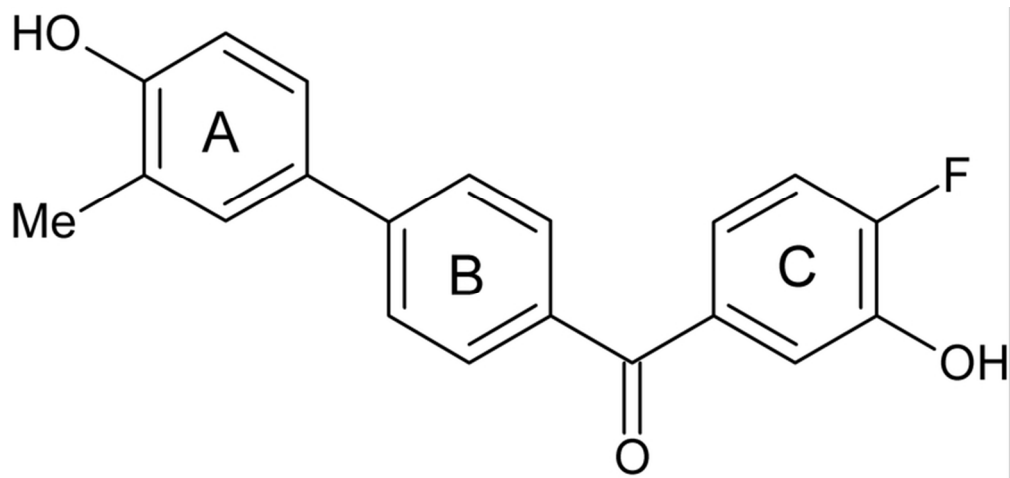
35x16mm (600 x 600 DPI)



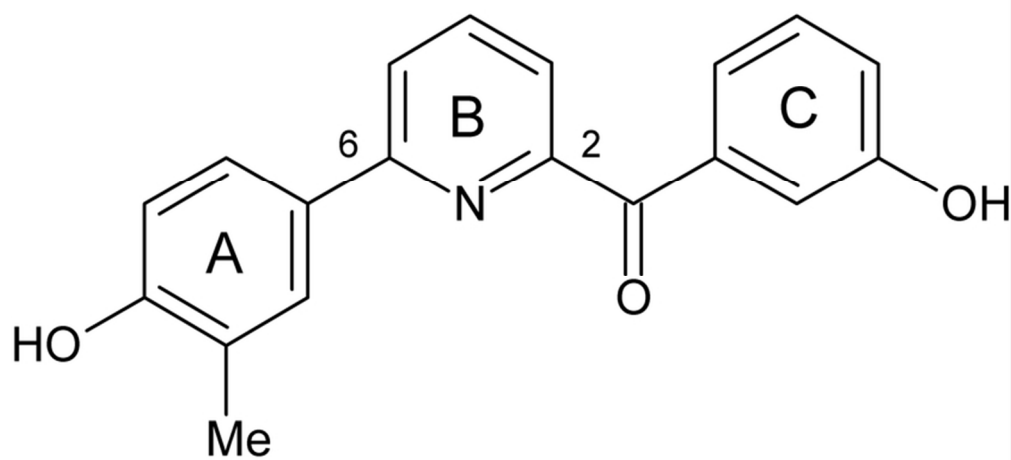
37  
38  
39  
40  
41  
42  
43  
44  
45  
46  
47  
48  
49  
50  
51  
52  
53  
54  
55  
56  
57  
58  
59  
60

Figure 1: Scaffold of inhibitors from a 17 $\beta$ -HSD1 and 17 $\beta$ -HSD2 library tested for 17 $\beta$ -HSD14 inhibitory activity.

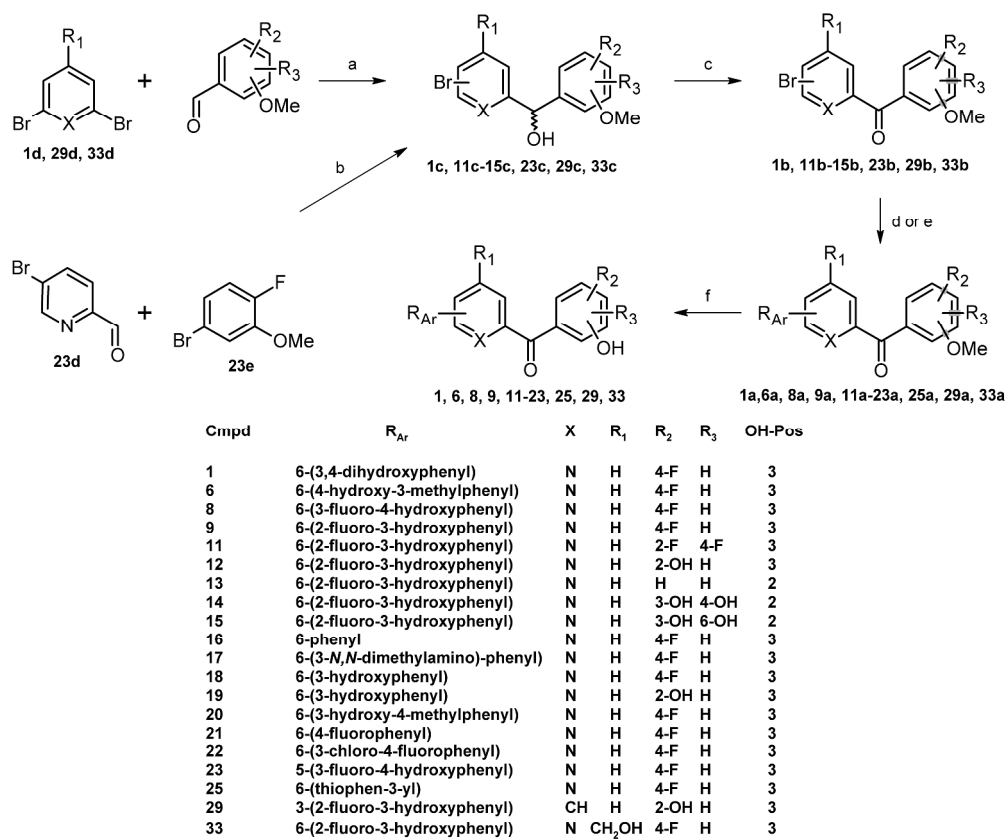
128x117mm (600 x 600 DPI)



35x16mm (600 x 600 DPI)

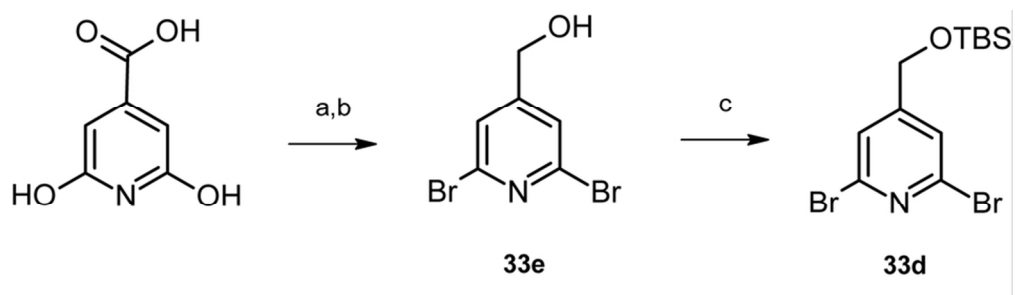


35x16mm (600 x 600 DPI)



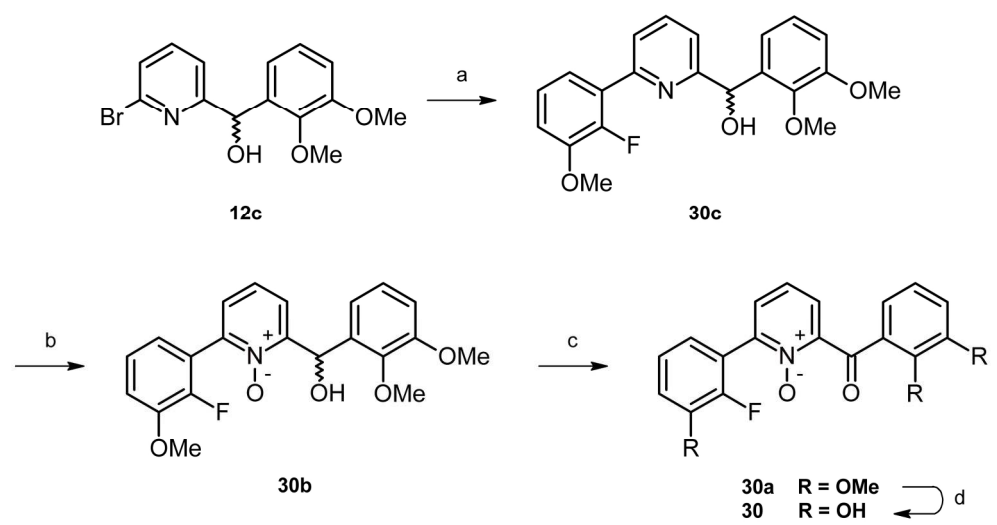
Scheme 1. Synthesis of compounds 1, 6, 8, 9, 11-23, 25, 29 and 33.

186x155mm (600 x 600 DPI)



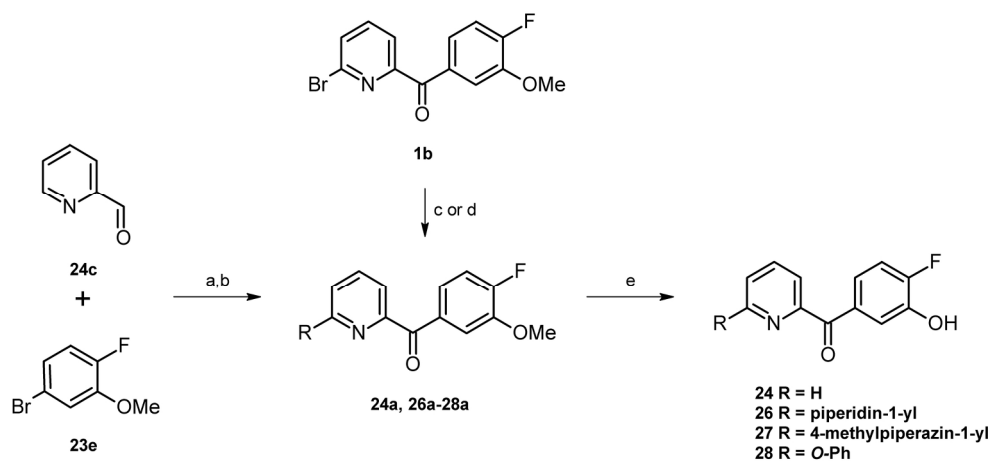
Scheme 2. Synthesis of precursor 33d.

40x11mm (600 x 600 DPI)



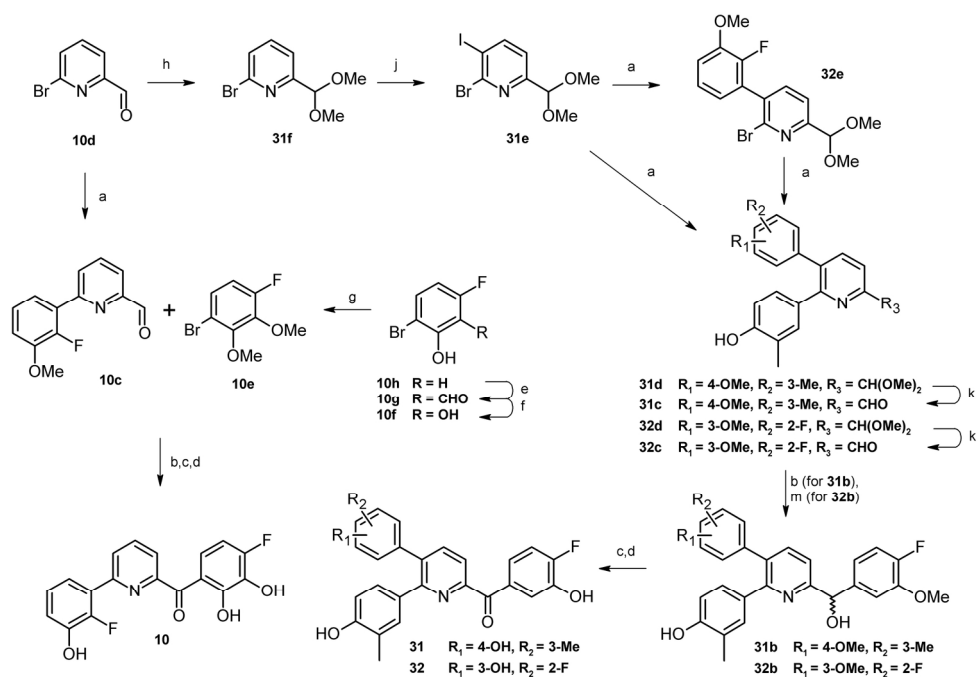
Scheme 3. Synthesis of N-oxide 30.

92x48mm (600 x 600 DPI)



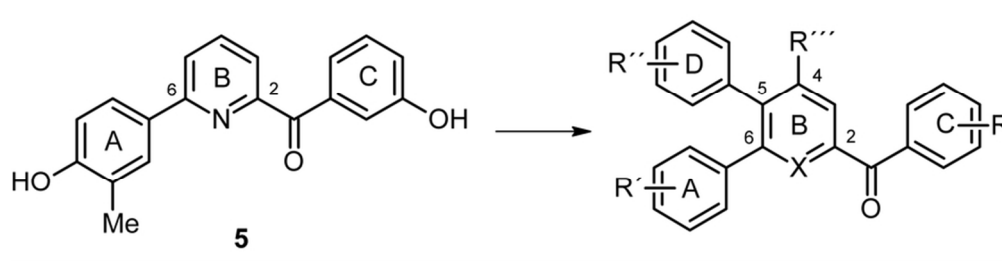
Scheme 4. Synthesis of compounds 24 and 26-28.

96x44mm (600 x 600 DPI)



Scheme 5. Synthesis of compounds 10, 31 and 32.

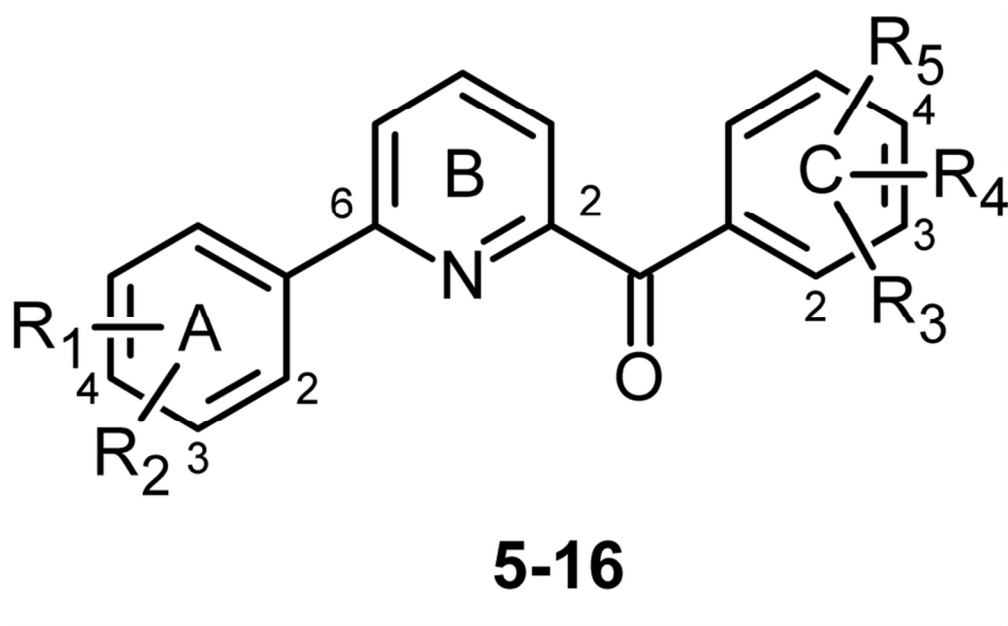
173x116mm (300 x 300 DPI)



16  
17  
18  
19  
20  
21  
22  
23  
24  
25  
26  
27  
28  
29  
30  
31  
32  
33  
34  
35  
36  
37  
38  
39  
40  
41  
42  
43  
44  
45  
46  
47  
48  
49  
50  
51  
52  
53  
54  
55  
56  
57  
58  
59  
60

Chart 1: Modifications undertaken on the hit compound 5.

40x10mm (600 x 600 DPI)



28 Table 2: 17 $\beta$ -HSD14 inhibitory activity and binding constant ( $K_i$ ) of 2,6-pyridine derivatives with different  
29 substituents at the C-ring

30 39x24mm (600 x 600 DPI)

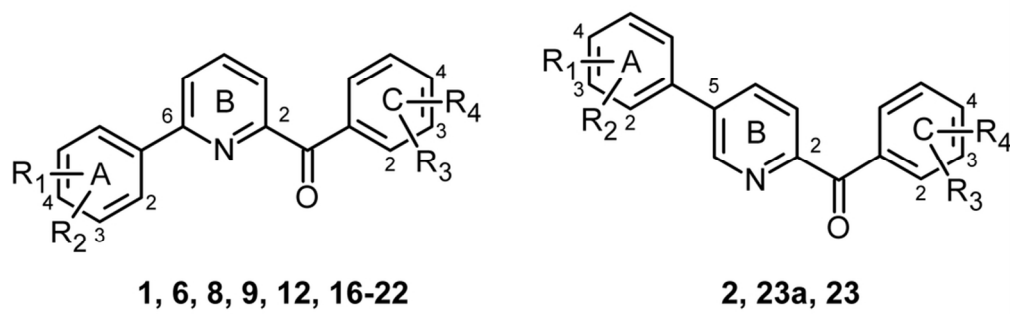
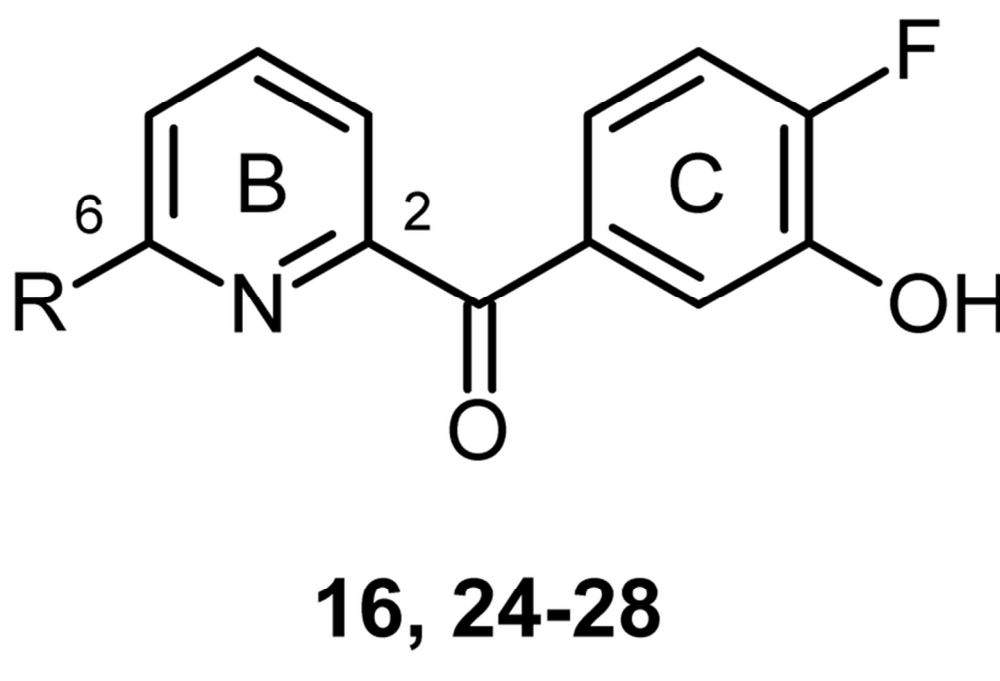


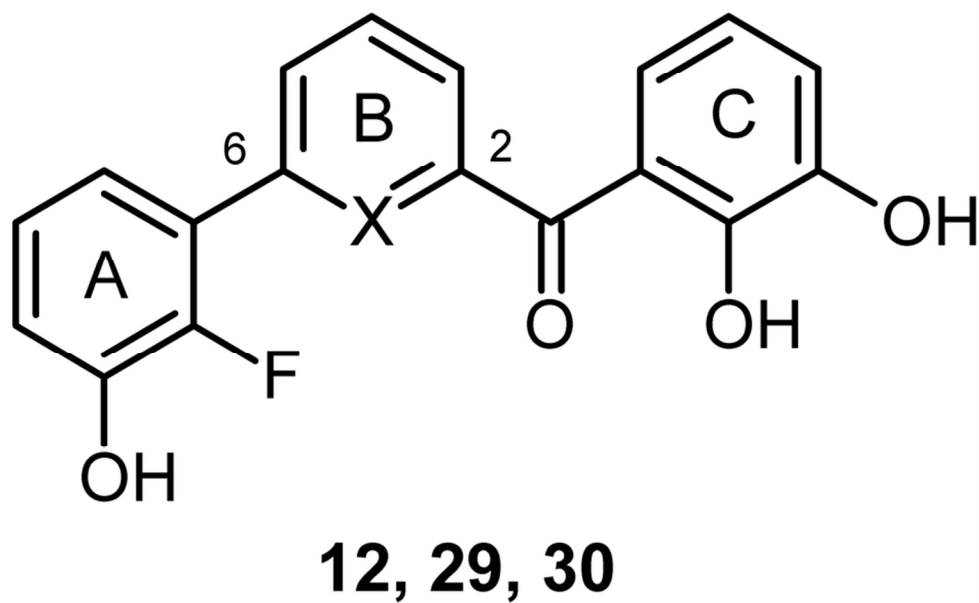
Table 3: 17 $\beta$ -HSD14 inhibitory activity and binding constant (K<sub>i</sub>) of pyridine derivatives with different substituents at the A-ring

44x14mm (600 x 600 DPI)



30 Table 4: 17 $\beta$ -HSD14 inhibitory activity and binding constant ( $K_i$ ) of 2,6-pyridine derivatives with different  
31 substituents in 6-position of the pyridine ring (different A-rings)

32 34x23mm (600 x 600 DPI)



28  
29 Table 5: 17 $\beta$ -HSD14 inhibitory activity and binding constant ( $K_i$ ) for compounds with different B-rings

30  
31 41x26mm (600 x 600 DPI)

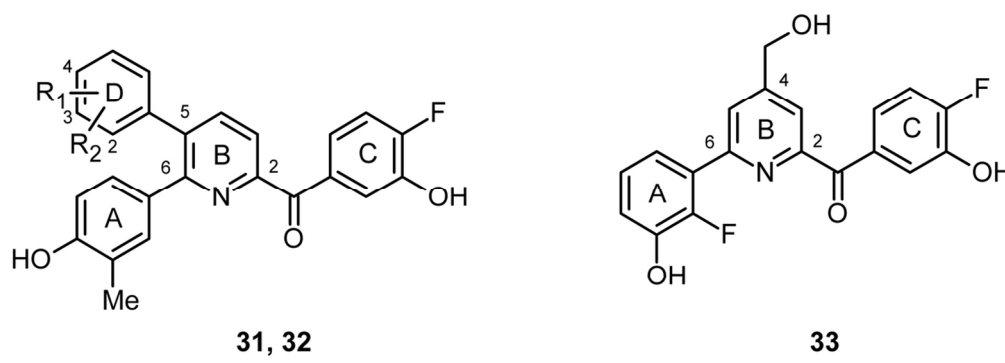


Table 6: 17 $\beta$ -HSD14 inhibitory activity and binding constant ( $K_i$ ) of pyridine derivatives with an additional D-ring or a substituent in 4-position

55x19mm (600 x 600 DPI)

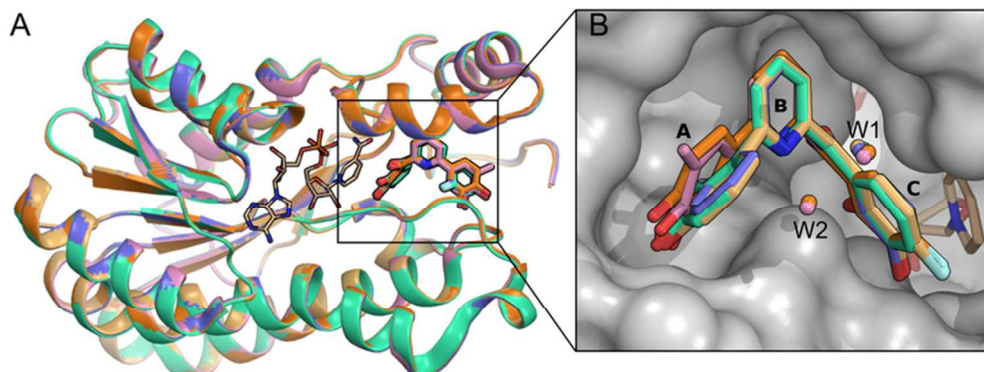


Figure 2. Superimposition of the crystal structures of 17 $\beta$ -HSD14 obtained in ternary complexes with five inhibitors: 1, 6, 9, 10, 12. (A) The enzyme 17 $\beta$ -HSD14 is shown as ribbon model (5ICM in orange, 5L7T in pink, 5L7Y in purple blue, 5L7W in ocher and 5EN4 in green); inhibitors are shown as stick models. The cofactor NAD<sup>+</sup> is shown as thin line. (B) Close-up view on the binding pocket. The protein 17 $\beta$ -HSD14 is displayed by use of the solvent accessible surface. The carbon atoms of the inhibitors are shown for 1 in orange 6 in pink, 9 in purple blue, 10 in ocher and 12 in green. Inhibitors are shown as stick models and cofactor as thin line. The water molecules W1 and W2 are represented in the same color as the corresponding inhibitor of the individual structures. W1 corresponds to water molecule 472 in 5ICM, 518 in 5L7T, 508 in 5L7Y, 496 in 5L7W, 450 in 5EN4; W2 corresponds to water molecule 530 in 5ICM and 502 in 5L7T, in the respective crystal structure. All structural representations were prepared with PyMOL.32

71x28mm (300 x 300 DPI)

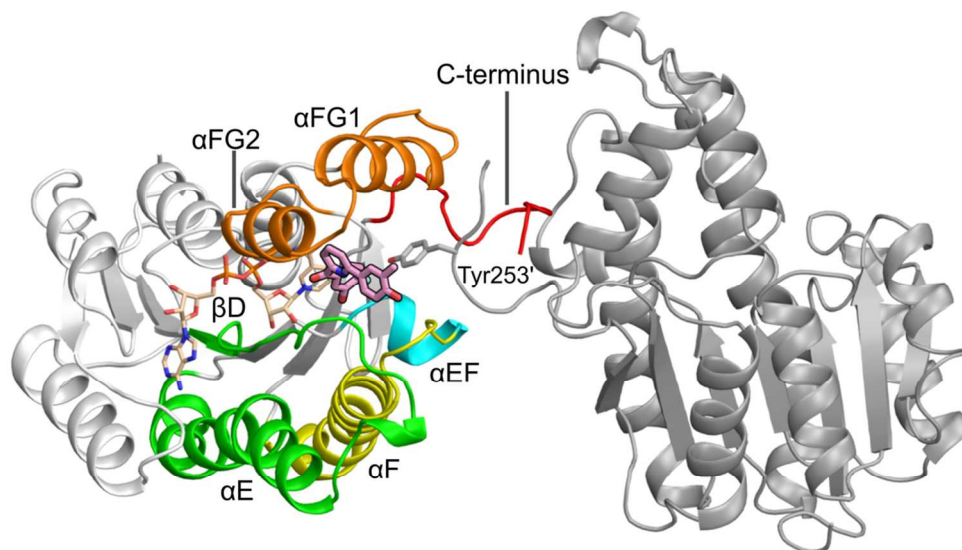
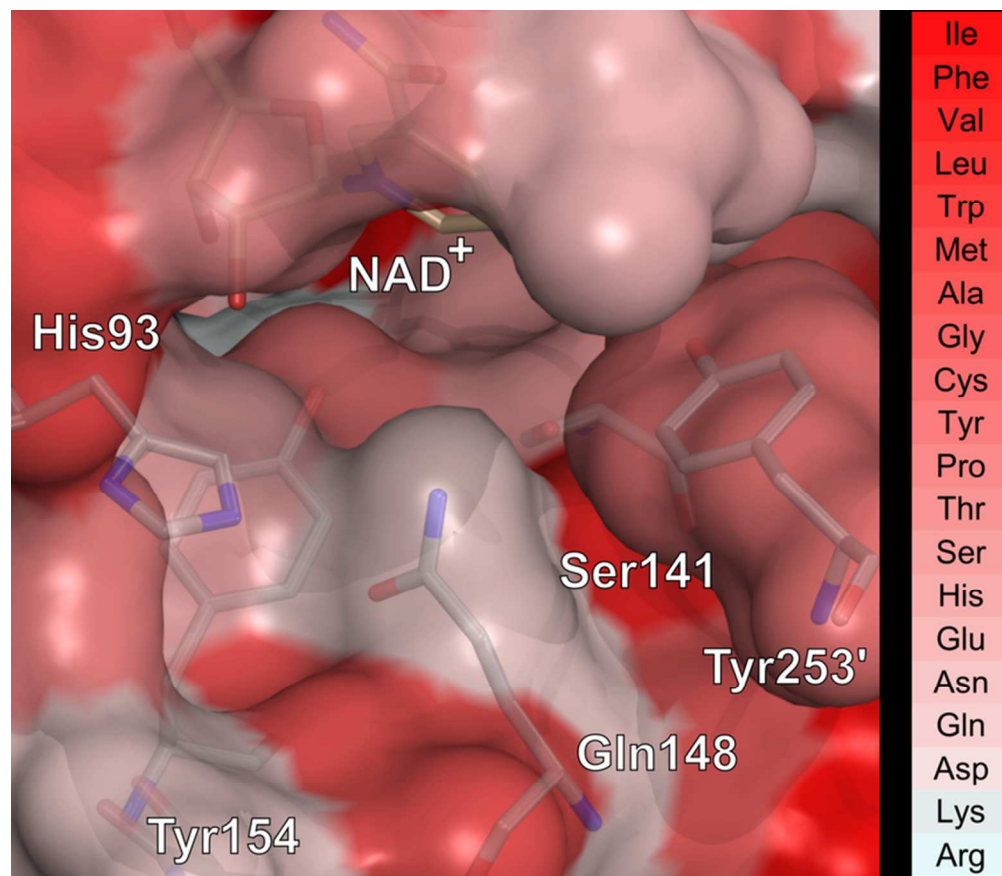


Figure 3. Ribbon representation of inhibitor 6 in complex with the protein 17β-HSD14 and cofactor NAD<sup>+</sup>. The inhibitor binding site is delimited by αFG1 and αFG2 (orange), αF (the helix containing the catalytic Tyr154 and Lys158, yellow), αEF (cyan), αE and βD (green) and C-terminal tail (red). Inhibitor 6 is shown as stick model and its carbon atoms are colored in pink. The symmetry equivalent molecule containing Tyr253' is shown in gray on the right hand side. The cofactor and Tyr253' are shown as thin lines.

101x57mm (300 x 300 DPI)



36 Figure 4. Surface representation of 17β-HSD14; color coded according to the Eisenberg hydrophobicity scale  
37 (from dark red for highly hydrophobic amino acids to white for highly hydrophilic amino acids).<sup>33</sup> The  
38 cofactor NAD<sup>+</sup> and amino acids are shown as stick models. The amino acid of the symmetry equivalent  
39 molecule is referred as prime (').

40 72x62mm (300 x 300 DPI)

41  
42  
43  
44  
45  
46  
47  
48  
49  
50  
51  
52  
53  
54  
55  
56  
57  
58  
59  
60

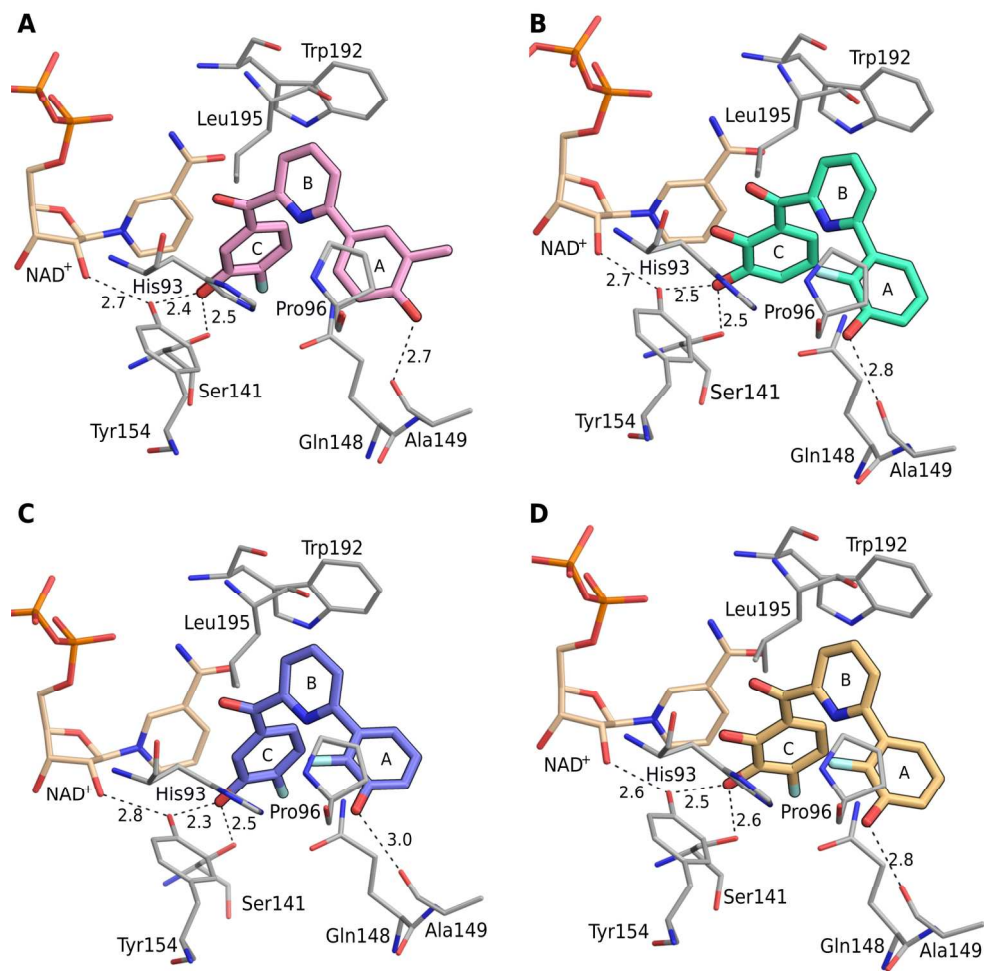


Figure 5. Crystal structures of 17β-HSD14 in complex with cofactor NAD<sup>+</sup>, and inhibitors 6 (in pink, A), 12 (in green, B), 9 (in purple blue, C) and 10 (in ocher, D). The inhibitors are shown as stick models. The amino acids, within a distance of 5 Å, and the cofactor are shown as thin lines. H-bonds are depicted as dotted lines. Distances are given in Å.

174x171mm (300 x 300 DPI)

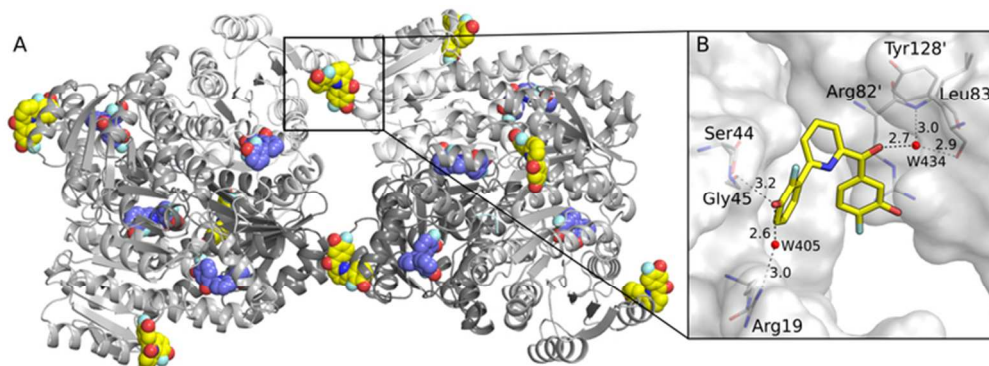


Figure 6. (A). Overall view of the crystal structure of two 17 $\beta$ -HSD14 tetramers in complex with 9. The protein monomers are shown as ribbon models and colored in gray. The inhibitors are shown as sphere models. The inhibitors located in the substrate binding site are colored in purple blue while the inhibitors located between the interfaces of the tetramers are shown in yellow. (B). Close-up view of the second ligand binding site of 9 located at the interface between two tetramers. The enzyme is displayed by use of the solvent accessible surface. Inhibitor 9 is shown as stick model. The amino acids are shown as thin lines. The amino acids of the symmetry equivalent molecule are referred to prime ('). H-bonds are depicted as black dotted lines. Distances are given in Å.

66x24mm (300 x 300 DPI)

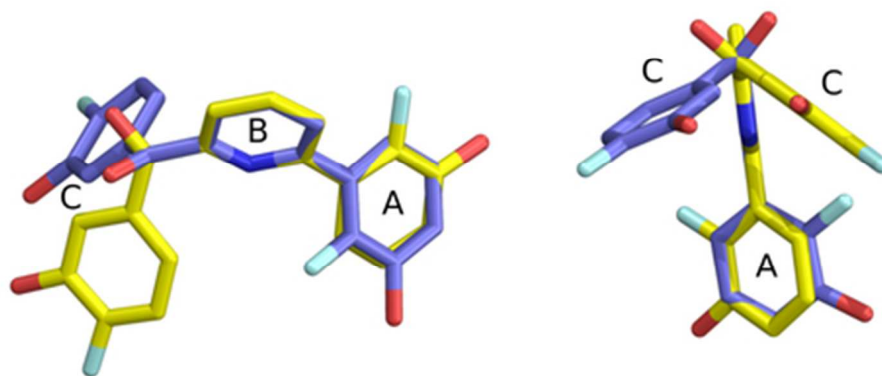


Figure 7. Superimposition of compound 9 based on the pyridine B-rings of the ligand at the interface (in yellow) and active site (in purple blue).

43x22mm (300 x 300 DPI)

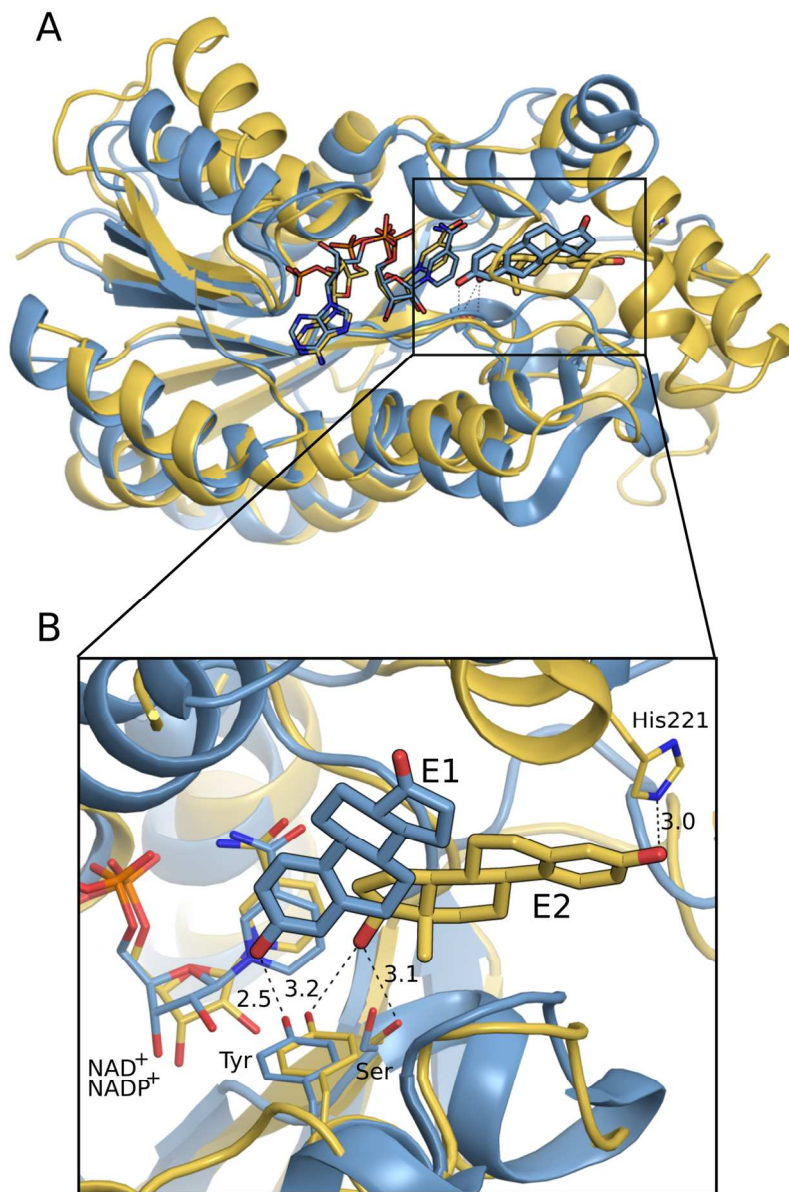


Figure 8. (A) Superimposition of 17 $\beta$ -HSD1 (yellow, PDB ID: 1FDT) and 17 $\beta$ -HSD14 (light blue, PDB ID: 5HS6) structures as ternary complexes. (B) Close-up view of the superimposed substrate binding pocket. The proteins are shown as ribbon model. The steroids are shown as stick models. The amino acids, involved in binding of the steroids (Tyr154 for 17 $\beta$ -HSD14; Tyr155, Ser142 and His 221 for 17 $\beta$ -HSD1), and the cofactors are shown as thin lines. The carbon atoms of estrone (E1) in complex with 17 $\beta$ -HSD14 are colored in light blue and the carbon atoms of estradiol (E2) in complex with 17 $\beta$ -HSD1 are colored in yellow. H-bonds are depicted as black dotted lines. Distances are given in Å.

123x179mm (300 x 300 DPI)

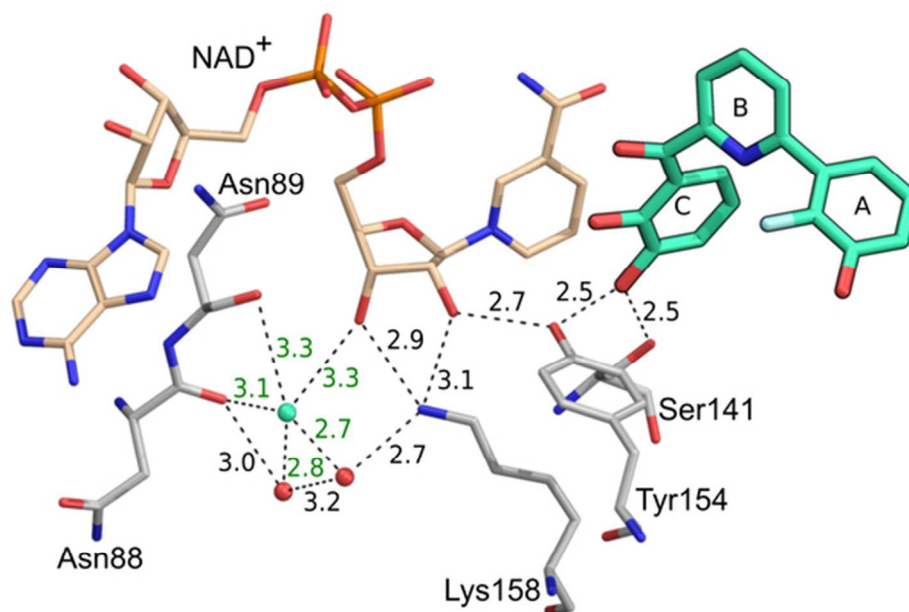


Figure 9. H-bonding network stabilizing the inhibitor 12 in the 17β-HSD14 binding site. The carbon atoms of 12 are colored in green and shown as stick model. The amino acids, involved in the H-bonding network, and the cofactor NAD<sup>+</sup> (beige) are shown as thin lines. H-bond interactions are depicted as dotted lines. Distances are given in Å. Water molecules are shown as spheres. The water molecules present in all protein-inhibitor complex structures are colored in red, an additional water molecule is visible in the case of the complexes with 1 and 12 (higher resolution crystal structures) and is colored in green.

55x36mm (300 x 300 DPI)

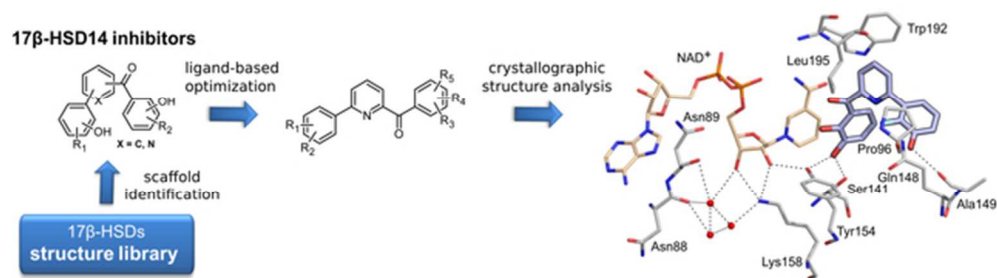


Table of content graphic

54x15mm (300 x 300 DPI)